Ignition Studies in a Motored Engine for Kinetic Mechanism Development and Validation

by

Shuqi Cheng

A dissertation submitted in partial fulfillment
of the requirements for the degree of
Doctor of Philosophy
(Mechanical Engineering)
in the University of Michigan
2021

Doctoral Committee:

Professor André L. Boehman, Chair
Professor Venkat Raman
Professor Angela Violi
Professor Margaret S. Wooldridge

Shuqi Cheng

chengsq@umich.edu

ORCID iD: 0000-0001-5481-1392

ACKNOWLEDGEMENTS

TABLE OF CONTENTS

LIST OF FIGURES

LIST OF TABLES

LIST OF ABBREVIATIONS

HCCI homogeneous charge compression ignition

LTO low-temperature oxidation

NTC negative temperature coefficient

HTO high-temperature oxidation

LTHR low-temperature heat release

HTHR high-temperature heat release

AHRR apparent heat release rate

IC internal combustion

SI spark ignited

GDI gasoline direct injection

RCM rapid compression machine

JSR jet-stirred reactor

CFD computation fluid dynamics

MFC Model Fuel Consortium

MCH methylcyclohexane

CFR Cooperative Fuel Research

RPM revolutions per minute

CR compression ratio

CCR Critical Compression Ratio

IVC intake valve closing

EVO exhaust valve opening

FTIR Fourier-transform infrared spectroscopy

GC gas chromatography

MS mass spectrometry

FID flame ionization detector

THC total hydrocarbon

ID inner diameter

RSD relative standard deviation

TS transition state

ABSTRACT

An accurate combustion model for real-world fuels is a key part of internal combustion engine simulation and design to reduce pollutants and greenhouse gas emissions. However, existing chemical kinetic mechanisms are not adequately accurate, especially for low-temperature oxidation (LTO). In this study, the autoignition of a jet fuel surrogate and pure components were investigated in a motored engine via coupled experiment and simulation to validate and improve the oxidation kinetic mechanism.

A multizone model was developed to simulate homogeneous charge compression ignition (HCCI) combustion in a modified CFR octane rating engine. In a simulation study for three pentane isomers, the multizone model was accurate for autoignition simulation and effective for kinetic mechanism validation. An existing mechanism for pentane isomers was found to be accurate in predicting reactivity, heat release, and oxidation intermediate species for all three pentane isomers. However, the low-temperature reactivity for iso-pentane was slightly underpredicted, with a 32.2% underprediction for the first-stage fuel consumption. Among the oxidation intermediate species, cyclic ethers were overpredicted by a minimum of 58.9%, while chain-branching products were underpredicted by more than 57.5%. 2-Pentene and 2-methyl-2-butene production was overpredicted by 104% and 126%, showing that concerted elimination reaction rates and the effect of H-atom availability need to be improved. In addition, acetone production should be negligible but was significantly overpredicted during iso-pentane oxidation. Chain-branching pathways following the first and second O_2 addition to the tertiary carbon were overestimated and needed

to be eliminated in the kinetic mechanism.

The ignition properties of the jet fuel surrogate and its pure components were investigated through coupled engine experiments and simulation. The UM-3 Jet-A surrogate showed strong low-temperature reactivity, which the kinetic mechanism, SKE360, successfully captured. However, the predicted transition from the negative temperature coefficient regime to high-temperature oxidation was too late. In the surrogate mixture, oxidation of iso-cetane, decalin, and toluene was significantly enhanced. The enhancement was more significant for iso-cetane than for decalin, although iso-cetane is less reactive as a pure component. The radical pool from n-dodecane low-temperature oxidation enhances H-atom abstraction, fuel radical formation, and production of small intermediate species via consecutive β-scission reactions. SKE360 successfully predicted the enhanced oxidation of iso-cetane and decalin but underpredicted toluene consumption in the surrogate mixture by 79.1%.

Low-temperature chemistry was important for n-dodecane and in a parallel investigation for n-heptane autoignition at the test conditions. However, existing mechanisms showed disagreeing predictions for n-dodecane (and n-heptane) reactivity. Although reaction pathways were similar, reaction rates differed in mechanisms and greatly influenced autoignition simulation in the motored engine. An existing n-heptane mechanism was updated and achieved improved accuracy, with the predicted critical compression ratio improved from 0.9 compression ratio higher to within 0.1 deviation from the measurements.

Low-temperature oxidation was insignificant during iso-cetane oxidation at the test condition. The jet fuel surrogate mechanism SKE360 overestimated the low-temperature reactivity of iso-cetane. In existing mechanisms, the ceiling temperature for iso-cetane was not properly addressed, and reaction rates for $\dot{R} + O_2 \Leftrightarrow RO\dot{O}$ need to be improved to eliminate O_2 addition to the iso-cetane fuel radical.

Decalin reactivity was underpredicted by SKE360. The production of benzene,

cyclohexadiene, and cyclohexene was overpredicted by more than 10 times during decalin oxidation, showing the opening of one ring in this bicyclic alkane molecule was overestimated. The main oxidation pathways following the C-C bond breaking between the two tertiary carbons were missing and need to be added.

In this work, motored engine experimental measurements were for the first time used for quantitative evaluations of kinetic mechanisms. The method developed in this study and the ignition data generated improved our fundamental understanding of combustion chemistry. Our discussions provided directions for future mechanism development.

Chapter 1

Introduction

The computation fluid dynamics (CFD) simulation coupled with the combustion model is a crucial part of combustor simulation and design, which is important for optimizing engine performance, especially nowadays with emerging low carbon fuels and the urgent need for engines to adapt to new fuel properties and meet tighter regulations for greenhouse gas emissions. However, "the development of validated, predictive, and multi-scale modeling capabilities" [1] was found to be the grand challenge in this need for advanced engine design, requiring significantly improved scientific understanding via experiments and simulations in multiple disciplines, including combustion chemistry.

Conventional and alternative diesel and jet fuels exhibit two-stage ignition behaviors [2, 3], mainly from the normal alkanes or the normal-chain-structure compounds in the fuels. The low-temperature oxidation (LTO) of diesel and jet fuels starts at $600-700K$ with low-temperature heat release (LTHR) and transitions to the negative temperature coefficient (NTC) heat release at $800-900K$. The heat released in the LTO and NTC regimes takes up a small amount of the total heat release (less than 30% depending on the fuel reactivity and the derived cetane number [3]). However, the radical pools and heat generated in this process are important to prepare the fuel for the high-temperature oxidation (HTO) and heat release once the temperature

reaches around $1000K$. Description of this ignition process is essential in simulations and engine designs, requiring a reliable kinetic mechanism that includes enough details of the chemical reactions.

The problem could be more complicated because real-world fuels, including gasoline, diesel, and jet fuels, are composed of hundreds of hydrocarbons and oxygenates, making it highly challenging to develop a computationally inexpensive combustion model for implementation in engine-level simulations. The thermochemical properties, rate constants, and reaction pathways data for the complex components of real-world fuels are unavailable [4]. Using such a large model in CFD simulation is also unrealistic. Therefore, to be useful in practical devices, the chemical model needs to be simplified to describe mixtures of a limited number of model compounds, referred to as surrogate fuels. In addition to gas-phase combustion behavior, surrogate fuels should also emulate real fuels' physical properties important in injection, atomization, vaporizing, and mixing processes. Unfortunately, physical and chemical properties result from fuel structures, so limiting the number of components in surrogate formulations is extremely difficult [5]. Each individual component also needs to have a reliable kinetic mechanism available to be put together, and important cross-reactions included [4]. Large kinetics mechanisms have been developed at an adequate level of accuracy and details to capture low-temperature reactivity of many fuels [6]. However, kinetic mechanisms for surrogate fuels need to be maintained at a reduced level (200-300 species) for use with the surrogate to enable practical simulation for future engine designs.

In the Combustion Chemistry Cluster, a collaboration between multi-university research groups engaging broad expertise in internal combustion (IC) engines, fuels, fuel chemistry, and computational models, made a great effort to significantly advance the predictive simulation capabilities for IC engine designs by improving the fundamental understandings of the effects of fuel properties and developing surrogate

2

fuel formulations and the kinetic mechanism.

Kim [7] developed evolving versions of surrogate formulations UM1, UM2, and UM3 for jet fuels. Target fuels included petroleum-derived Jet-A POSF-4658, coal-derived Iso-Paraffinic Kerosene (IPK) POSF-5642, and natural-gas-derived S-8 POSF-4734, which are complex mixtures of linear alkanes, cyclic alkanes, and aromatic compounds. The surrogate component palette consisted of six pure components: n-dodecane, n-decane to represent normal alkane compounds; iso-cetane, iso-octane to represent branched alkane compounds; decalin to represent cyclic alkane compounds; and toluene to represent aromatic compounds. Among the pure components, four representative components (n-dodecane, iso-cetane, decalin, and toluene) were investigated in this work. Kang et al. [3] validated the UM1 and UM2 surrogate formulations via autoignition experiments in a constant-volume combustion chamber and a single-cylinder motored engine. The UM2 Jet-A surrogate precisely emulated the physical properties of the target fuel in physical ignition delay measurements in the constant-volume combustion chamber. Reactivity of the surrogate reasonably matched the target fuel in autoignition experiments in the motored engine under a boosted intake condition. Kim et al. [8] found that the UM3 surrogate captured the ignition pattern in an optical engine experiment compared to the target fuel, although it showed a slightly earlier ignition. Kim et al. [9] developed a skeletal mechanism consisting of 360 species and 1851 reactions for the jet fuel surrogates, in response to the need for a reliable and computationally inexpensive chemical model for jet fuel surrogates. Ignition delay time simulation showed that the mechanism successfully predicted the ignition delay trends observed in shock tube experiments, but notable discrepancies were observed at low-to-intermediate temperatures, which unfortunately laid within the range of temperatures critical to the diesel ignition process.

Now come the questions of how significant these discrepancies are for combustion simulation at engine-related conditions, and how we could improve the mechanism.

Those are the two questions we aim to answer in this work. The objectives are to generate ignition data for fuel reactivity quantification and mechanism validation, to support the development of kinetic mechanisms that we will be confident to use in engine modeling and design.

In Chapter 2, we will review the literature of fundamental combustion facilities for mechanism development and validation, and recent progress in mechanism development for jet fuel surrogates and pure components. In Chapter 3, we will discuss the details of our experiment and simulation method. In Chapters 4-6, we will discuss the results on autoignition properties and simulations for fuels of different structures. Finally, Chapter 7 is the conclusions and recommendations for future work.

Chapter 2

Literature Review

2.1 Fundamental combustion facilities for low-temperature oxidation (LTO) mechanism development and validation

A chemical kinetic mechanism is a set of parameters to determine the thermochemical properties of species, rate constants of reactions, and species transport properties in a wide range of pressure, temperature and concentration conditions, for simulation of the combustion processes of a specified fuel [10]. As discussed in Chapter 1, the mechanism is the basis for CFD simulation and design of combustors.

Thermochemical data of species were in many mechanisms estimated using group additivity rules [10, 11]. A few reaction rates could be directly measured in experiments. Most reaction rates were difficult to measure directly and were calculated using quantum chemistry [10]. Hence, the overall quality of a mechanism needs to be evaluated with indirect experimental data. Widely used prediction targets included the ignition delay time, the flame speed, and the species time history measured in fundamental combustion facilities. The flame speed was insensitive to low-temperature chemistry [10], so we will briefly discuss the experimental facilities for the ignition delay time and the species time history measurement.

2.1.1 Ignition delay time in the shock tube (ST) and the rapid compression machine (RCM)

The ignition delay time measured in the shock tube was the most widely used prediction target for mechanism development and validation due to the large dataset available in the literature for various fuels and the accessibility and simplicity of the simulation model. Species time histories, especially for the OH radical, were also widely used in mechanism validation and optimization. The investigation temperature in the traditional shock tube is usually $> 1000K$. To measure the ignition delay time at lower temperatures, the driver section needed to be lengthened significantly [12]. The high-pressure shock tube could expand the temperature range to as low as $665K$ for fuels exhibiting strong negative temperature coefficient (NTC) behavior [13, 14]. In mechanism validation and optimization, the autoignition process in a shock tube could be treated as a zero-dimensional process in a closed homogenous reactor. A gas dynamic model CHEMSHOCK was also developed [15] for a more accurate simulation of the species time history in the shock tube.

The rapid compression machine (RCM) is another experimental facility for ignition delay time measurement, especially at low-to-intermediate temperatures where shock tube data are unavailable. Goldsborough et al. [16] reviewed the recent advances in RCM studies and compared the operating conditions of different experimental facilities for autoignition studies, as shown in Figure 2.1. The strength of RCM is that it offers well-controlled conditions (compared to motored engines), realistic mixtures (compared to jet reactors), and low-temperature experiment capability (compared to the shock tube). Premixed autoignition in an RCM could be treated as in a closed homogeneous reactor in the same way as for a shock tube (at a constant volume) or by applying effective volume histories of experiments to account for heat loss [11, 17].
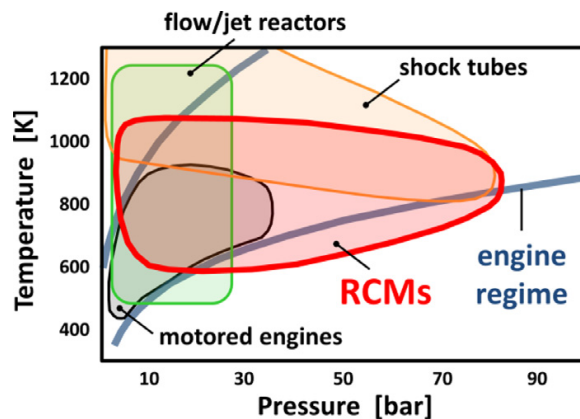
Figure 2.1: Operation temperature and pressure range for autoignition experimental facilities [16].

2.1.2 Pyrolysis and oxidation intermediate species in the flow and jet reactors

Species time histories in the flow and jet reactors have been widely used to provide constraints for constructing mechanisms and quantifying mechanism accuracy. The flow reactor could be simplified as an ideal plug flow reactor for simulating the chemical reactions in the axial direction, permitting the usage of large-scale chemical mechanisms [18]. The jet-stirred reactor (JSR) is another facility widely used for intermediate species measurement. Recently, concentration measurements for hydroperoxide [19], ketohydroperoxide, and dione [20] species were performed in the JSR, which was modeled as a perfectly stirred reactor in the simulation. Those are species produced in the early stage of fuel consumption at low temperatures and were previously too unstable to be detected in other experimental facilities.

2.1.3 Motored engine experiment and simulation

Motored engine autoignition experiments were widely performed to evaluate the reactivity of a wide variety of fuels. Although providing valuable information for fuel reactivities and reaction pathways, few of the engine study results were used quantitatively for mechanism development and validation. Wang et al. [21] measured

7

n-heptane oxidation intermediates in a motored engine and a JSR and for the first time, demonstrated the similarity in the distribution of intermediate species in an engine and an ideal reactor. They found that the species pool was more complex than considered in existing mechanisms and unconsidered species mattered under engine conditions. Cheng [22] simulated the autoignition of pentane isomers in a motored engine and found that adding motored engine experiments as constraints significantly reduced the uncertainty of modeling and rate coefficients.

As discussed in Section 2.2, existing mechanisms were validated with measured data from the shock tube, the RCM, and the flow and jet reactors. However, few mechanisms were evaluated with measured data from the motored engine, due to the lack of a reliable and computationally inexpensive engine simulation model. The method developed in this work was aimed to fill this gap.

2.2 Kinetic mechanism development and validation for jet fuel surrogates and pure components

2.2.1 Jet fuel surrogates

The mechanism evaluated in this work, SKE360, for UM3 jet fuel surrogates was developed from the Model Fuel Consortium (MFC) of CHEMKIN-PRO. In MFC, the mechanism was based on the Westbrook et al. [23] mechanism for normal alkanes, the Oehlschlaeger et al. [24] mechanism for branched alkanes, the Naik [25] mechanism for decalin, and the Naik et al. [26] mechanism for aromatics. The mechanism prediction agreed well with the ignition delay time measured in the shock tube, except for slight deviation from measurements at intermediate temperatures, as shown in Figure 2.2.

Recently, new jet fuel surrogate mechanisms were developed based on improved mechanisms of the pure components. Liu et al. [27] investigated the autoignition of

8
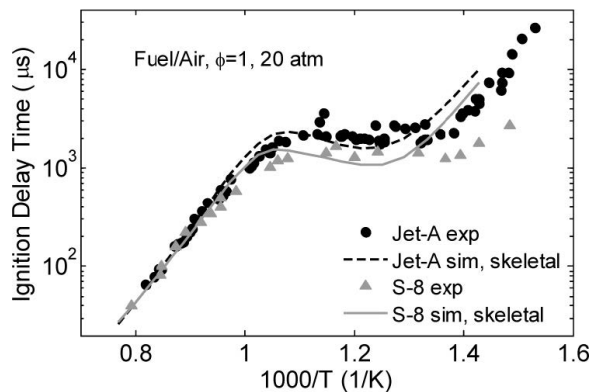
Figure 2.2: Ignition delay time predicted by SKE360 compared to shock tube igntion delay time [9].
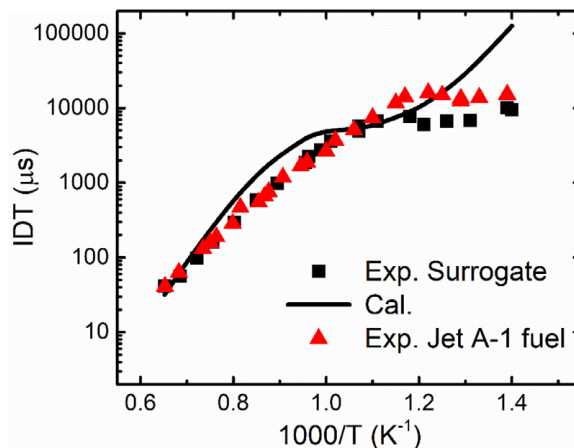
Figure 2.3: Ignition delay time predicted by a jet fuel surrogate mechanism and measured in a shock tube at $\phi = 1.0$ and $P = 16$ bar [27].

a jet fuel surrogate consisting of n-dodecane, propyl-benzene, and trimethyl-benzene, in a JSR, a shock tube, and a laminar flame burner. They developed a 401-species 2838-reactions mechanism for the surrogate. The n-dodecane chemistry was based on the Banerjee et al. [28] mechanism. Figre 2.3 shows that the mechanism prediction was in good agreement with the ignition delay time measured in a shock tube at high temperatures, but deviated from the measurements at low temperatures. Mao et al. [29] updated the surrogate mechanism in Ranzi et al. [30] with the n-dodecane submechanism from Chang et al. [31], and acquired a 233-species 5689-reactions mechanism for a jet fuel surrogate consisting of n-dodecane, iso-cetane, and

toluene. The mechanism prediction showed improved agreement with ignition delay time measured in a shock tube and an RCM at low temperatures, and maintained satisfactory agreement at high and intermediate temperatures.

2.2.2   n-Dodecane

Among the pure components, n-dodecane contributed the most to the NTC behavior of the jet fuel surrogate. Due to the long-normal-chain structure, n-dodecane has strong LTO reactivity. Ranzi et al. [30] found that the reactivity and product distribution of a normal$-C_N$ alkane could be correctly and conveniently estimated using the linear combination of normal$-C_{N-i}$ and normal$-C_{N+j}$ properties. This similarity in homologous hydrocarbons allowed fewer pure components to be included in the surrogate formulation. Hence, n-dodecane reactivity is representative of the reactivities of the normal alkane compounds in real jet fuels.

2.2.2.1   Development of n-dodecane mechanisms

Based on the Westbrook et al. [23] mechanism that SKE360's n-dodecane submechanism was developed from, plenty of improvement and optimization work has been done to to achieve better prediction accuracy. Sarathy et al. [32] developed a 7200-species 31400-reactions mechanism (often referred to as the LLNL mechanism) and included an updated Westbrook et al. [23] C_8-C_{16} n-alkane submechanism. Narayanaswamy et al. [33] reduced the LLNL mechanism to a skeletal level, and updated rate constants for important reactions selected in sensitivity analysis. As shown in Figure 2.4, the new 255-species 2289-reactions mechanism showed significantly improved accuracy.

Based on the LLNL mechanism, Cai et al. [34] updated the species thermochemical properties using the group additivity method, updated rate rules with those from Bugler et al. [11] and for H-atom abstractions by OH radicals at various carbon sites,

10

(a) Effect of Change A   (b) Effect of Change B   (c) Effect of Change C   (d) Effect of Changes D, E, and F
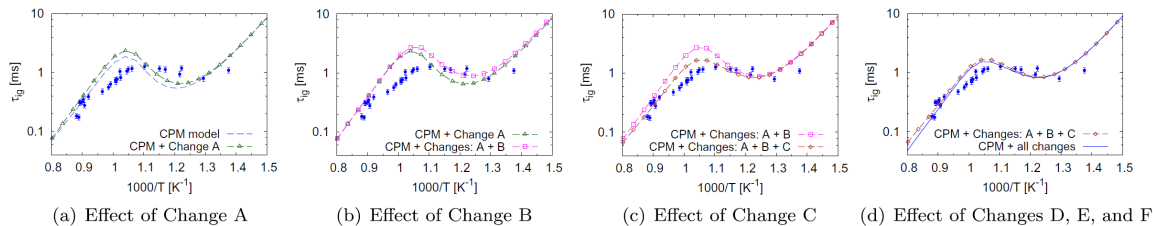
Figure 2.4: Modifications to rate constants improved prediction (lines and markers with lines) accuracy for ignition delay time measured in the shock tube (markers). Modifications: (A) updated H_2/O_2 chemistry, (B) rate of formation of ketohydroperoxide and OH, (C) rate of H-abstraction by HO_2 from n-dodecane, (D, E, F) alkene/alkenyl decomposition and H-abstraction rates [33].
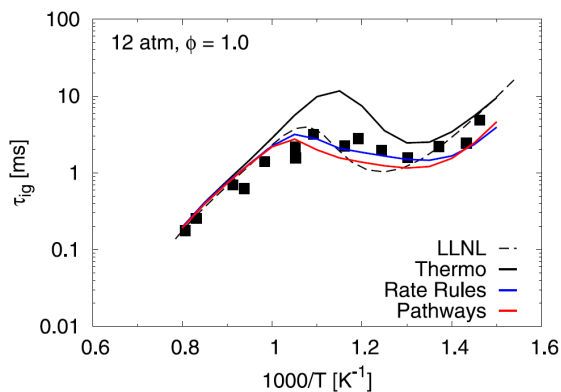
Figure 2.5: The Cai et al. [34] mechanism showed improved prediction for n-decane ignition delay time. Markers are shock tube data [34].
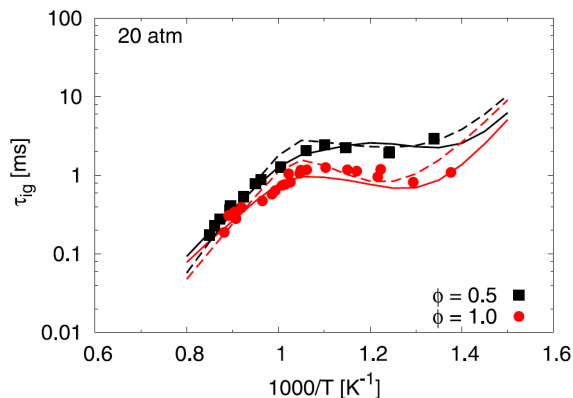
Figure 2.6: n-Dodecane ignition delay measurement in the shock tube (markers) and prediction by the Narayanaswamy et al. [33] mechanism (dashed lines) and the Cai et al. [34] mechanism (solid lines) [34].

11

and added alternative isomerization pathways from O_2QOOH radicals to $P(OOH)_2$ radicals. This updated mechanism was then optimized statistically using ignition delay time measured in the shock tube as prediction targets. The optimized mechanism showed improved accuracy as shown in Figure 2.5 compared to the original LLNL mechanism, and in Figure 2.6 compared to the Narayanaswamy et al. [33] [33] mechanism. At $\phi = 0.5$, the Cai et al. [34] mechanism showed better predictions at high temperatures while the Narayanaswamy et al. [33] mechanism showed better predictions at low temperatures. At $\phi = 1.0$, the Narayanaswamy et al. [33] mechanism overpredicted n-dodecane reactivity.
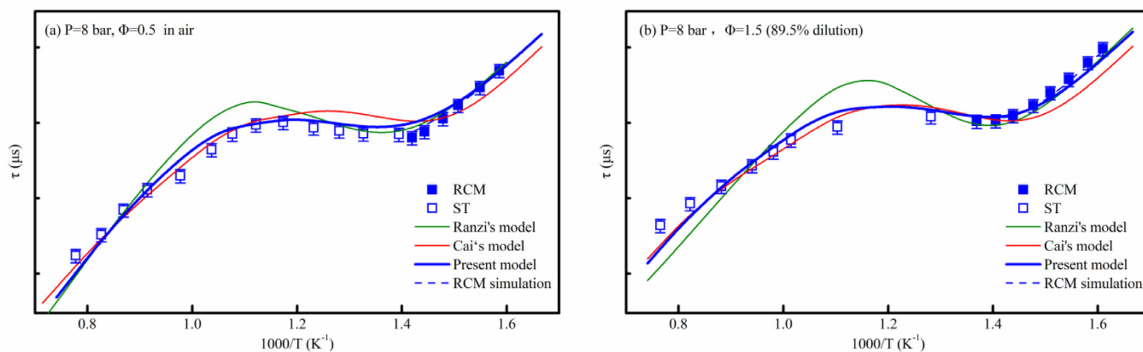
Figure 2.7: The Mao et al. [29] mechanism showed improved accuracy compared to the Ranzi et al. [30] mechanism and the Cai et al. [34] mechanism over a wide range of temperatures [29].

Mao et al. [29] evaluated six n-dodecane mechanisms (the Ranzi et al. [30] mechanism, the Banerjee et al. [28] mechanism, the LLNL mechanism, the Narayanaswamy et al. [33] mechanism, the Cai et al. [34] mechanism and the Zeng et al. [35] mechanism) in experiments and simulations in a shock tube, an RCM and a flow reactor, and found that the Cai et al. [34] mechanism provided best prediction over a wide range of temperatures, but still needed improvement. They utilized the AramcoMech 2.0 mechanism [36], the high-temperature mechanism from [35] and the low-temperature mechanism from [34], and modified selected low-temperature reaction rates. The new mechanism showed improve agreement with shock tube and RCM ignition delay time

measurements, as shown in Figure 2.7.

2.2.2.2   Validation of n-dodecane mechanisms

Existing n-dodecane mechanisms were validated in fundamental combustion facility experiments in various studies, and similarities in reaction pathways were observed. Dasgupta et al. [37] investigated three n-dodecane mechanisms (the You et al. [38] mechanism, the Luo et al. [39] mechanism, and the Narayanaswamy et al. [33] mechanism) in counter-flow flame and perfectly-stirred reactor (PSR) simulations, to evaluate the difference in reaction pathways in the mechanism. They found that though quantitatively different, the mechanisms were qualitatively similar in reaction pathways.

However, quantitative differences were found to matter in other studies. Desantes et al. [40] evaluated seven n-dodecane mechanisms ([32, 33, 34, 39, 41, 42, 43]) in RCM experiment and simulation, and observed overpredicted ignition delay time by most of the mechanism, except for the Cai et al. [34] mechanism predicting shorter cool-flame ignition delay time than other mechanisms, and the Yao et al. [43] mechanism being overtuned. Payri et al. [44] used four n-dodecane mechanisms ([33, 34, 42, 43]) in a CFD simulation for the Spray A flame structure, and found that different mechanisms led to different laminar flame structure and consequently different turbulent flame structures, especially different lift-off lengths. Fang et al. [45] also found in a Spray A simulation that low-temperature chemistry was a driving force for the 2nd-stage ignition in diesel spray end-of-injection ignition. Their studies showed the extreme importance of low-temperature chemistry in turbulent reacting spray simulation.

Despite the importance of mechanism selection, improvements are also needed. Shao et al. [14] measured n-dodecane ignition delay time in a high-pressure shock tube at $665 - 1250K$ and found that the LLNL mechanism over-predicted the 1st-stage fuel consumption at stoichiometric conditions. They also observed highly repeatable

13

pressure oscillations after the 1st-stage fuel consumption in the n-dodecane NTC regime, which was missed in the LLNL model simulation, showing that the low-temperature chemistry needed improvement.

Although n-dodecane was a widely-studied fuel, differences in mechanisms still need to be evaluated, and improvements in low-temperature chemistry are needed.

2.2.3   iso-Cetane

Compared to n-dodecane and another highly-branched alkane, iso-octane, iso-cetane autoignition properties were not adequately investigated to develop a reliable kinetic mechanism. A most widely-used iso-cetane mechanism (Oehlschlaeger et al. [24]) was developed based on analogy to an iso-octane mechanism (Curran et al. [46]). Kukkadapu and Sung [47] found that the Oehlschlaeger et al. [24] mechanism predicted an NTC behavior that was not captured in their RCM experiments as shown in Figure 2.8, because the mechanism had not been well validated using experimental data.
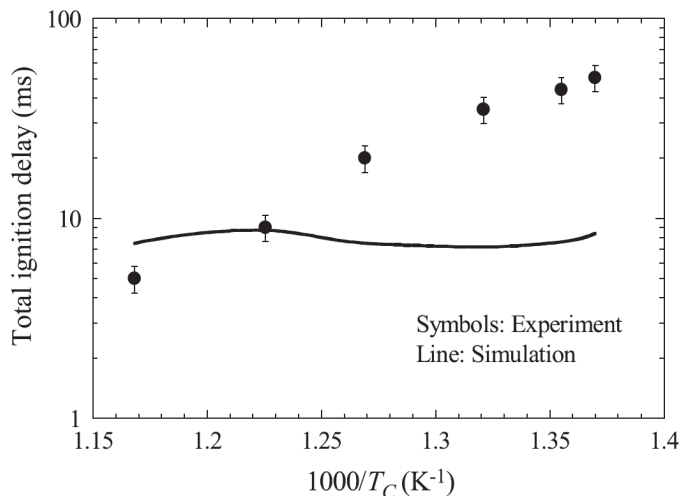
Figure 2.8: The Oehlschlaeger et al. [24] mechanism predicted an NTC behavior that was not observed in iso-cetane autoignition experiments in an RCM [47].

Yu et al. [17] extended the temperature range for iso-cetane ignition delay time

measurement to as low as 620K in RCM experiments, and found that the NTC behavior of iso-cetane did exist, but shifted to a very low temperature compared to iso-octane. They updated the species thermochemical properties and rate rules in the Oehlschlaeger et al. [24] mechanism, using values from a new iso-octane mechanism (Atef et al. [48]), but still found large discrepancies between measurements and model predictions, as shown in Figure 2.8. They suggested that new reaction pathways were needed for iso-cetane low-to-intermediate-temperature oxidation.
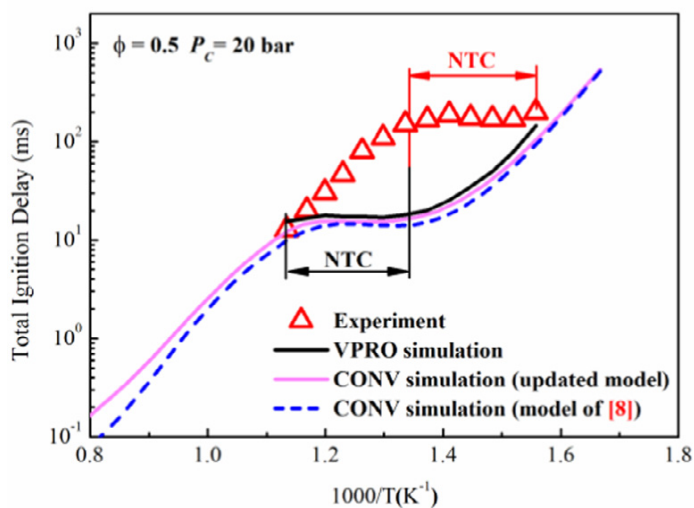
Figure 2.9: Updated Oehlschlaeger et al. [24] mechanism still needed to be improved to match the ignition delay time measured in an RCM [17].

Raza et al. [49] modified rate coefficients in the Yu et al. [17] mechanism. Wang et al. [50] updated the reaction rates of H-atom abstraction by OH radicals for the isocetane submechanism in a diesel surrogate mechanism. Both updated mechanisms improved accuracy for iso-cetane ignition delay time prediction, but significant discrepancies were still observed between the simulation and the experiment. iso-Cetane mechanisms available in the literature are listed in Table 2.1

Fuel	Mechanism	Number of Species	Number of Reactions
iso-Cetane	Yu et al. [17]	2,458	9,685
	Raza et al. [49]	2,465	10,348
	Wang et al. [50]	3,137	12,506
Decalin	Dagaut et al. [51]	357	10,741
	Wang et al. [52]	2,198	8,896
Toluene	Costa et al. [53]	349	1,631
	Metcalfe et al. [54]	329	1,888
	Yuan et al. [55]	272	1,698
	Kukkadapu et al. [56]	935	4,863

Table 2.1: Mechanisms available in the literature for iso-cetane, decalin and toluene oxidation.
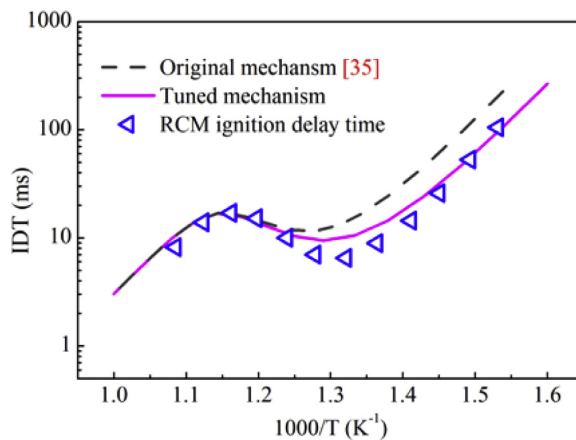
Figure 2.10: Tuned mechanism showed improved accuracy for decalin ignition delay time prediction at 15 *bar* and $\phi = 0.5$. The figure is from Yu et al. [57].

2.2.4 Decalin

The Naik [25] mechanism, from which SKE360's decalin submechanism was developed, was constructed based on analogy to other alkanes, including branched alkanes and cyclohexane groups. The mechanism was not validated with low-temperature oxidation data. Yu et al. [57] found that another decalin mechanism (Dagaut et al.
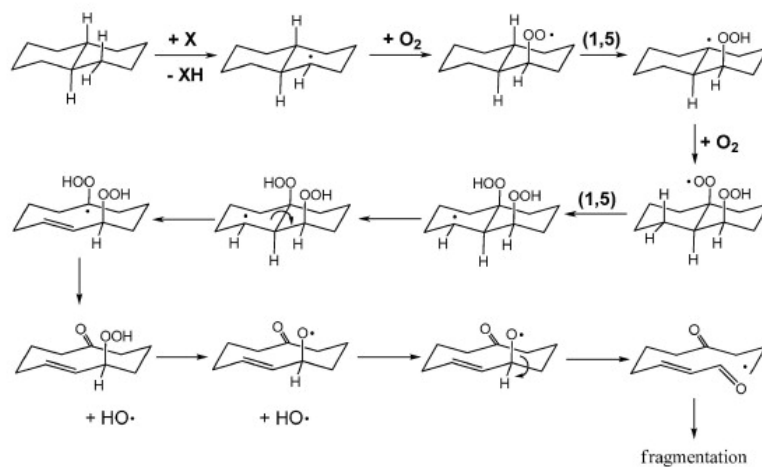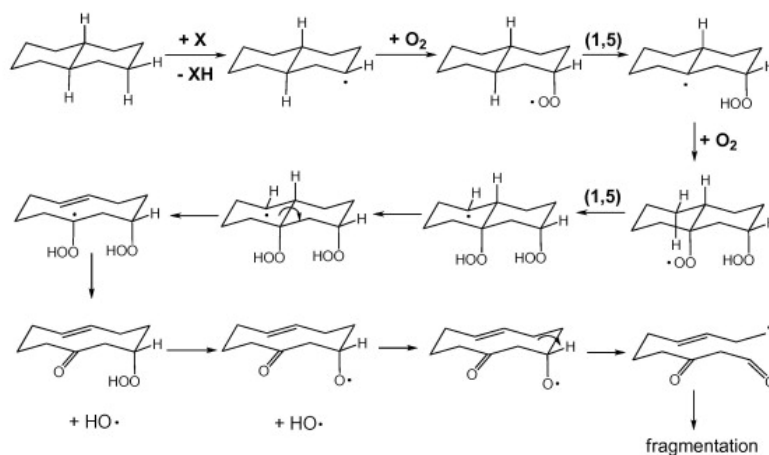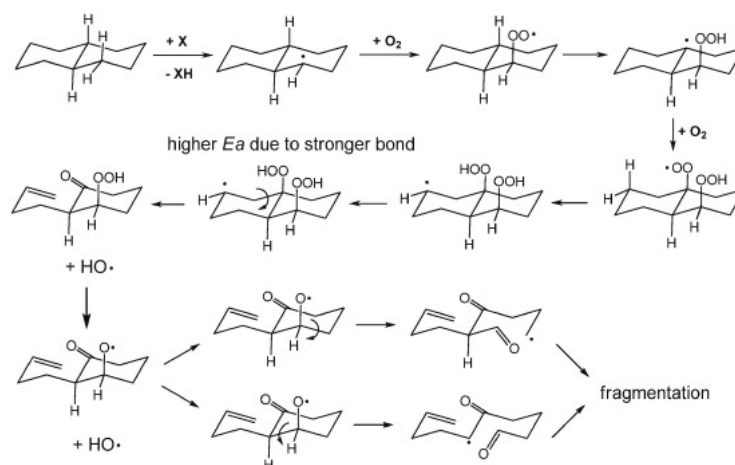
Figure 2.11: Ring-opening pathways in decalin oxidation. (a) and (b) are favored pathways of breaking the common C-C bond and their adjacent bonds. (c) is the less favored pathway of breaking one ring first [58].

[51]) was also developed based on analogy to cyclohexane and was not validated with experimental data either. They measured the ignition delay time of decalin at low temperatures in an RCM, and changed the activation energy of ketohydroperoxide decomposition reactions from 43 $kcal/mol$ to 40.5 $kcal/mol$, to match the ignition delay time measurements, as shown in Figure 2.10. Wang et al. [52] developed a decalin oxidation mechanism based on analogy to cyclohexane oxidation, and validated the new mechanism with ignition delay time measured in a shock tube and an RCM.

Yang and Boehman [58] investigated decalin oxidation in motored engine autoignition experiments. It was found that although intermediate species from decalin low-temperature oxidation was complicated, the dehydrogenation path was clear via formation of octahydronaphthalene, hexahydronaphthalene, tetralin, decalin and naphthalene. The ethylene/propene ratio in decalin oxidation was close to that of cyclohexane and significantly higher than that of methylcyclohexane (MCH). The formation of propene was favored in MCH oxidation because the ring breaking took place at the carbon connecting the methyl group. Propene formation during decalin oxidation was closer to cyclohexane oxidation rather than MCH oxidation, showing that it's unlikely for decalin to break one ring first to form a methyl side chain. Instead, it's more likely to break the common C-C bond and its adjacent bonds. These ring-breaking pathways are shown in Figure 2.11.

2.2.5 Toluene

Toluene autoignition showed no significant pre-ignition energy release below $900K$ in a shock tube [59], an RCM [60] and a flow reactor [54], so developing a precise kinetic mechanism for toluene should be relatively easier. The toluene submechanism used in SKE360 [53] was developed based on shock tube ignition delay time at $8.0 - 9.4\ atm$ and $1300 - 1900K$, and species time histories in an atmospheric-pressure flow reactor at an initial temperature of $1137K$. However, this mechanism was found to

be too reactive in shock tube experiments at $10 - 61$ bar and $1021 - 1400K$ [59], and RCM experiments at $25 - 45$ bar and $960 - 1100K$ [60].

Efforts were made to develop a more accurate toluene pyrolysis and oxidation mechanism. Metcalfe et al. [54] improved the Bounaceur et al. [61] mechanism based on time histories measured in a flow reactor for benzene, cyclopentadiene, and phenol. Yuan et al. [55] also developed a mechanism based on pyrolysis intermediates measured in a flow reactor, and oxidation intermediates measured in a JSR at $950 - 1200K$ [62]. Wang et al. [63] measured the OH time history in a shock tube at $1513 - 1877$ K and 1.2 atm, and found that the Yuan et al. [55] mechanism showed excellent agreement with the measurement, as shown in Figure 2.12. Kukkadapu et al. [56] recently improved the Mehl et al. [64] mechanism and the Zhang et al. [65] mechanism by adopting new reaction rates and reaction channels from the literature, and measured the ignition delay time in an RCM for validation. Recent toluene mechanisms available in the literature are listed in Tabel 2.1.
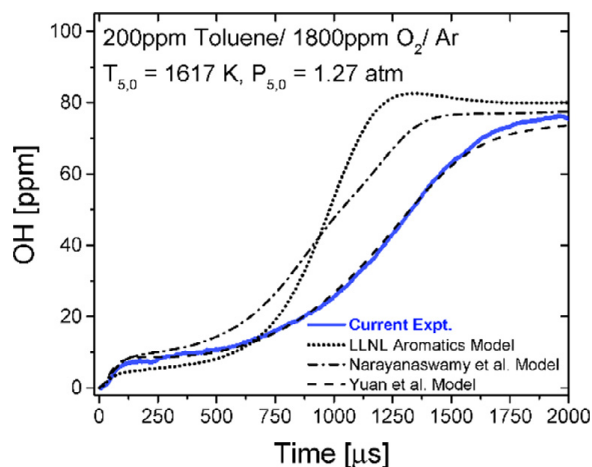
Figure 2.12: OH time-history measured in a shock tube and predicted by three mechanisms [63].

Chapter 3

Method

3.1 Motored engine experiment

3.1.1 Engine setup

The experimental autoignition studies were performed in a modified octane rating engine. The Cooperative Fuel Research (CFR) engine at the University of Michigan was modified to run in homogeneous charge compression ignition (HCCI), and could be motored at an engine speed of 600 RPM or 900 RPM, with intake dry air pressure up to 3 bar, and compression ratio (CR) from 4.0 to 15.7.

The intake pipe was heated from approximately 11 ft upstream of the engine intake port to maintain a constant intake temperature up to 280℃. The original carburetor of the CFR engine was removed, and fuel was injected approximately 5 ft upstream of the engine intake port, using a gasoline direct injection (GDI) injector, at an injection pressure of 700 psi. Fuel was injected continuously into the heated intake pipe to create a fully vaporized and homogenous intake gas mixture.

The in-cylinder pressure was measured using a Kistler 6052B piezoelectric pressure transducer at the port where there originally was a detonation sensor for octane rating tests. The apparent heat release rate (AHRR) was calculated from cylinder pressure traces using the equation from Heywood [66]:

$$\frac{dQ_n}{dt} = \frac{\gamma}{\gamma - 1} p \frac{dV}{dt} + \frac{1}{\gamma - 1} V \frac{dp}{dt} \qquad (3.1)$$

The ignition delay timing was defined as the crank angle degree when the AHRR started to rise and being a zero point of the 2nd derivative of cylinder pressure. The amount of heat release was the integral of AHRR from the onset to the end of the heat release event.

The engine was first modified by Szybist et al. [67] to run in HCCI mode, for autoignition studies of alternative diesel fuel-relevant compounds. The exhaust composition was monitored via FTIR. Condensable exhaust gas was collected for subsequent gas chromatography/mass spectrometry (GC/MS) analysis. Since then, the modified engine has been used for ignition studies of a wide variety of fuels, including gasoline [68], jet fuels [3], fatty acid esters [69], and many more. While the change to engine setup was kept minimal to that in [67], different emission analyzers were used in later studies and in this work, which will be discussed in Section 3.1.2

3.1.2 Exhaust gas sampling

At each test condition, a sample of the exhaust gas was pulled through a heated headline filter at $190°C$ to remove particulate matters, and through a chiller at -5 to $5°C$ to remove hydrocarbons, then to California Analytical Instrument (CAI) 600 series O_2/CO_2 and CO analyzers. The degree of low-temperature CO production was used in the flow reactor as a measure of reactivity, and autoignition tendency [70, 71]. CO was a major product when a fuel underwent low- and intermediate-temperature oxidation, and was not converted to CO_2 at a significant rate until a critical concentration was formed and the high-temperature heat release (HTHR) began. Other intermediates were also produced in this process, but their species and

reactivity could be fuel-specific. CO was a common product at a significantly higher concentration than other intermediates. Hence CO was the best indicator of the stage of oxidation and the reactivity of fuels, and has been used in previous autoignition studies (e.g. Agosta et al. [71]).

Another exhaust sample was pulled from the engine, through a heated line at $190°C$, to an AVL SESAM i60 FT analyzer, for FTIR measurement of small hydrocarbons and oxygenates (methane, ethylene, propene, formaldehyde, and acetaldehyde). Details of the CAI bench setup and the AVL SESAM FTIR analyzer could be found in [68].

Newly added to the engine exhaust sampling system was a Thermo Scientific Trace 1310 gas chromatography-mass spectrometry (GC-MS) coupled with a customized auxiliary oven. The aux oven inlet was connected to the engine exhaust pipe with a heated sample line and a heated headline filter, both kept at $190°C$. The aux oven was kept at $260°C$ to avoid condensation of heavy compounds (especially the fuel molecules). Exhaust sample was pulled with a vacuum pump at a constant flow rate to fill the sample loop of the GC-MS. Flow after the GC column was split into two flows to the MS and a utilized FID simultaneously. The mass spectrums and the retention times were used to determine the species, and the FID peak areas were used to quantify the species concentrations. The column used was a Restek Rtx-VMS column, which was 30m in length with 0.25 mm inner diameter (ID). This column was good at separating C_3-C_7 hydrocarbons and oxygenates [58].

FID quantification was achieved via an approach similar to external standards. Three fuels, n-heptane (a normal-alkane), iso-cetane (a highly-branched alkane), and toluene (an aromatic compound), were injected into the engine at the lowest compression ratio 4.0. Oxidation was found to be negligible at this compression ratio for the three fuels. Exhaust gas during this calibration process was sampled and the FID areas of the fuel molecules were used to determine the FID signal correlation to

species concentrations in the unit of ppmC1. Figure 3.1 (a) shows the correlation.
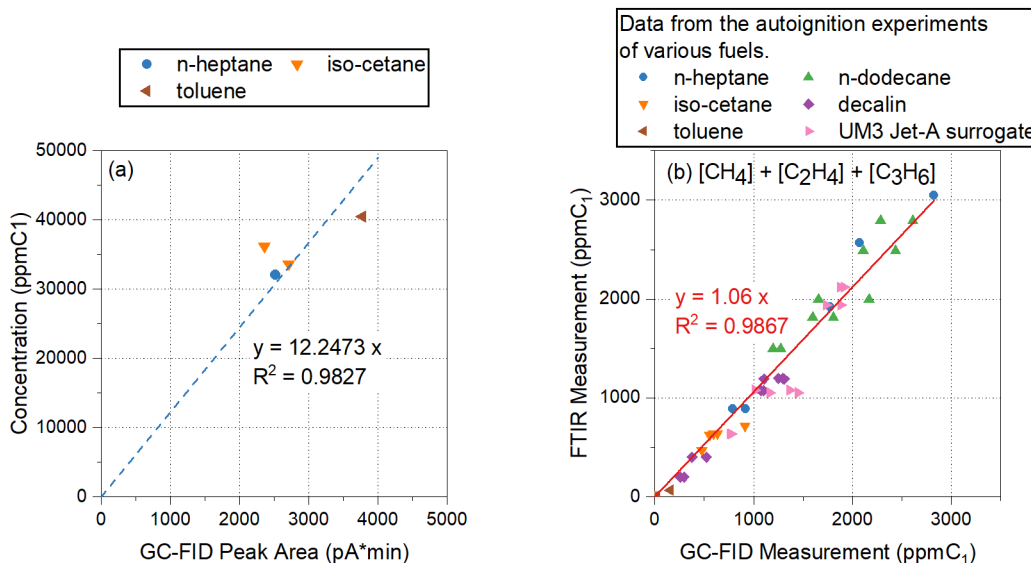
Figure 3.1: (a) Correlation used for FID quantification.
(b) Comparison of results from the GC-FID and the FTIR analyzer.

To evaluate the reliability of this correlation, total concentrations of methane, ethylene and propene from the GC-FID were compared with the values from the FTIR, as shown in Figure 3.1 (b). Measurements using the two instruments were in good agreement in autoignition experiments of all fuels investigated. Compared to the FTIR analyzer, the GC-FID measurements were 6% lower. In the future, it would be beneficial to inject unreacted fuels at a set of different concentrations in a similar way to the five-point calibration process, to re-calibrate species concentrations reported in this work for more accurate quantification.

Because oxygenates have low response factors in the FID, the total carbon in the exhaust gas could not balance with the total carbon of the fuel injected into the engine intake pipe, especially at test conditions when oxygenate concentrations were high in the exhaust gas. However, the total hydrocarbon (THC) concentrations and the CO/CO_2 concentrations measured with different analyzers agreed well, at the same conditions in repeated experiments, showing eliminated sample loss and satisfying
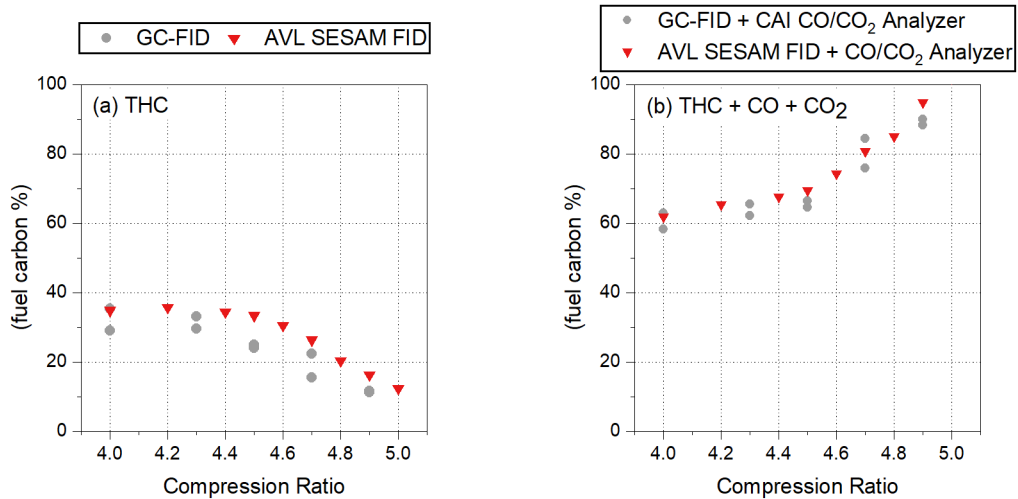
Figure 3.2: THC and carbon balance in n-dodecane autoignition experiments in the motored engine at Tin=260℃, Pin=1bar, and an engine speed of 600 RPM.
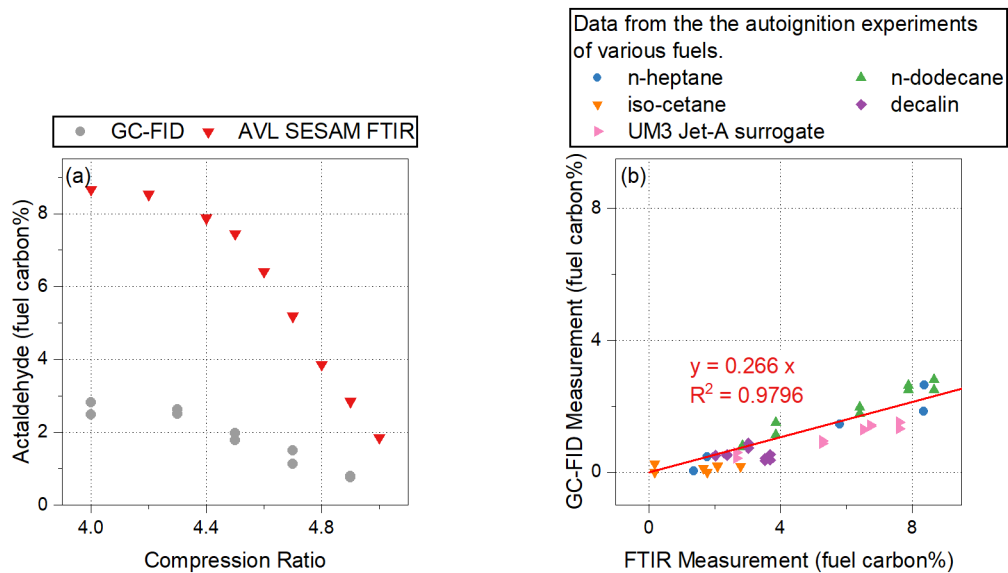
Figure 3.3: Acetaldehyde concentrations measured with the GC-FID and the AVL SESAM FTIR. Results are from (a) n-dodecane and (b) various fuel autoignition experiments in the motored engine.

repeatability in the experiment. Figure 3.2 (a) shows the THC concentrations measured with the two FIDs. Figure 3.2 (b) shows the total carbon balance (THC + CO + CO_2) in repeated experiments using different FIDs and CO/CO_2 analyzers. In this study, total carbon in the exhaust reached >90% of fuel carbon at the beginning of LTO and near the Critical Compression Ratio (CCR). During NTC, carbon balance was the worst and could be as low as 60%-80% because a large amount of oxygenates was produced.

The response factor, defined as the ratio of the FID measurement and the actual concentration, is almost 0 for formaldehyde, 0.14-0.51 for acetaldehyde [72, 73, 74, 75], and gradually increases when O/C decreases with a larger molecular size [76]. The response factor of acetaldehyde was found to be 0.266 in this study. Figure 3.3 shows the correlation of acetaldehyde concentrations measured with the GC-FID and the FTIR. An interesting observation from this correlation is that the FTIR analyzer might have a very small offset too.

Estimation of response factors is complicated and unreliable. In the following chapters, formaldehyde and acetaldehyde concentrations were from the FTIR. Original concentrations for other oxygenates were used, and no response factors were applied. Hence, C_3-C_{12} oxygenate concentrations could be as low as 0.266 of the actual concentrations.

Although carbon balance was poor in this experiment, the repeatability of species measurements was good in repeated experiments and with different instruments. Hence, alkane and alkene concentrations were reliable, and the general trends for C_3-C_{12} oxygenates were reliable. In the future, measurements of the response factors of oxygenates (i.e. C_3-C_{12} aldehydes and cyclic ethers) could be added to re-calibration oxygenate concentrations reported in this study for a better quantification.

3.1.3 Engine experiment repeatability

In addition to exhaust sampling repeatability, engine experiment repeatability was also evaluated. Peak cylinder pressure from repeated tests could be an indicator of the test repeatability. Figure 3.4 shows the peak cylinder pressures from repeated experiments. The relative standard deviation (RSD) of the peak cylinder pressure was within 2% in repeated motoring tests. In autoignition tests, peak pressures near CCR might have larger RSDs for some fuels. The onset of high-temperature oxidation (HTO) could be very sensitive to the engine coolant temperature, depending on the fuel type and the operating condition. $< 0.1°C$ increase in engine coolant set temperature might trigger HTO, leading to a significantly higher peak cylinder pressure. In general, fuels with more intensive low-temperature oxidation (LTO) are less sensitive to coolant temperature. For example, n-dodecane autoignition peak pressures showed RSDs $< 0.6\%$. In contrast, the autoignition of single-stage fuels, such as iso-cetane and toluene, is extremely sensitive to engine coolant temperature.
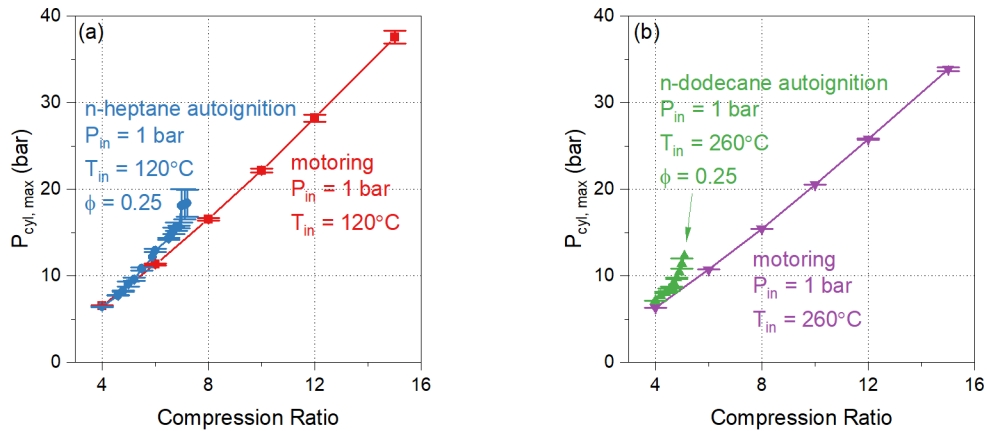
Figure 3.4: Peak cylinder pressure in repeated experiments.

The Critical Compression Ratio (CCR) could be another indicator of test repeatability. The critical compression ratio is the compression ratio at which intensive autoignition was triggered and [CO] starts to drop in the exhaust gas. It was used as a fuel reactivity indicator and was highly repeatable within a 0.1 compression ratio in previous autoignition studies [3, 68].

For fuels exhibiting strong low-temperature oxidation (LTO) behavior, CO concentration in the negative temperature coefficient (NTC) regime, $[CO]_{NTC}$, was also highly repetitive. In n-heptane autoignition experiment at $T_{in} = 120°C$ and $\phi = 0.25$, RSD of [CO] was 0.62% at $CR = 6.0$. In n-dodecane autoignition experiment at $T_{in} = 260°C$ and $\phi = 0.25$, RSD of [CO] was 3.56% at $CR = 4.0$.

It was also found that the CCR was not very sensitive to intake temperature. Figure 3.5 shows that when T_{in} increased from $110°C$ to $130°C$, CCR decreased by 0.2 at $\phi = 0.25$ and by 0.3 at $\phi = 0.50$ in n-heptane autoignition experiments. Hence, a small variance in intake temperature would not induce a significant error in CCR.
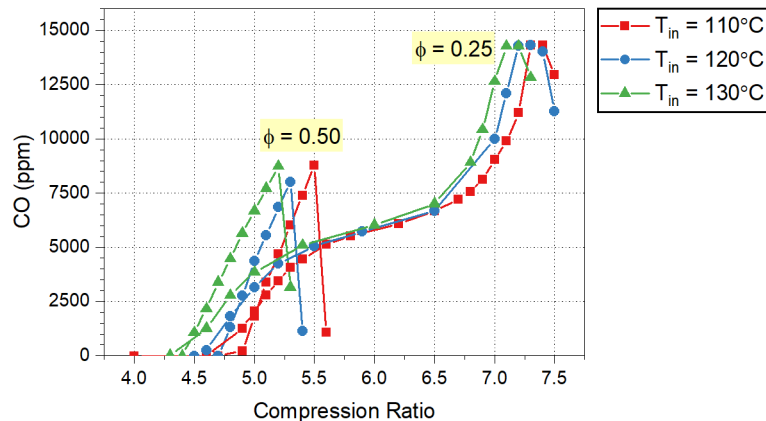
Figure 3.5: n-heptane autoignition in a motored engine, at $P_{in} = 1bar$ and $T_{in} = 110 - 130°C$.

3.1.4   Test fuels

Table 3.1 shows the brands and purities of the fuels used in this study. The UM3 Jet-A surrogate was blended on a mass base.

Fuel	Brand and Purity
n-Dodecane	Alfa Aesar, 99%
2,2,4,4,6,8,8-Heptamethylnonane (iso-cetane)	ACROS Organics™, 98%
Decahydronaphthalene (decalin, cis and trans Mixture/Reagent)	Fisher Chemical, >97%

Table 3.1: Test fuel information.

3.2 Simulation

A multizone model was developed to simulate HCCI combustion in the motored engine. The model was adapted from the stand-alone balloon-type multizone model AMECS developed by Kodavasal et al. [77]. In the AMECS model, the engine cylinder was divided into 40 zones, assuming no mass transfer between zones, which was a simplification suitable for HCCI combustion. Each zone would behave like a balloon that would shrink and swell to maintain a uniform cylinder pressure. These features were kept the same for the multizone model developed in this study.

Heat loss distribution among the zones was re-calculated based on the temperature distribution acquired from a CFD simulation of this engine. This temperature distribution is shown in Figure 3.6 (a). The CFD mesh of the engine was modified from the virtual CFR engine developed by Pal et al. [78]

The adapted stand-alone multizone model was then embedded into GT-Power as a user-defined function for the cycle calculation part of the engine system simulation. While the multizone model calculated the chemical reactions from intake valve closing (IVC) to exhaust valve opening (EVO), GT-Power simulated the gas exchange processes and the cooling system of the motored engine. Instead of being a closed-cycle simulation as for the stand-alone multizone model, the developed multizone model was used to perform open cycle simulation. Intake temperature adjustment was no longer needed to compensate for residuals and charge heating effect. Multiple

28
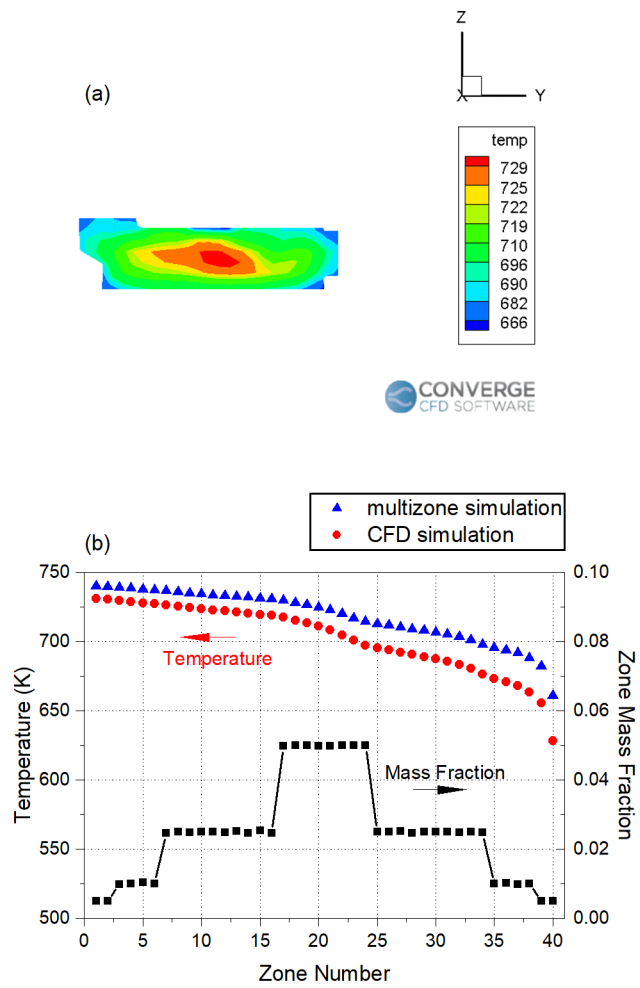
Figure 3.6: Simulation of the engine motoring at $T_{in} = 120°C$ and CR = 6.0. (a) Temperature contour from the CFD simulation. (b) Temperature profile and zone mass distribution in the CFD and multizone simulations.

		Experiment	Simulation
Engine Specifica- tion	Bore	3.25 in	3.25 in
	Stroke	4.5 in	4.5 in
	Connecting Rod Length	10 in	10 in
	Clearance Height	1.5 to 0.321 in (compression ratio 4.0 to 15.0)	Same as experiment
Operating Condition	Engine Speed	600 or 900 RPM	Same as experiment
	Intake Pressure	1 to 3 bar	Same as experiment
	Intake Temperature	40 to 260 ℃	Same as experiment (set as the intake pipe wall temperature)
	Coolant Temperature	90 ℃	$90°C$ (same for the lubricant oil temperature)
	Equivalence ratio	0.25 to 0.5	Same as experiment

Table 3.2: Experiment and simulation parameters.

cycle simulation was performed until convergence was reached. Table 3.2 shows the engine specifications and operating conditions in the experiment and simulation.

Valve lifts were measured, and a modified CFR engine valve lift curve as in Figure 3.7 was used in the simulation. The original CFR engine valve lifts and flow coefficients were acquired from Morganti [79]. The zoomed-in cylinder pressure trace in the intake and exhaust strokes (Figure 3.8) shows that the simulation's valve lifts and flow coefficients were accurate.
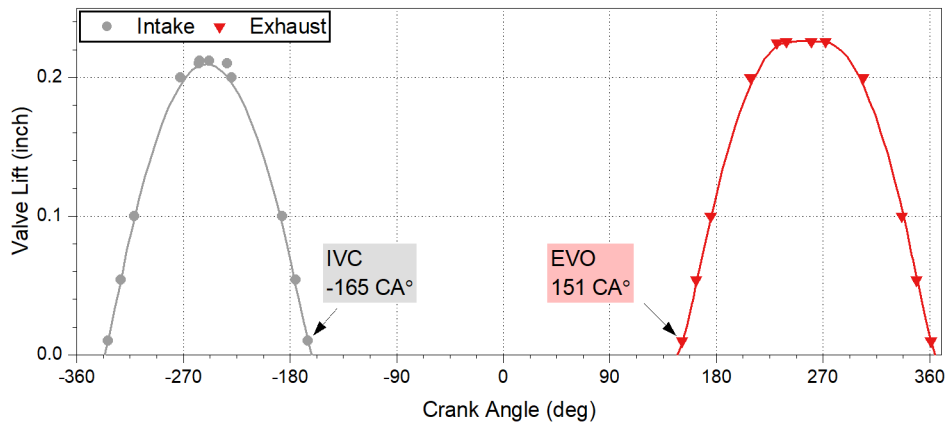
Figure 3.7: Valve lifts measured (markers) and used in the simulation (solid lines).
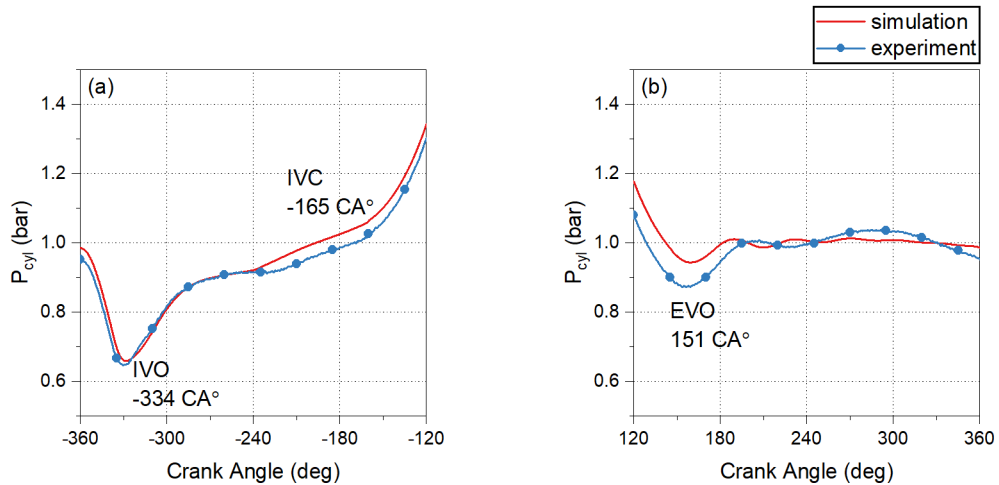
Figure 3.8: Cylinder pressure trace of the engine motoring at an engine speed of 600 RPM, $P_{in} = 1bar$, $T_{in} = 120°C$ and CR=6.0.

The modified Woschni model [80] was used to calculate the total heat loss. The heat loss coefficient was calibrated to match the peak cylinder pressures at motoring conditions. Figure 3.9 shows that the simulated peak cylinder pressure $P_{cyl,max}$ agreed well with the measurements at all simulated conditions.
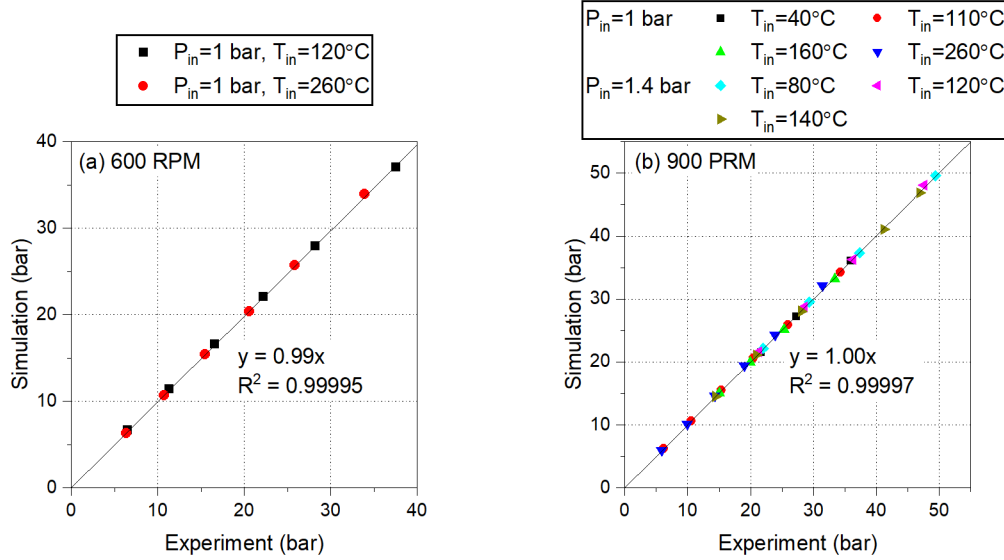
Figure 3.9: Correlation between measured and predicted peak cylinder pressure at motoring conditions. Experiment data at 900 RPM were from [68]. All simulation results were from this work.

In Figure 3.6, the CFD model over-predicted the peak cylinder pressure, likely because blow-by flow was not considered in the CFD simulation. In the multizone model, peak pressure prediction matched the measurement because the blow-by flow was "compensated" in heat loss calibration. This "compensation" might have induced an error in mass flow rate prediction. Yoo [68] reported that the blow-by flow rates measured in this motored engine showed a good agreement with calculations using the orifice flow equation from [66]. The calculated blow-by flow rate was 0.0008335 g/cycle at $600 RPM$, $P_{in} = 1 bar$, $T_{in} = 120°C$, and $CR = 6.0$, equal to 1.6% of the mass airflow rate measured at the test condition.

This multizone model is especially suitable for HCCI combustion, where the charge is homogeneous. In the model, thermal stratification was considered, but computa-

32

tional cost remained low. According to Kodavasal et al. [77], the multizone model was 100X faster than the CFD model. In this study, we were also able to use large chemical kinetic mechanisms containing 1000+ species and 5000+ reactions.

Chapter 4

Simulation of Pentane Isomers Autoignition in a Motored Engine

4.1 Introduction

Pentane isomers are components of gas turbine, gasoline, and diesel engine fuels, but they were less investigated than reference fuels n-heptane and iso-octane. They have long been fuels of interest in ignition studies due to their relative simplicity compared to longer alkanes. At the same time, a reactivity comparison of their variety of branched structures provides helpful information for studies of longer alkanes.

In previous pentane studies, ignition delay timings measured in a rapid compression machine (RCM) and a shock tube (ST) were widely used as prediction targets for mechanism validation and optimization. Cai and Pitsch [81] developed a rate rule optimization method, which was then applied to an n-pentane mechanism, incorporating low- to high-temperature ignition delay timings as prediction targets. Bugler et al. [11] updated species thermochemical properties, the C_0-C_4 sub-mechanism, and rate rules for pentane isomers oxidation and showed significantly improved accuracy of the mechanism in predicting the ignition delay timing. Wang and Sarathy [82] and Hansen et al. [83] found that the third O_2 addition was insignificant for n-pentane and neo-pentane ignition delay timing. Sudholt et al. [84] for the first time, measured

the ignition delay timing at very low temperatures (550 to $800K$) in a laminar flow reactor for n-pentane.

In addition to matching ignition delay timings, Cheng et al. [85] found that the mechanism from Bugler et al. [11] accurately predicted laminar flame speeds for n-pentane. Cheng [22] evaluated the same mechanism in an spark ignited (SI) engine, found that to reasonably predict the knocking onset for pentane isomers, the mechanism needs to reach higher accuracy, and suggested that adding the engine experiment as a constraint would reduce model uncertainty by 84%.

Speciation data are available for oxidation of pentane isomers in a jet stirred reactor (JSR). Rodriguez et al. [86] measured hydroperoxides in n-pentane oxidation. They found that the mechanism from Bugler et al. [11] gave a good prediction for pentyl-hydroperoxide but observed significant discrepancies for unsaturated peroxides. Bugler et al. [87] measured intermediate oxidation species during n-pentane oxidation and added reaction classes for C_5 aldehydes (pentanal and 2- and 3- pentanones). Bourgalais et al. [88] measured the low-temperature reaction products of n-pentane, found a higher formation of acetone and methyl ethyl ketone than the mechanism predicted, and found products not considered previously (methoxyacetylene, methyl vinyl ketone, and 2-furanone). Battin-Leclerc et al. [20] measured n-pentane low-temperature oxidation products at 585-665 K, confirming that the dominant ketohydroperoxide is 4-hydroperoxyl-pentan-2-one and observed species with a ketone and an enol function.

 Kang et al. [89] investigated the reactivity of three pentane isomers in a motored engine, which is a more complicated experiment but closely mimics real engines, and measured the detailed intermediate species. It was the first intermediate species measurement for all three pentane isomers. However, those informative data were not used for mechanism validation or improvement due to the lack of a simulation tool.

To fill this gap, we developed a multizone model from the AMECS model of Ko-

davasal et al. [77] and integrated it into GT-Power, to simulate the autoignition process in the modified CFR octane rating engine at the University of Michigan. The C_5 isomers mechanism of Bugler et al. [11] was selected for use in this study, as it was shown to be accurate for ignition delay timing and laminar flame speed prediction. Experiment data are from Kang et al. [89] , at an engine intake air pressure of 1 bar and an intake mixture temperature of 120℃, serving as a benchmark for the simulation of autoignition of n-pentane, iso-pentane, and neo-pentane in the motored engine.

4.2   Objectives

The objectives of this simulation work are

- to evaluate the effectiveness of the multizone model as a tool for mechanism validation,

- to improve the fundamental understanding of C_5 isomers autoignition chemistry and

- to provide detailed information for C_5 mechanism improvement

4.3   Results and discussion

4.3.1   Global reactivity

In the modified CFR octane rating engine experiment, CO concentration in the exhaust gas indicates reaction intensity and fuel oxidation stages [89]. While the engine compression ratio was gradually increased, fuel oxidation underwent three regimes which could be identified by CO production:

- Low-temperature oxidation (LTO) regime, including stages

(I) $<700K$ when barely any CO was produced, but initial fuel consumption began, a small amount of formaldehyde was formed and

(II) 700-800K when CO started to accumulate in the exhaust, indicating that the low-temperature oxidation intensified

- Negative temperature coefficients (NTC) regime, or

(III) 800-900K, when CO concentration leveled out, showing a slow-down of reaction and fuel consumption although the in-cylinder temperature was increased

- High-temperature oxidation (HTO) regime, including stage

(IV) 900-1200K, when CO concentration increased intensely, representing intensive reaction and fuel consumption, followed by

(V) $>1200K$, a sharp drop of CO concentration when CO was oxidized to CO_2, accompanied by intensive heat release and in-cylinder temperature rise

Figure 4.1 shows a prediction of CO emissions by the multizone model, compared to experimental data from Kang et al. [89], with an example of LTO, NTC, and HTO regimes for n-pentane autoignition.

In previous motored CFR engine experimental studies, the compression ratio at which CO emissions started to drop was defined as the critical compression ratio (CCR) [89]. CCR has been highly repeatable for specified fuels and is an effective fuel reactivity indicator. At an equivalence ratio of 0.25, CCR prediction was within 0.3 compression ratio (2.3% of measured CCRs) for pentane isomers, showing a high degree of consistency of both the engine model and the chemical kinetics mechanism.

Peak CO emission ($[CO]_{max}$) prediction was 14.2% of fuel carbon too high for n-pentane, 10.7% of fuel carbon too high for iso-pentane, and 11.5% of fuel carbon too high for neo-pentane. One reason for the higher $[CO]_{max}$ in the prediction than
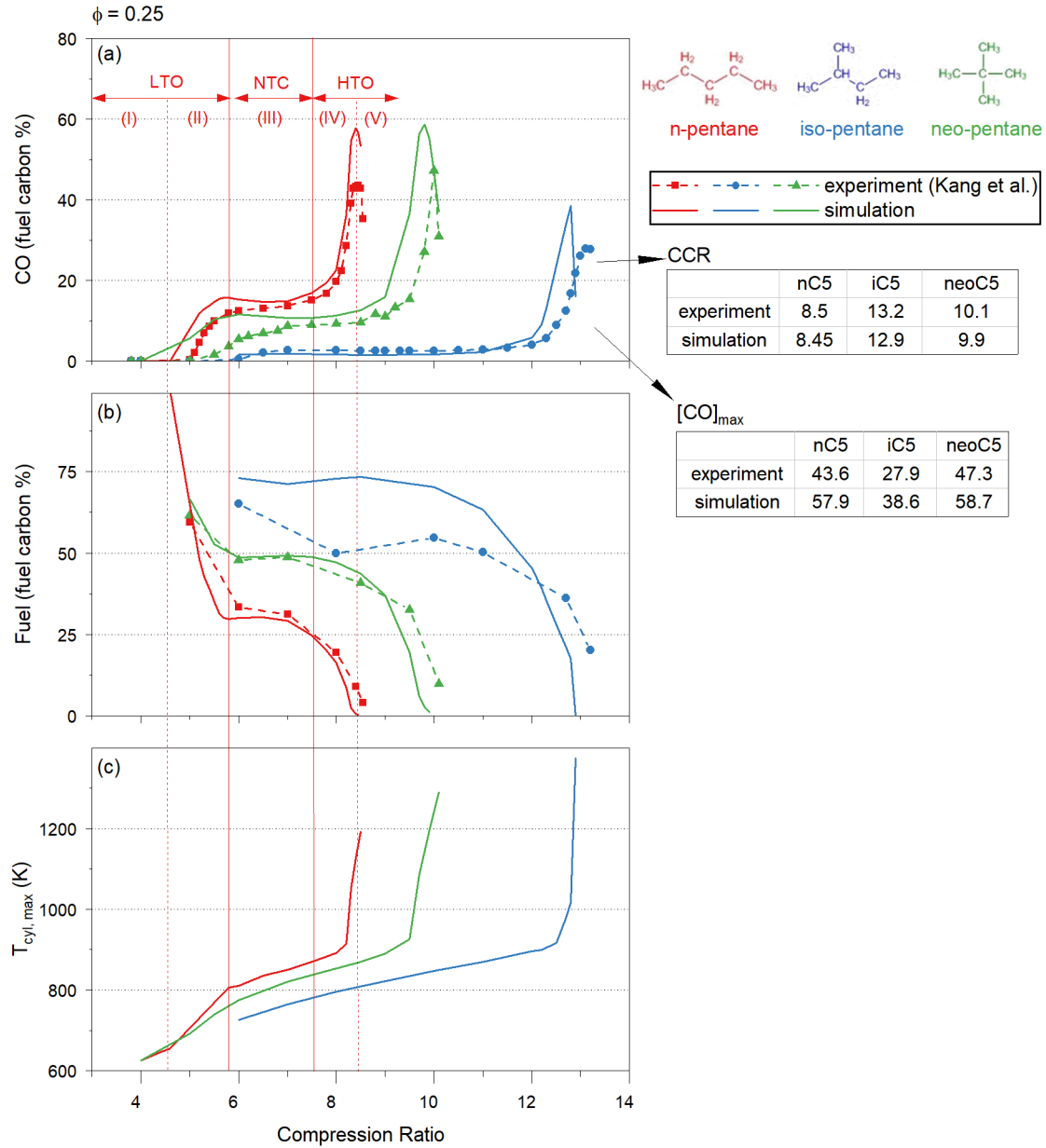
Figure 4.1: Autoigitnion of pentane isomers in a compression ratio (CR) sweep in the motored CFR engine

in the experiment is the experiment measurement limit. The emission bench used in the experiment had an upper limit of 14000 ppm, which is equivalent to 44% of fuel carbon, so the true $[CO]_{max}$ was above 44% of fuel carbon in n-pentane and neo-pentane oxidation. New experiments for n-heptane and n-dodecane in Chapter 5 show that $[CO]_{max}$ is around 50% of fuel carbon for n-alkanes. Another reason is

that fuel consumption in the simulation was more complete in HTO, probably due to simplified assumptions in the multizone model. In the experiment, there might be some inhomogeneity not considered in the simulation, including the crevice volume, that led to a small amount of unburned fuel in the exhaust gas.

Figure 4.1 (b) shows unreacted fuel concentration. The simulation effectively predicted fuel consumption at the early stage, with a 3.8% overprediction of fuel consumption for n-pentane and 5.2% for neo-pentane. A more significant discrepancy was observed for iso-pentane with a 32.2% underprediction of fuel consumption, showing that iso-pentane reactivity was underestimated at low to intermediate temperatures.
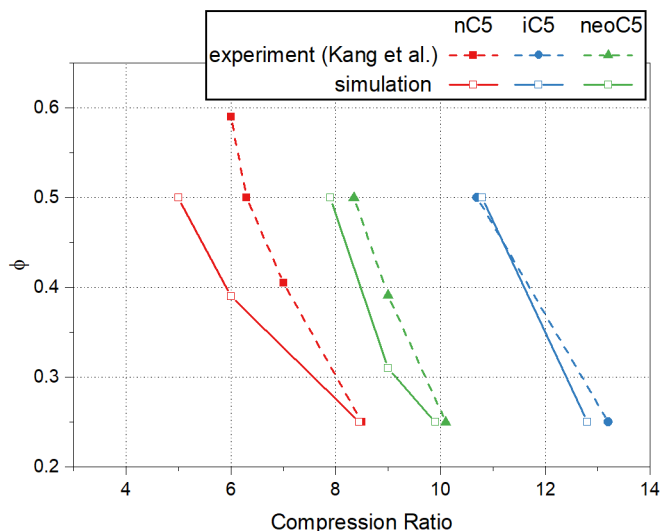
Figure 4.2: Critical equivalence ratios (CEQs) and critical compression ratios (CCRs) of the three pentane isomers

At extended test conditions, simulation was performed to evaluate the effectiveness of the multizone model and the mechanism. Figure 4.2 shows the predicted equivalence ratio and compression ratio, at which intensive heat release started to be observed and CO concentration dropped (i.e., CEQ and CCR). At $\phi = 0.25$, CCR was underpredicted for n-pentane and neo-pentane for < 0.3. This discrepancy was magnified to > 0.4 at $\phi = 0.50$. It is likely that at a higher equivalence ratio, inaccuracy

in the LTO mechanism would introduce a more significant temperature difference due to the increased amount of fuel and would be reflected in worse CCR prediction. It was in the opposite direction for iso-pentane as CCR prediction was improved as phi increased. This trend is because the LTO discrepancy is in the opposite direction for iso-pentane (i.e., underprediction).

4.3.2 Heat release analysis

Figure 4.3 shows the apparent heat release rate for pentane isomers at a compression ratio of 8.5 and at their respective CCRs.
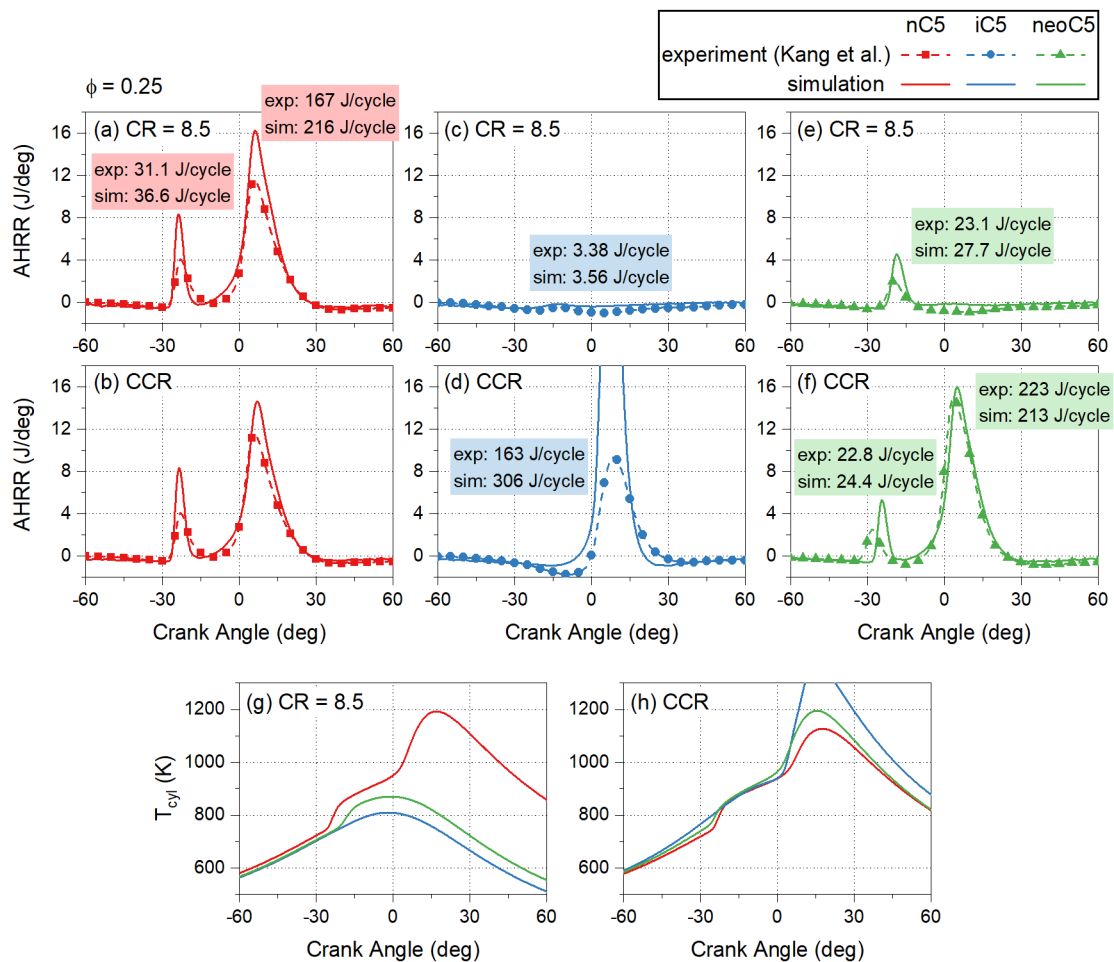
Figure 4.3: Apparent heat release rate (AHRR) and in-cylinder temperature of the pentane isomers autoignition in the motored engine

For n-pentane, at $CR = 8.5$, the timing of the low-temperature apparent heat release (LTHR) prediction was 3.1 $CA°$ late, and the amount was 8.9 J/cycle more. The high-temperature heat release (HTHR) prediction was 5.1 $CA°$ early and the amount was 50 J/cycle too high. The slight overprediction of HTHR and global reactivity might be a result of overestimated LTHR.

Although significant fuel consumption was observed at the early stage of iso-pentane oxidation, LTHR was not observed, either in simulation or experiment. At $CR = 8.5$, the predicted timing of HTHR was 4.1 $CA°$ early, and the amount was 0.23 J/cycle lower; while at CCR, predicted HTHR was 7.2 $CA°$ early, and the amount was twice the amount from the experiment.

For neo-pentane at CCR, the predicted timing of LTHR was 5.8 $CA°$ early, and the amount was 4.1 J/cycle lower, with HTHR only 0.3 $CA°$ late and the amount was 9.06 J/cycle higher than the experiment.

4.3.3 Intermediate species

Predicted intermediate species and concentrations were compared to measurement, together with reaction pathways analysis, to enable a more detailed evaluation of the mechanism.

4.3.3.1 Intermediate species during n-pentane oxidation

As shown in Figure 4.4, there are three different H atoms in an n-pentane molecule, hence three isomers of alkyl-peroxyl radicals, produced by O_2 addition to the fuel radicals at low and intermediate temperatures. In LTO, intramolecular isomerization via 6-membered TS rings and the second O_2 addition were the most important reactions for ignition delay timing prediction [11]. As temperature increases, flux shifts towards 5- and 7-membered TS rings, and more conjugate olefins and cyclic ethers are produced.

Figure 4.4: n-Pentane low- and intermediate-temperature oxidation pathways. Red arrows represent chain-propagating pathways producing conjugate olefins. Pink arrows represent chain-propagating pathways producing cyclic ethers. Blue arrows represent chain-propagating pathways involving the breaking of a C-C bond.
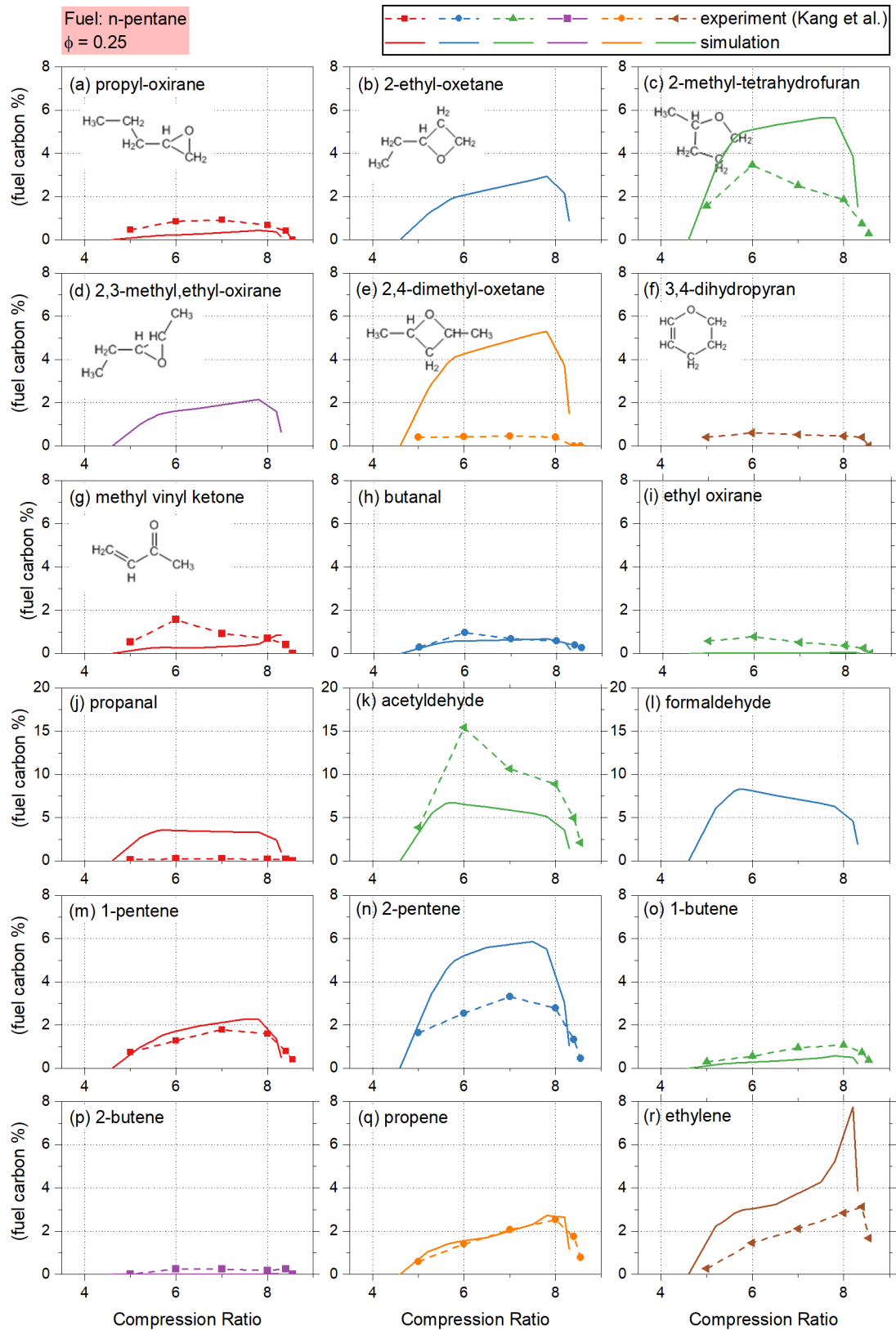
Figure 4.5: Species during n-pentane oxidation: (a-f) cyclic ethers, (g-i) other major oxygenates and (m-r) alkenes.

43
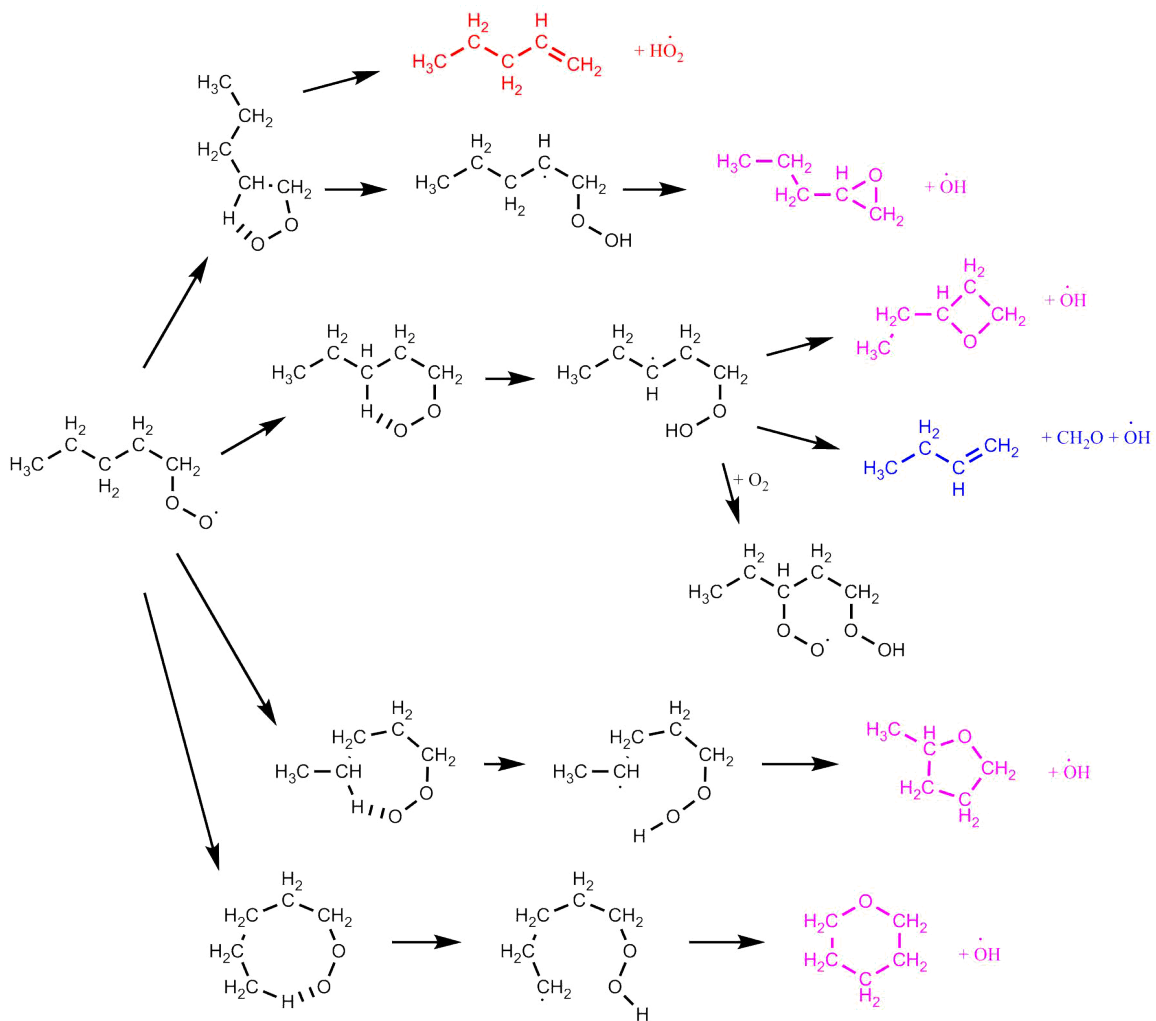
Figure 4.6: Intramolecular isomerization of a pentyl-peroxyl radical and the pathways producing cyclic ethers. Pink arrows represent chain-propagating pathways producing cyclic ethers. Blue arrows represent chain-propagating pathways involving the breaking of a C-C bond.

Figures 4.5 (a-f) show the cyclic ether concentrations. Among the cyclic ethers, the dominant product in the experiment was 2-methyl-tetrahydrofuran, which was overpredicted by the mechanism. 2,4-dimethyl-oxetane was predicted to be another dominant cyclic ether but the measured concentration was <0.5% of fuel carbon. 2-Ethyl-oxetane and 2,3-methyl,ethyl-oxirane were predicted to be >1.5% of fuel carbon but not detected in the experiment. In contrast, dihydropyran was not included in the mechanism but detected in the experiment. As shown in Figure 4.6, the formation of tetrahydro- and dihydro-pyran involves an 8-membered TS ring and might be worth adding to the mechanism.
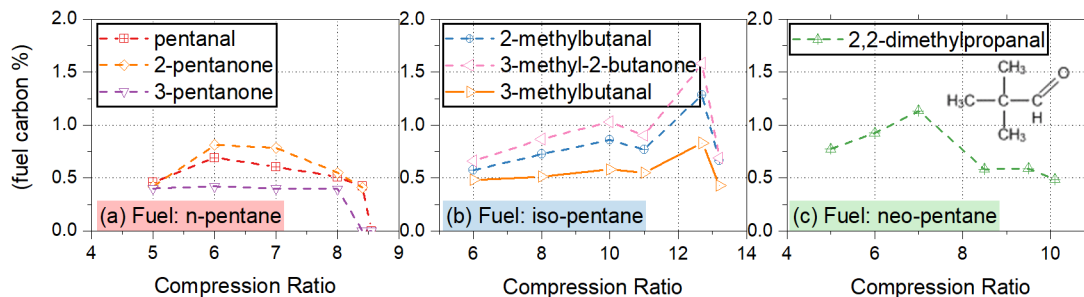
Figure 4.7: C$_5$ aldehyde concentrations replotted from Kang et al. [89].

C$_5$ aldehydes and ketones were not considered in the mechanism but detected in the experiment. Figure 4.7 shows C$_5$ aldehyde and ketone concentrations from Kang et al. [89]. Reactions are missed in the mechanism from alkyl-peroxyl radicals, possibly via 4-membered TS ring, to C$_5$ aldehydes and ketones, as shown in Figure 4.8. Those missing species would partially explain the overprediction of C$_5$ cyclic ethers during n-pentane and iso-pentane oxidation. Though Bugler et al. [87] suggested that a 4-membered TS ring is less likely to form due to a high energy barrier, their proposed pathways involved C$_5$ alcohol species that were not detected in the experiment. Furthermore, C$_5$ aldehydes and ketones are in one-to-one correspondence with the alkyl-peroxyl radicals, so they would be beneficial in evaluating the initial H-atom abstraction from different carbon atoms.
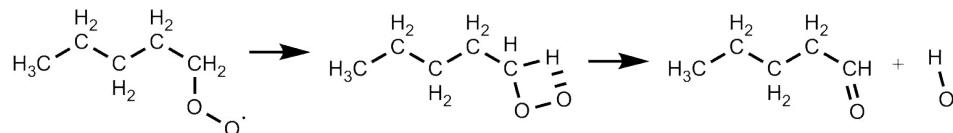
Figure 4.8: Formation of pentanal via a 4-membered TS ring.

Figures 4.5 (m-r) show the alkene concentrations. 2-Pentene and ethylene were significantly overpredicted. Competing reactions to the formation of C_5 cyclic ethers and 2-pentene are the formation of 6-membered TS rings, leading to the production of CO, formaldehyde, and acetaldehyde. Acetaldehyde was significantly underpredicted by the mechanism, as shown in Figure 4.5 (k). The underprediction of acetaldehyde and overprediction of 2-pentene and 2,3-methyl,ethyl-oxirane is consistent with the observation in a JSR (Bugler et al. [87]) at $10bar$, $800 - 900K$ and $\phi = 0.3$.

4.3.3.2 Intermediate species during iso-pentane oxidation

Figure 4.9 shows major species concentrations during iso-pentane oxidation. While four C_5 cyclic ether isomers were predicted to be >1% of fuel carbon, only one isomer, 3-methyl-tetrahydrofuran, which is also the only possible tetrahydrofuran, was detected in the experiment.

Three conjugate olefins could be produced, and all of the three isomers were detected in the experiment. As shown in Figure 4.11, in an iso-pentane molecule, there are four different H atoms, the abstraction of which could lead to the formation of four different fuel radicals. The flux analysis shows that at $600 - 800K$, most of the conjugate olefin isomers are produced following H-atom abstraction from the secondary and tertiary carbons. H-atom abstraction from the primary carbons does not significantly contribute to conjugate olefin production. From the flux analysis, 2-methyl-1-butene production is at a similar rate to 2-methyl-2-butene, both about twice of 3-methyl-1-butene. Same for the engine simulation results, which were fairly accurate for the other two conjugate olefins, but too high for 2-methyl-2-butene.

46
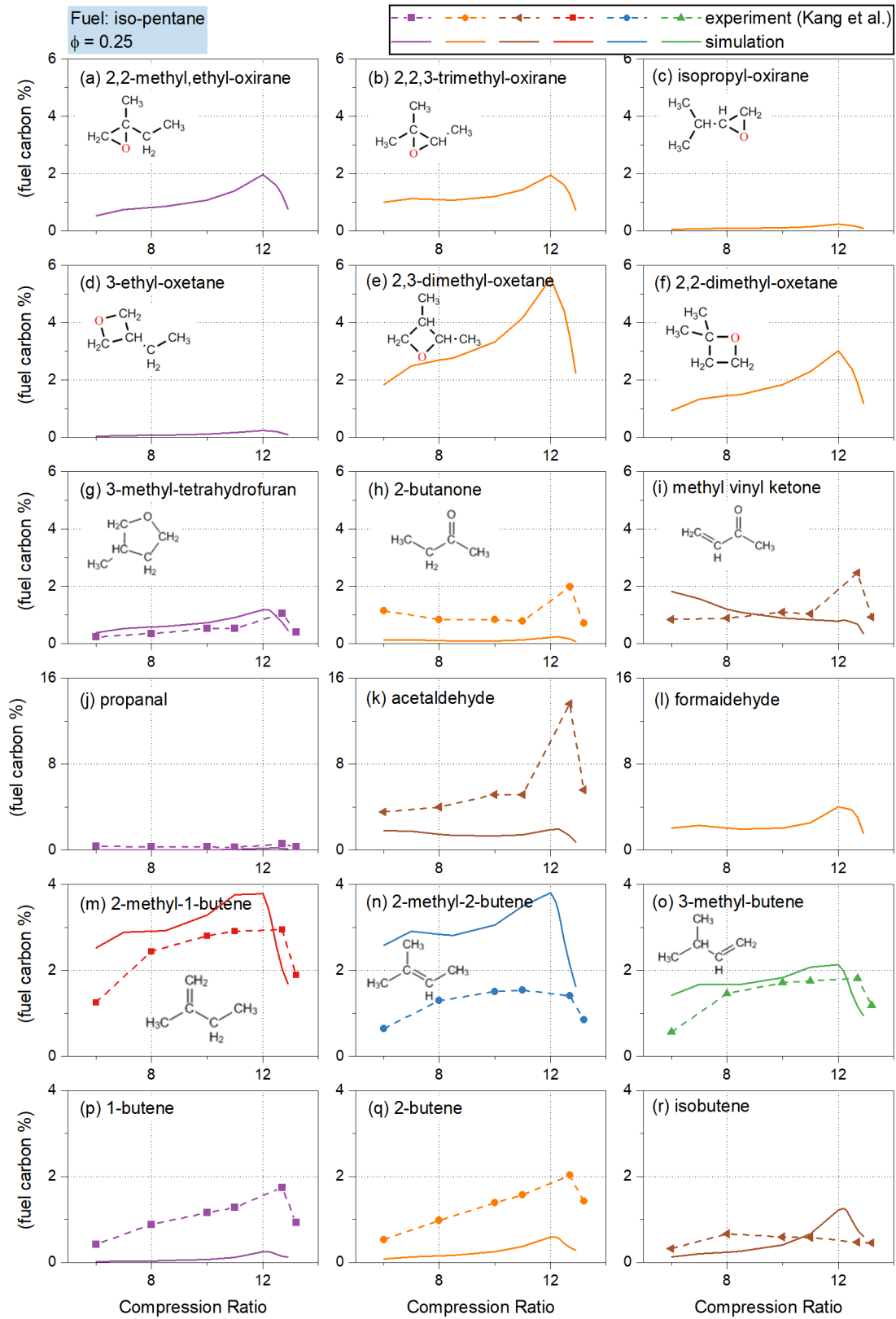
Figure 4.9: Species during iso-pentane oxidation.

47
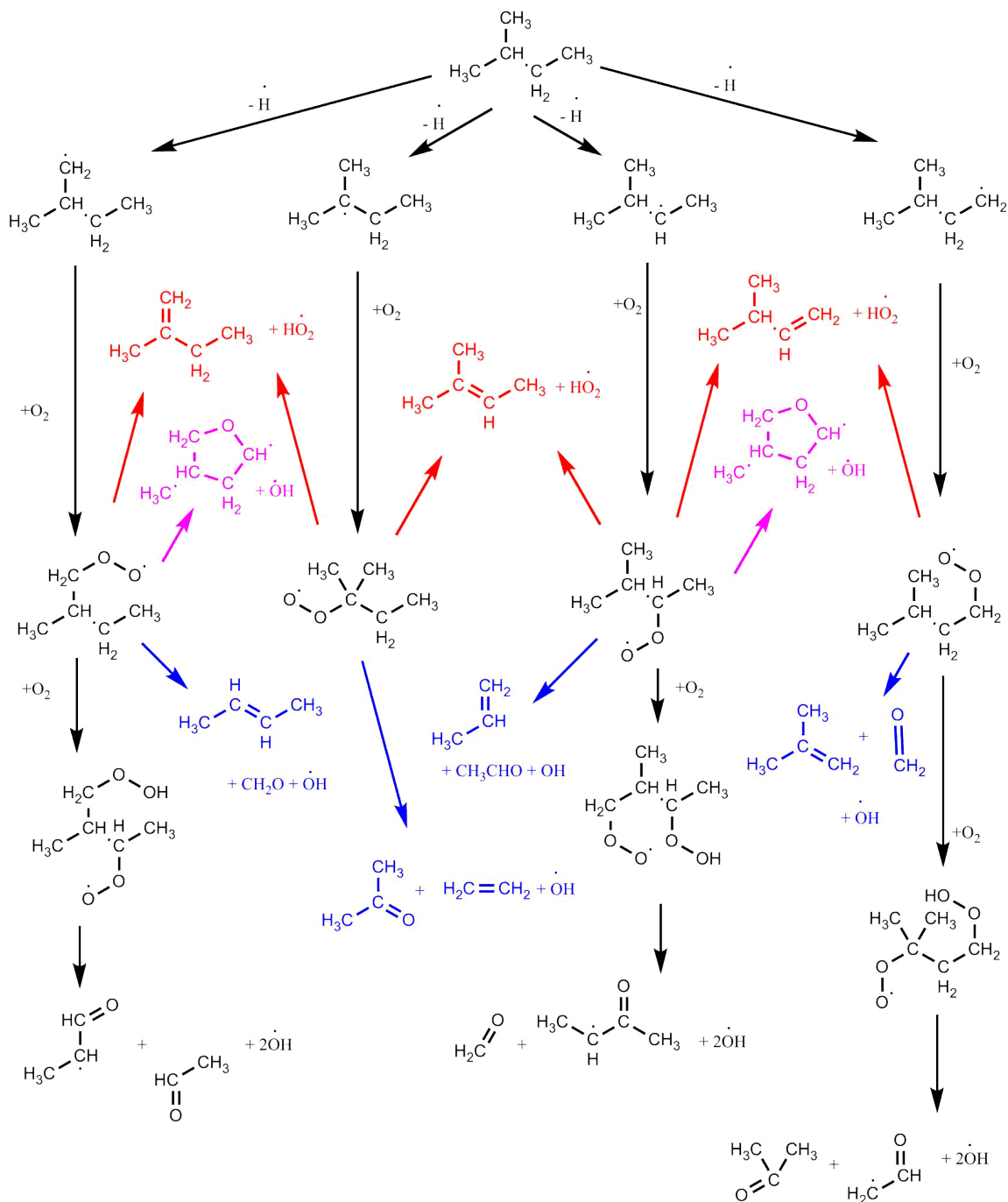
Figure 4.10: iso-Pentane low- and intermediate-temperature oxidation pathways. Red arrows represent chain-propagating pathways producing conjugate olefins. Pink arrows represent chain-propagating pathways producing cyclic ethers. Blue arrows represent chain-propagating pathways involving the breaking of a C-C bond.
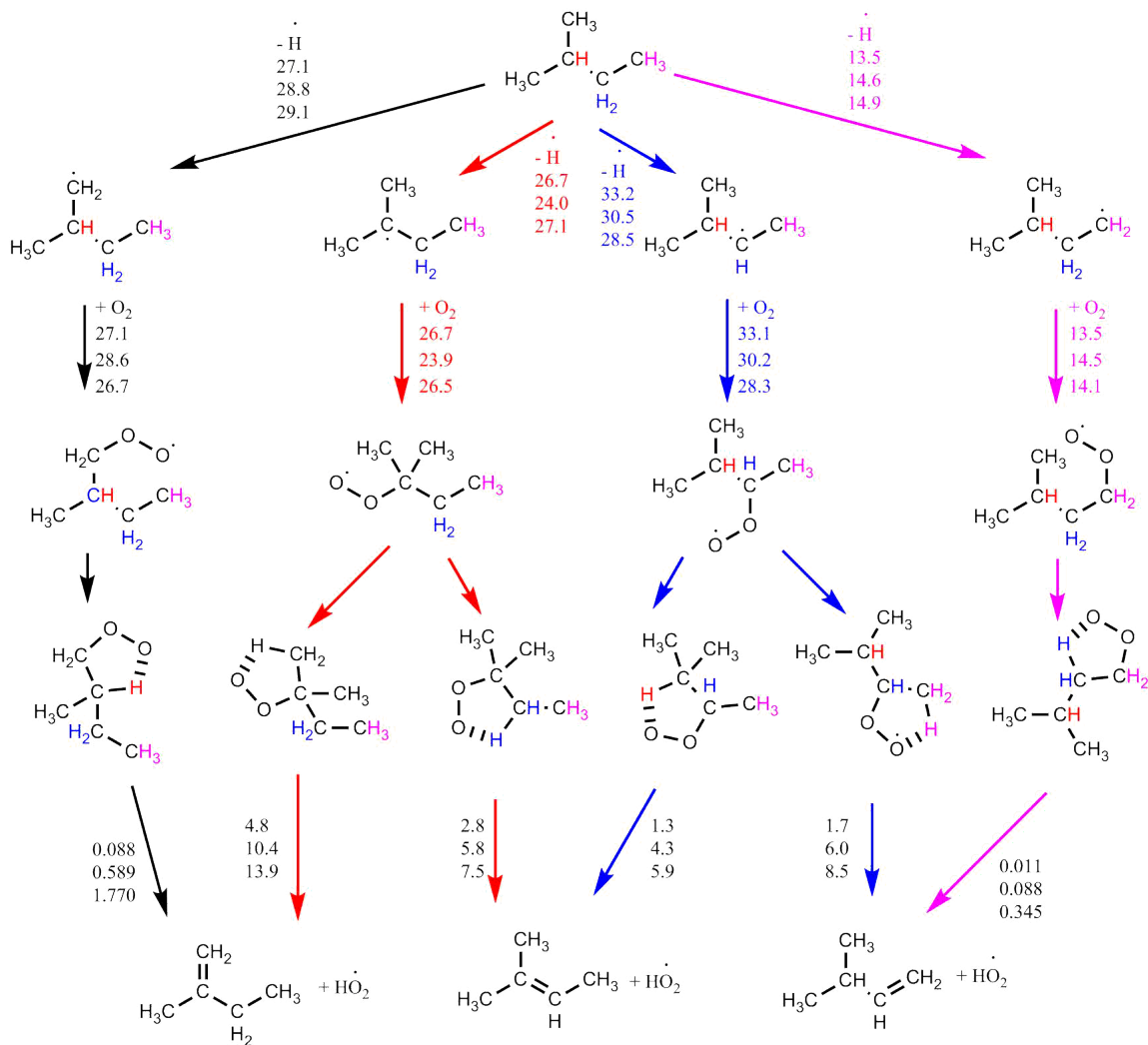
Figure 4.11: Conjugate olefin formation pathways during iso-pentane oxidation. Numbers are fluxess in % of fuel carbon, at $T = 600K$, $700K$ and $800K$, $P = 15$ bar, $\phi = 0.25$ and 20% fuel consumption. Flux analysis was performed in a closed homogeneous reactor in Cantera.

There is an interesting observation with this inaccurate simulation. There are 7 H atoms in a iso-pentane fuel molecule, that are related to production of 2-methyl-1-butene. 5 H atoms are related to 3-methyl-1-butene. The ratio of the concentrations of the two correspondent conjugate olefins were close to this ratio of available H atoms 7/5. Similarly, 3 H atoms are related to 2-methyl-2-butene formation, and the concentration of 2-methyl-2-butene was lower than 3-methyl-1-butene, but only slightly, because losing the H atom from the tertiary carbon is easier making 2-methyl-2-butene slightly easier to form. This comparison among the three conjugate olefin isomers shows that H availability might be a dominant factor in conjugate olefin production. How easy an H atom could be abstracted might be a secondary factor, but its importance was overestimated in the mechanism.

A major chain-branching product, acetaldehyde, was significantly underpredicted. It is worth mentioning that peak acetone prediction was over 2.0% of fuel carbon but acetone was not detected in the experiment. Figure 4.10 shows that acetone production follows the first or second O_2 addition to the tertiary carbon. Hence, these pathways are very unlikely and should be eliminated in the mechanism. These pathways being unlikely might be why branched alkanes are generally less reactive than normal alkanes. iso-Pentane is less reactive than neo-pentane, maybe also because there is no tertiary carbon in the neo-pentane molecule. There are no other data available in the literature for acetone production during iso-pentane oxidation. Hence, more species concentration measurements are necessary to confirm this observation and to support further improvement of the iso-pentane oxidation mechanism.

4.3.3.3 Intermediate species during neo-pentane oxidation

As shown in Figure 4.12, because all H atoms are identical in the neo-pentane molecule, only one type of alkyl-peroxyl radical is formed. The flux analysis shows that at 600-800K, the β-scission pathway is insignificant, and the first O_2 addition
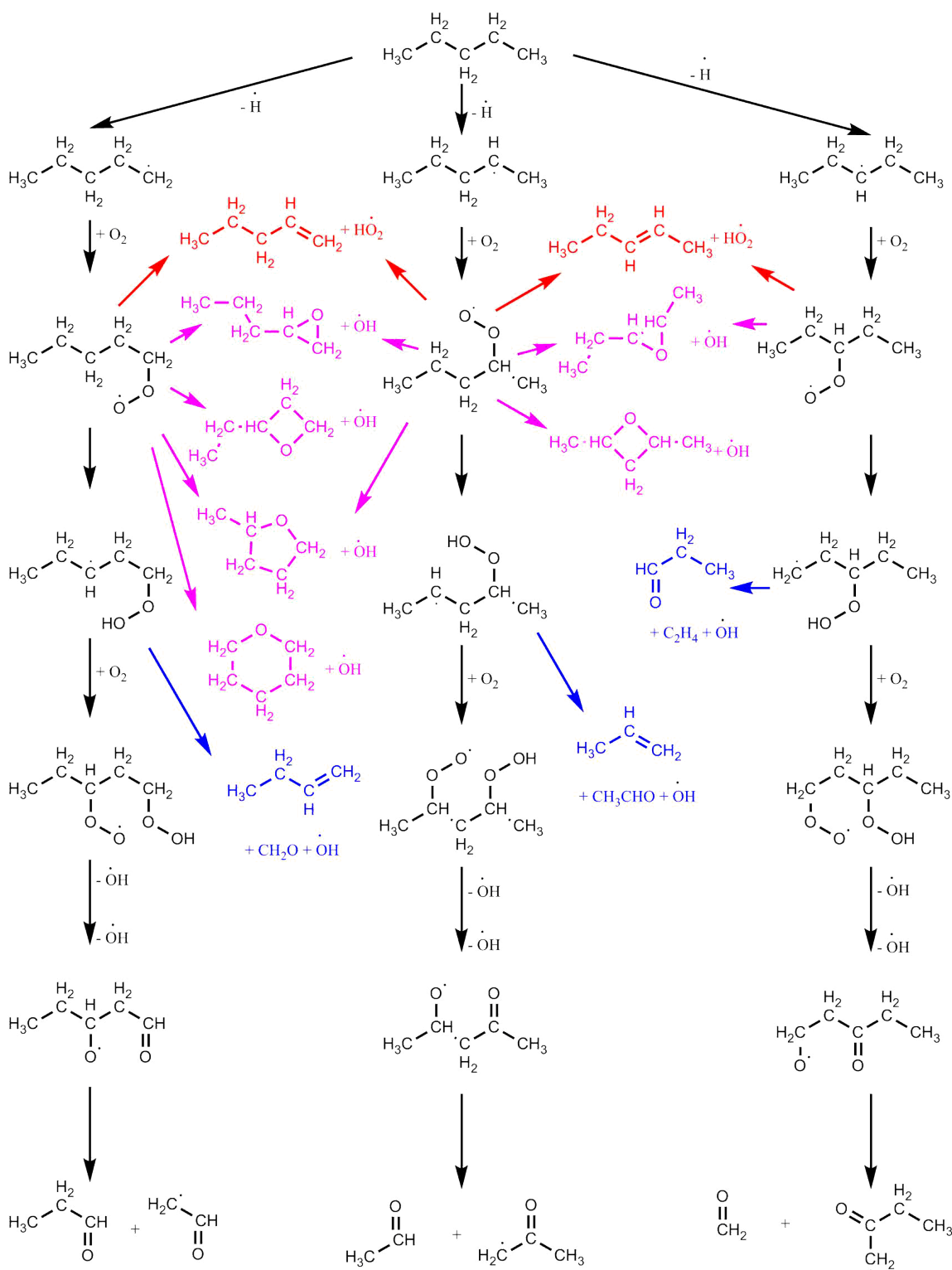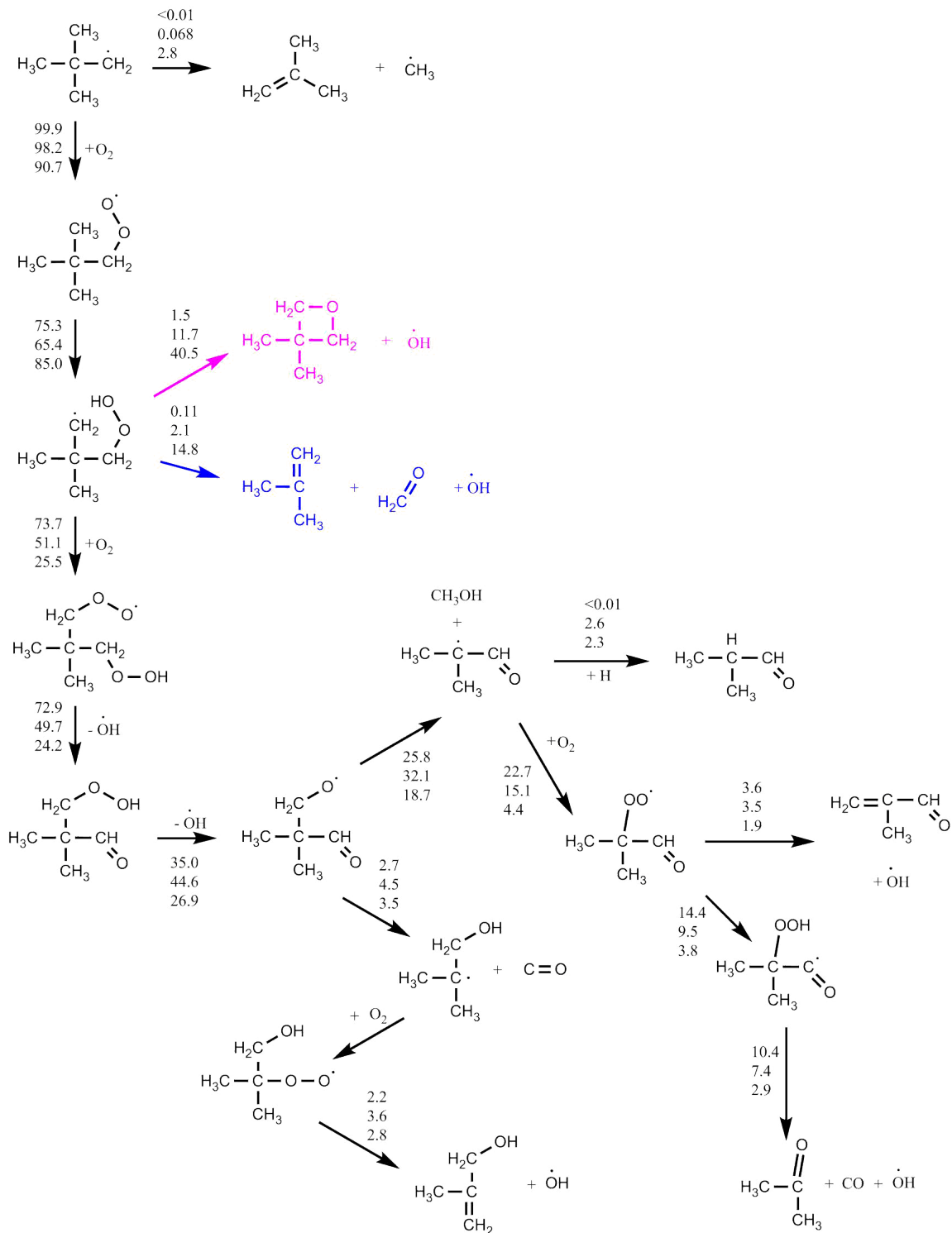
Figure 4.12: neo-Pentane low- and intermediate-temperature oxidation pathways. The pink arrow represent the chain-propagating pathway producing the cyclic ether. Numbers are fluxes in % of fuel carbon, at $T = 600K$, $700K$ and $800K$, $P = 15$ bar, $\phi = 0.25$ and 20% fuel consumption. Flux analysis was performed in a closed homogeneous reactor in Cantera.
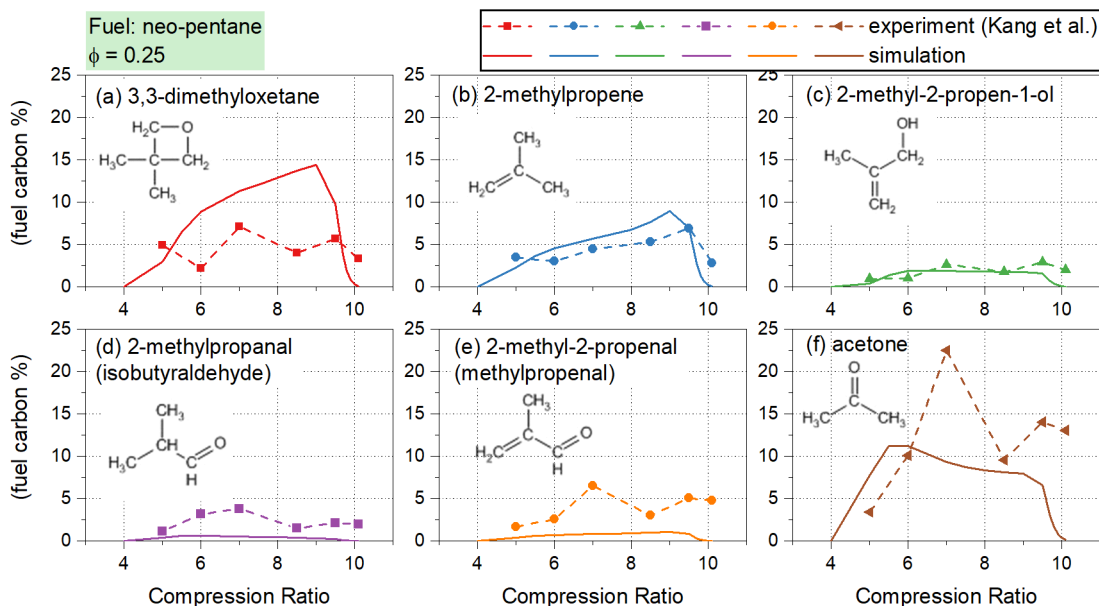
Figure 4.13: Species during iso-pentane oxidation.

is dominant. There is also only one way for the intramolecular isomerization of the alkyl-peroxy radical to the hydroperoxyl-alkyl radical. At 800K, flux analysis shows a 40% flux to the cyclic ether, a 14.8% flux to iso-butene, and a 25.5% flux undergoing the second O_2 addition. However, as shown in Figure 4.13, the only possible cyclic ether was overpredicted by the mechanism, while LTO chain-branching products 2-methylpropanal, 2-methyl-2-propenal, and acetone were underpredicted. Hence, pathways following the second O_2 addition need to be enhanced in the mechanism.

4.3.4 Intermediate species comparison for pentane isomers

Figure 4.14 shows the concentrations of conjugate olefins (iso-butene for neo-pentane), $C_5H_{10}O$ isomers (including cyclic ethers, aldehydes and ketones) and acetaldehyde (or acetone for neo-pentane) during oxidation of pentane isomers, to give a direct comparison for the reactivity of the pentane isomers.

Conjugate olefin concentrations during NTC seemed to be insensitive to the fuel structure. Conjugate olefin concentrations were around 5% of fuel carbon for all three

52
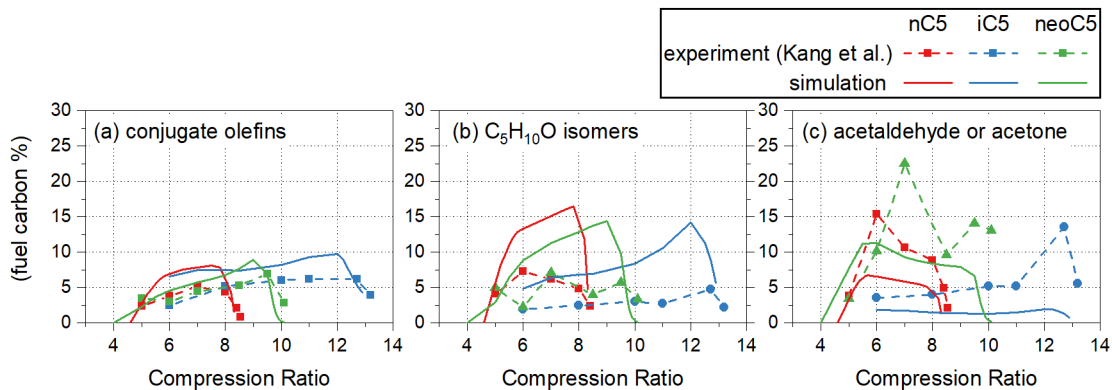
Figure 4.14: Species during iso-pentane oxidation.

pentane isomers. The mechanism successfully predicted this insensitivity. For another LTO chain-branching product group, $C_5H_{10}O$ isomers, concentrations during NTC seemed to be more sensitive to the fuel structure, with the least reactive iso-pentane having the lowest $C_5H_{10}O$ concentration during NTC. Bugler et al. [11] mentioned that the ignition delay timing is most sensitive to the reaction rate of cyclic ether formation following the second O_2 addition. This might also hold true for the first O_2 addition. Less cyclic ether formation might in turn weaken O_2 addition to the fuel radical, resulting in a lowered fuel reactivity. The difference in $C_5H_{10}O$ concentration was successfully predicted by the mechanism. This observation might also help in understanding the oxidation chemistry of larger branched alkanes.

Production of the LTO chain-branching products, acetaldehyde and acetone, was also sensitive to the fuel structure. In the experiment, the least reactive pentane isomer, iso-pentane produced the lowest acetaldehyde concentration. The mechanism captured this trend. However, significant underprediction of acetaldehyde was observed for n-pentane and iso-pentane, and acetone for neo-pentane, though the global reactivity prediction was accurate. This indicates that the ignition delay timing might not be very sensitive to reactions producing acetaldehyde.

4.4 Conclusions

In this study, the autoignition of pentane isomers in a motored engine was simulated using a multizone model. The model was an effective tool to validate an available chemical kinetics mechanism (Bugler et al. [11]), improve fundamental understanding of autoignition chemistry, and provide detailed information for mechanism improvement. The predicted global reactivity, fuel consumption, and heat release profiles were in excellent agreement with experiment data in Kang et al. [89]. At the same time, slight improvements could be made in the mechanism, as LTO was slightly overestimated for n-and neo-pentane and slightly underestimated for iso-pentane.

For all pentane isomers considered here, C_5 cyclic ethers were overpredicted. Conjugate olefins for n- and iso-pentane were slightly over-predicted. Low-temperature chain-branching products acetaldehyde (for n- and iso-pentane) and acetone (for neo-pentane) were underpredicted. Hence, cyclic ether production pathways could be weakened, and 4- and 8-membered TS ring pathways also need to be added to include missing species. Concerted elimination reaction rates need to be improved. Second O_2 addition pathways could be enhanced. Specifically for iso-pentane, chain-branching pathways following first and second O_2 addition to the tertiary carbon were also found to be unlikely.

In a comparison of the three pentane isomers, conjugate olefin production was found to be insensitive to the fuel structure. $C_5H_{10}O$ and acetaldehyde/acetone formation is sensitive to the fuel structure, with the least reactive pentane isomer, iso-pentane producing the least $C_5H_{10}O$ and acetaldehyde. The mechanism successfully predicted these trends.

Chapter 5

Autoignition of n-Heptane and n-Dodecane in a Motored Engine: Experiment and Simulation

5.1 Introduction

A major motivation for this thesis was to investigate the autoignition behavior of the UM3 jet fuel surrogate, of which n-dodecane is a major component, making up 40.84% volume fraction or 52.01% of the fuel carbon of the UM3 Jet-A surrogate. To better understand n-dodecane oxidation, we investigated the autoignition of n-dodecane together with another normal alkane with a shorter chain length, n-heptane, in the motored engine via coupled experiment and simulation.

Like n-dodecane, there has been a continuing effort to develop a reliable n-heptane oxidation mechanism in the research community. Lu and Law [90] developed a 188-species skeletal mechanism of n-heptane oxidation from a detailed 561-species mechanism (Curran et al. [46]), using the temperature profile in a perfectly stirred reactor (PSR), the ignition delay timing and JSR species concentrations as prediction targets. Seidel et al. [91] constructed a 360-species n-heptane mechanism based on their temperature and species measurement in a fuel-rich low-pressure laminar flat premixed flame. Zhang et al. [92] developed a detailed mechanism based on the AramcoMech 2.0 C_0-C_4 submechanism and rate rules from the pentane isomers mechanism

in Bugler et al. [11]. This detailed mechanism showed a generally good agreement with the species concentration measurement in a JSR, except for underpredicted reactivity at $\phi = 0.25$ and around $750K$.

Existing n-heptane mechanisms have also been widely evaluated in experiments and simulations of fundamental combustion facilities. Rodriguez et al. [19] measured hydroperoxides during n-heptane oxidation in a JSR and found that unsaturated hydroperoxide production pathways needed improvement in the Zhang et al. [92] mechanism. Ferris et al. [93] measured n-heptane oxidation intermediates in a shock tube at $4.9atm$ and $760K$, modified the LLNL mechanism (Mehl et al. [94]) by lowering the rate of heptyl-peroxy isomerization reactions, and achieved improved prediction for n-heptane, C_2H_4, C_3H_6, CO, and H_2 prediction. Sarathy et al. [95] found 3-stage ignition behavior in the n-heptane ignition prediction using the Zhang et al. [92] mechanism at lean ($\phi = 0.3$) and high-pressure ($40atm$) conditions. They found that in addition to $H + O_2 \, (+M) = HO_2 \, (+M)$ reaction, $OH + HO_2 <=> H_2O + O_2$ reaction might also be important in n-heptane high-pressure lean combustion. He et al. [96] measured the temperature and CO concentration in a high-pressure shock tube and found that the Zhang et al. [92] mechanism predicted too fast a rise in temperature and CO concentration.

Despite the inaccuracy found with these mechanism reaction rates, Wang et al. [21] suggested that even for one of the most common reference fuels, n-heptane, new species were still being discovered that are not considered in existing mechanisms, based on their species measurements in a JSR and a motored engine. Herbinet et al. [97] found that dione species formation was significantly enhanced at 10 bar in a JSR than at lower pressures. Belhadj et al. [98] also measured the highly oxygenated molecules not included in the existing mechanism during n-heptane oxidation in a JSR at $10atm$, $580 - 790K$, and $\phi = 0.5$. They recommended RCM and IC engine experiments to further investigate the importance of those newly observed species in

n-heptane LTO.

In this study, we evaluated the performance of three n-heptane mechanisms and three n-dodecane mechanisms listed in Table 5.1 in coupled experiments and simulation of the motored engine.

Fuel	Mechanism	Number of Species	Number of Reactions
n-Heptane	Lu and Law [90]	188	842
	Seidel et al. [91]	349	3686
	Zhang et al. [92]	1268	5336
n-Dodecane	SKE360 [9]	360	1851
	Narayanaswamy et al. [99]	255	2289
	Mao et al. [29]	737	3629

Table 5.1: n-heptane and n-dodecane mechanisms evaluated in this study.

5.2 Test conditions

n-Heptane engine experiment was performed at an intake temperature of 120℃, the same as that of the pentane isomers in Kang et al. [89] n-Dodecane engine experiment was performed at an intake temperature of 260℃, to fully vaporize n-dodecane, and also to be consistent with the engine experiment for other pure components and the mixture of UM3 jet fuel surrogates. Consequently, even at the lowest compression ratio (CR), a significant amount of n-dodecane was oxidized. However, there was still space from the starting compression ratio to the critical compression ratio (CCR), so our method effectively evaluated n-dodecane reactivity and mechanism accuracy.

Details of the test conditions are listed in Table 5.2.

Fuel	n-Heptane	n-Dodecane
Boiling Point	98.4℃	216.2℃
Engine Intake Pressure	1 bar	1 bar
Engine Intake Temperature	120℃	260℃
Engine Compression Ratio (CR)	4-7.2	4-5.1
Equivalence Ratio (ϕ)	0.25	0.25
Peak Cylinder Pressure	6.5-20.5 bar	7.2-12.3 bar
Peak Cylinder Temperature	$623 - 1358K$	$814 - 1453K$

Table 5.2: Test conditions for n-heptane and n-dodecane autoignition studies in the motored engine.

5.3 Global reactivity

Figures 5.1 shows the CO concentration ([CO]), unreacted fuel concentration, and simulated peak cylinder temperature during n-heptane and n-dodecane autoignition in the motored engine. Both fuels are known for strong LTO and NTC behaviors, which were captured in this experiment too.

For n-heptane global reactivity, both the Lu and Law [90] and the Seidel et al. [91] mechanisms predicted late CCRs, indicating an overall underestimation of n-heptane reactivity. CCR prediction from the Zhang et al. [92] mechanism was not obtained due to a precision problem in the simulation.

The Seidel et al. [91] mechanisms showed a lower [CO] during NTC, indicating an underestimated LTO, and a lower peak [CO], which might be a result of lower NTC [CO]. The Lu and Law [90] and the Zhang et al. [92] mechanisms were very accurate for [CO] during NTC (at $CR = 5.0 - 6.5$). The Lu and Law [90] mechanism also provided a reasonably precise peak [CO] prediction.

Interestingly, for the two mechanisms predicting similar [CO] during NTC, their predictions for the peak cylinder temperature were also close in that regime. The Seidel et al. [91] mechanism underpredicted [CO] during NTC by around 6% of fuel
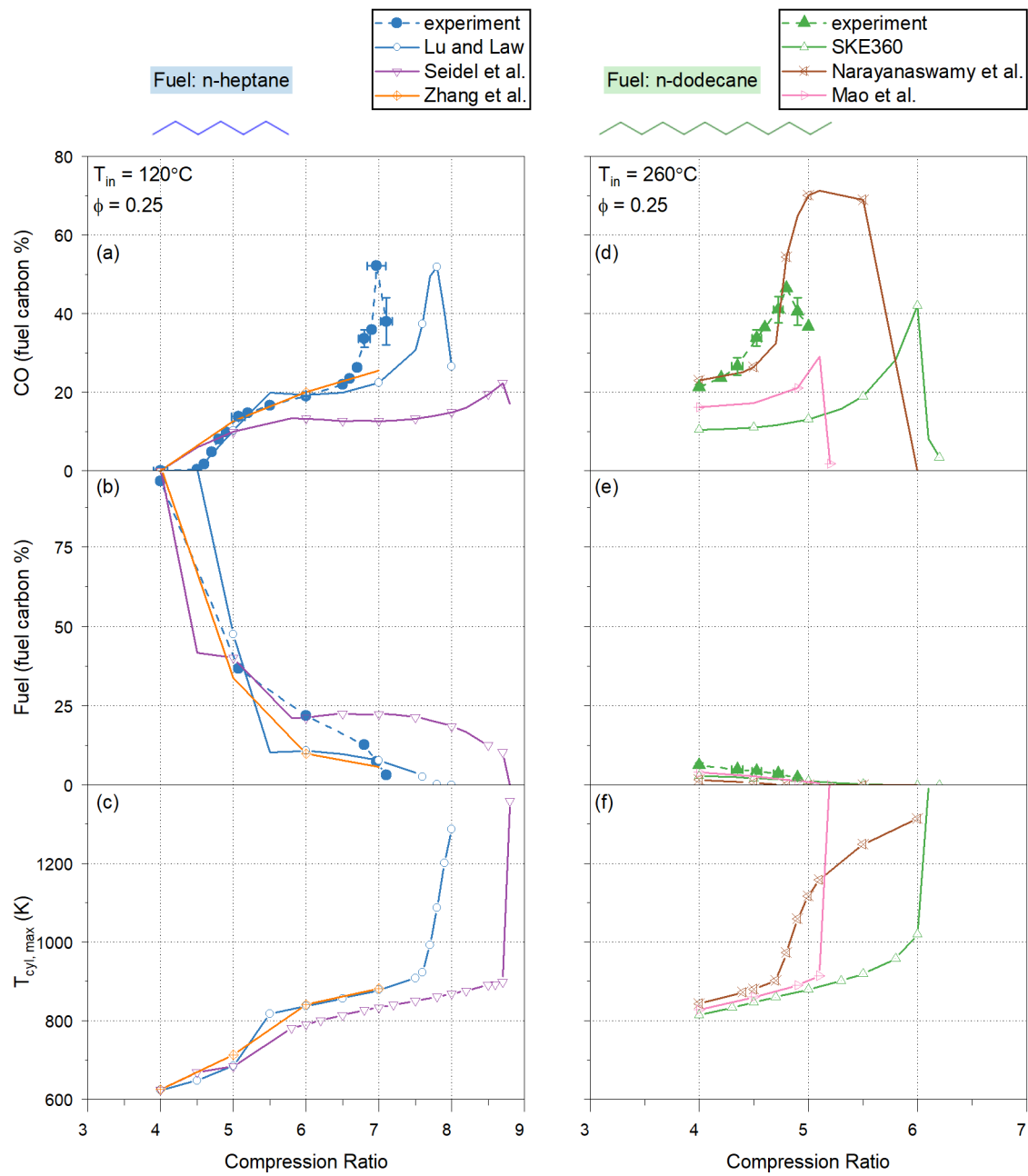
Figure 5.1: Autoignitoin of n-heptane and n-dodecane in the motored engine, (a),(c),(e) at 120℃, (b),(d),(f) at 260℃.

carbon (equal to about 2400 ppm). At the same time, the Seidel et al. [91] mechanism underpredicted the peak cylinder temperature by around 50 K. The Lu and Law [90] and the Zhang et al. [92] mechanisms also gave very accurate predictions of the amount of LTHR, as shown in Table 5.3. This comparison indicates that [CO] during NTC, in-cylinder temperature, and the amount of LTHR are strongly correlated, all being indicators of LTO intensity. Among those three parameters, [CO] might be the best prediction target for future LTO mechanism development and validation.

	CCR	$[CO]_{max}$	[CO] at $CR = 6.0$	$T_{cyl,max}$ at $CR = 6.0$	LTHR at $CR = 6.0$
unit		fuel carbon %	fuel carbon %	K	J/cycle
Experiment	7.1 ± 0.08	52.1	19.0	-	66.54 ± 4.33
Lu and Law [90]	7.9	51.9	19.2	838	64.6
Seidel et al. [91]	8.8	22.3	13.23	791	42.9
Zhang et al. [92]	-	-	20.03	841	61.6

Table 5.3: Critical compression ratio (CCR), CO concentration ([CO]), maximum cylinder temperature, and the amount low-temperature heat release (LTHR) of n-heptane autoignition in the motored engine.

For the Lu and Law [90] mechanism, [CO] prediction was accurate during LTO and NTC, until transitioning from NTC to HTO, at $CR = 6.5 - 7.0$ and peak cylinder temperatures of $850 - 900K$. This transition is usually controlled by HO_2 radical reactivity. Sensitivity analysis in Zhang et al. [92] for their n-pentane mechanism showed that the ignition delay timing at both $820K$ and $1000K$ is sensitive to two reactions:

$$HO_2 + HO_2 \Leftrightarrow H_2O_2 + O_2 \qquad (5.1)$$

$$H_2O_2\,(+M) \Leftrightarrow OH + OH\,(+M) \qquad (5.2)$$
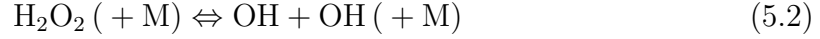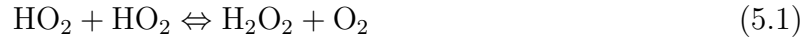
Figure 5.2 shows the reaction rates of the two reactions and their reverse reactions at 15 bar. At $850 - 900K$, the Lu and Law [90] mechanism has higher rate constants for $HO_2 + HO_2 \Rightarrow H_2O_2 + O_2$ and $OH + OH\,(+M) \Rightarrow H_2O_2\,(+M)$, both weakening the reactivity of the mixture and increasing the ignition delay timing.
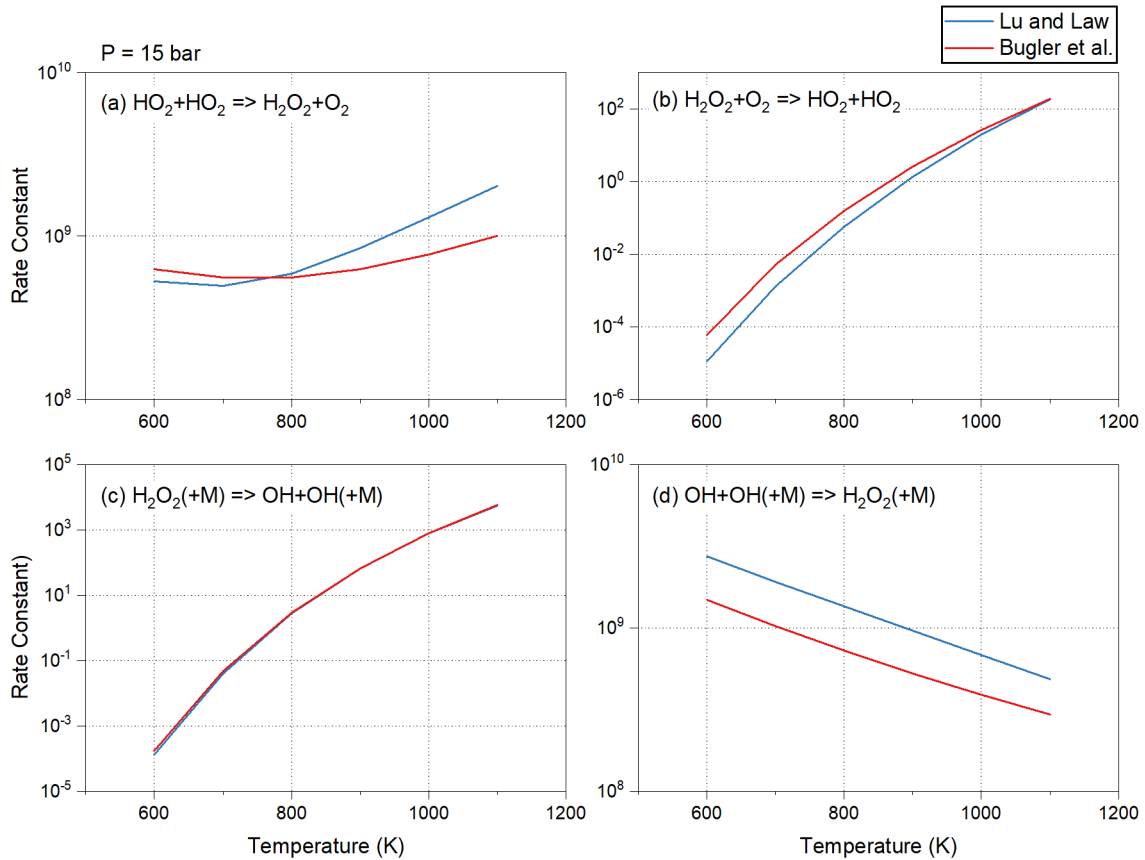
Figure 5.2: Key reactions in the transition from negative temperature coefficient (NTC) regime to high-temperature oxidation (HTO) regime.

Another way to improve the Lu and Law [90] mechanism is to slightly increase the amount of LTHR to compensate for somehow underestimated LTO reactivity. In

the n-pentane simulation in Chapter 4, the amount of LTHR was overpredicted by 8.9 J/cycle but CCR prediction was very accurate.

Because the Bugler et al. [11] n-pentane mechanism has shown excellent CO and CCR prediction in Chapter 4, we replaced the H_2/O_2 and CO submechanisms and common species' thermochemical properties in the Lu and Law [90] mechanism, with those from Bugler et al. [11] The new [CO] and CCR prediction in Figure 5.3 showed significant improvement, though the timing of LTHR was slightly late.

n-Dodecane results were similar to the n-heptane results. First, for the three n-dodecane mechanisms, all three predicted CCRs were late, showing an overall underestimation of n-dodecane reactivity. The Mao et al. [29] mechanism gave the most accurate CCR prediction among the three mechanisms. SKE360 [9] gave the best $[CO]_{max}$ prediction and the Narayanaswamy et al. [33] mechanism gave the best [CO] prediction during NTC and early HTO, and the highest prediction of the amount of LTHR.

	CCR	$[CO]_{max}$	[CO] at $CR = 4.0$	$T_{cyl,max}$ at $CR = 4.0$	LTHR at $CR = 4.0$
		fuel carbon %	fuel carbon %	K	J/cycle
Experiment	4.9	43.9	21.3	-	60.0 ± 2.7
SKE360 [9]	6.1	42.0	10.4	814	35.1
Narayanaswamy et al. [99]	5.5	71.4	22.8	844	44.5
Mao et al. [29]	5.2	29.1	16.2	828	39.0

Table 5.4: Critical compression ratio (CCR), CO concentration ([CO]), maximum cylinder temperature, and the amount low-temperature heat release (LTHR) of n-dodecane autoignition in the motored engine.

Predicted [CO] from the Narayanaswamy et al. [33] mechanism was fairly accurate during NTC and at the beginning of HTO, indicating that LTO reactivity was
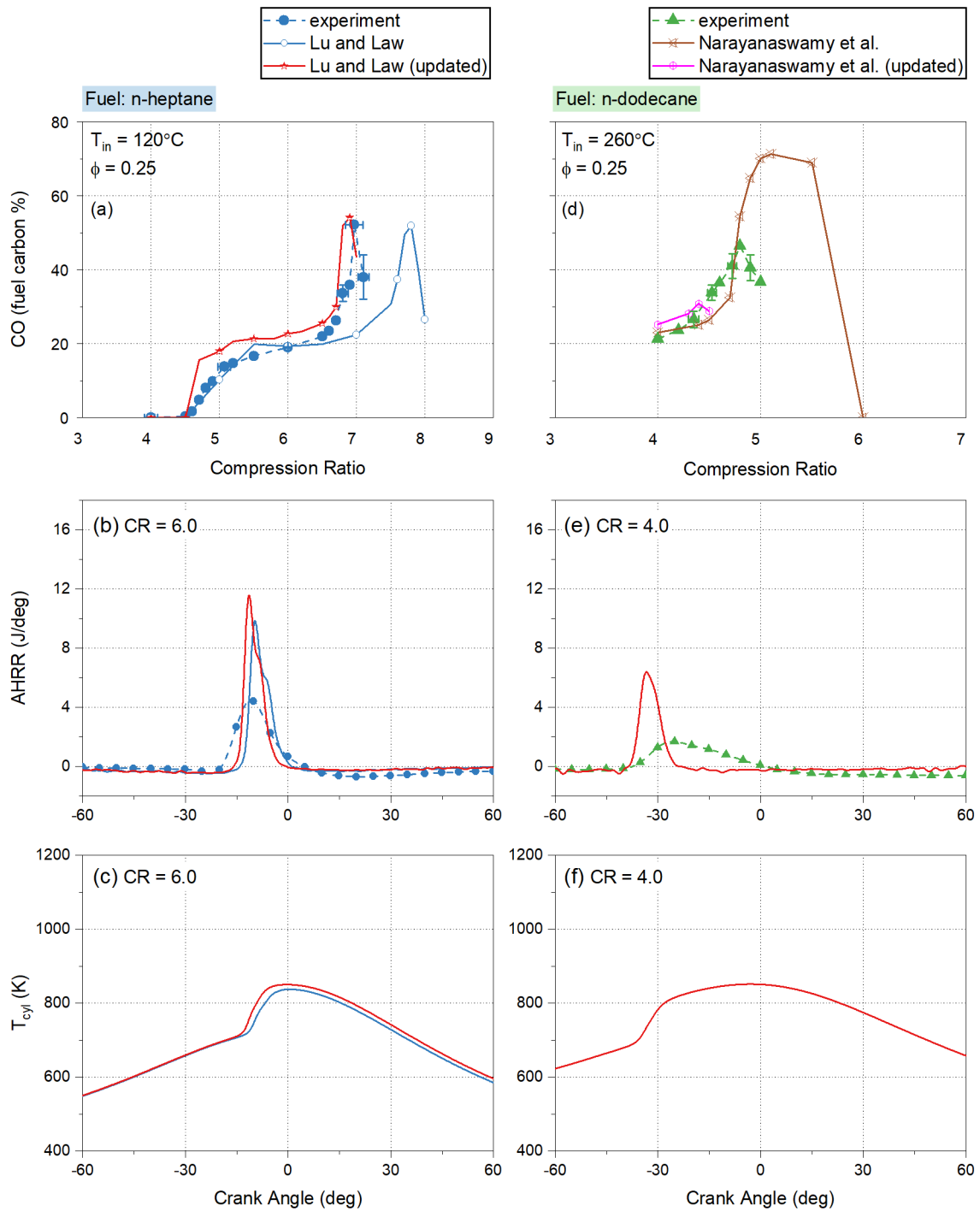
Figure 5.3: Predicted autoignition of n-heptane and n-dodecane by the updated mechanisms.

accurate in this mechanism at $CR = 4.0 - 4.8$ and a peak cylinder temperature of $850 - 1050K$. However, [CO] accumulated to an unreasonable 71.36% of fuel carbon and was slowly oxidized with increasing CR. Peak in-cylinder temperature also increased slowly during HTO, which contradicts observations in the experiment and other mechanisms. This indicates that the Narayanaswamy et al. [33] mechanism needs major improvements for reactions that are important in HTO at temperatures $> 1050K$. Sensitivity analysis for n-pentane and n-heptane ignition delay timing in Bugler et al. [11] and Zhang et al. [92] showed that at high temperatures, the ignition delay timing is sensitive to the β-scission reactions of the fuel molecule and these C_1 and H_2/O_2 reactions:

$$CH_3 + HO_2 \Leftrightarrow CH_4 + O_2 \tag{5.3}$$

$$HO_2 + HO_2 \Leftrightarrow H_2O_2 + O_2 \tag{5.4}$$

$$H_2O_2 \, (+M) \Leftrightarrow H + OH \, (+M) \tag{5.5}$$

$$CH_3 + HO_2 \Leftrightarrow CH_3O + OH \tag{5.6}$$

$$H + O_2 \Leftrightarrow O + OH \tag{5.7}$$
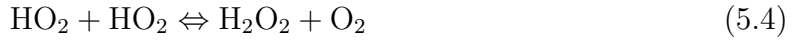
Figure 5.4 shows the reaction rates for the listed reactions, 5.3 - 5.7. For the two $CH_3 + HO_2$ reactions, it's difficult to tell the combined influence of the discrepancies in both reactions. For $HO_2 + HO_2 \Leftrightarrow H_2O_2 + O_2$, the Narayanaswamy et al. [33] mechanism shows a higher rate constant at temperatures $> 800K$, which leads to longer ignition delay timings in this temperature range. Because the C_0-C_1 submechanism sizes are comparable in the two mechanisms, we replaced the C_0-C_1 submechanism, and the thermochemical properties of common species in the Narayanaswamy et al. [33] mechanism with the data in Bugler et al. [11] Figure 5.3 shows the result of the updated mechanism. While no significant differences were observed in
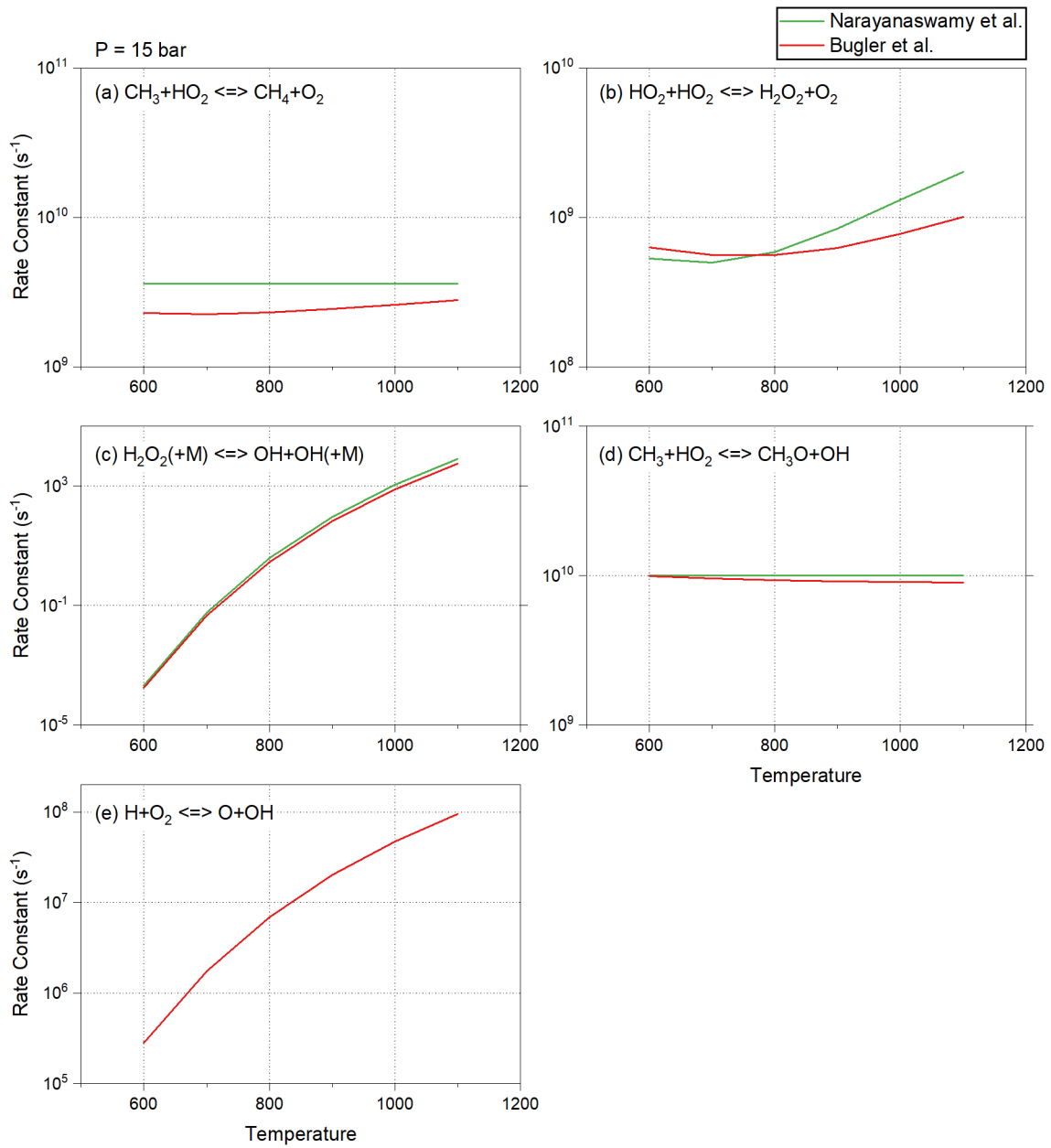
Figure 5.4: Key reaction in high-temperature oxidation (HTO) regime.

the heat release profile or in-cylinder temperature prediction, CCR prediction was too early by the updated mechanism, likely due to overtuned LTO reactions in the original Narayanaswamy et al. [33] mechanism.

5.4 Heat release analysis

Figure 5.5 shows the apparent heat release rate (AHRR) from experiment and simulation and the in-cylinder temperature from simulation. For n-heptane at $CR = 6.0$, the predicted timings of LTHR from all three mechanisms were late. The Zhang et al. [92] mechanism gave the most accurate predicted timing of LTHR among the three n-heptane mechanisms, but a too high and narrow LTHR curve. Similarly, for n-dodecane at $CR = 4.0$, the original and updated Narayanaswamy et al. [33] mechanisms gave accurate predictions for the timing of LTHR, but too sharp and narrow predicted LTHR curves. The Mao et al. [29] mechanism and SKE360 gave too late predictions for the timing of LTHR.

For the in-cylinder temperature of n-heptane and n-dodecane, predictions of different mechanisms started from the motoring temperature and deviated from the motoring temperature at around $700K$ after the onset of LTO.

5.5 Intermediate species

5.5.1 Low-to-intermediate temperature chain-propagating products: conjugate olefins and cyclic ethers

Figure 5.6 shows the conjugate olefin, cyclic ether isomer, and acetaldehyde concentrations. During n-heptane oxidation, predictions for the C_7H_{14} isomer concentration from all three mechanisms were fairly accurate. For $C_7H_{14}O$ isomers, the Lu and Law [90] and the Zhang et al. [92] mechanisms overpredicted the concentration, while the Seidel et al. [91] mechanism slightly underpredicted the concentration.
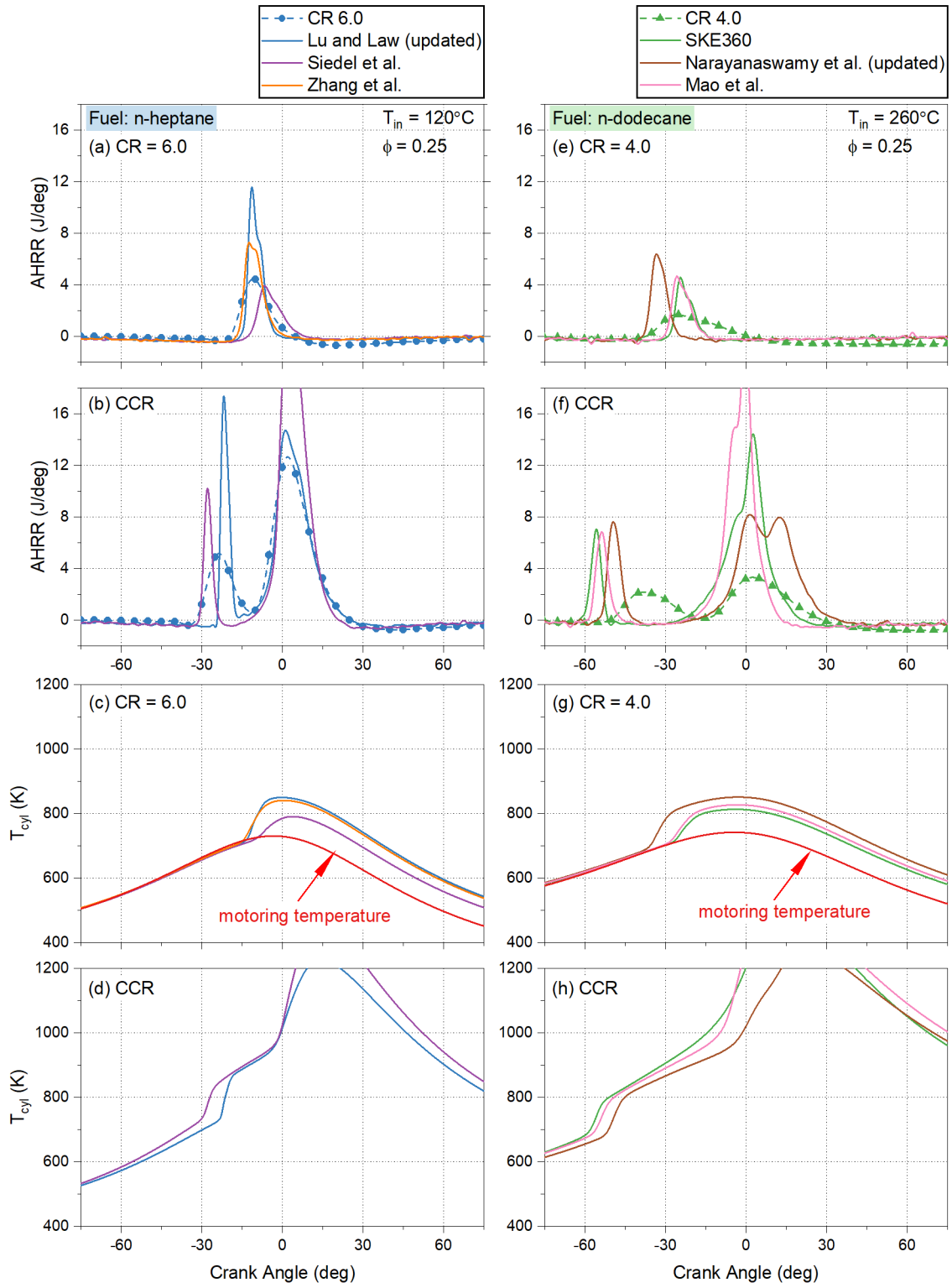
Figure 5.5: Heat release analysis of n-heptane and n-dodecane autoignition in the motored engine.

During n-dodecane oxidation, predictions for the $C_{12}H_{24}$ isomer concentration from the Narayanaswamy et al. [33] and the Mao et al. [29] mechanisms were fairly accurate, while SKE360 significantly overpredicted the concentration. All three mechanisms overpredicted the $C_{12}H_{24}$ isomer concentration.
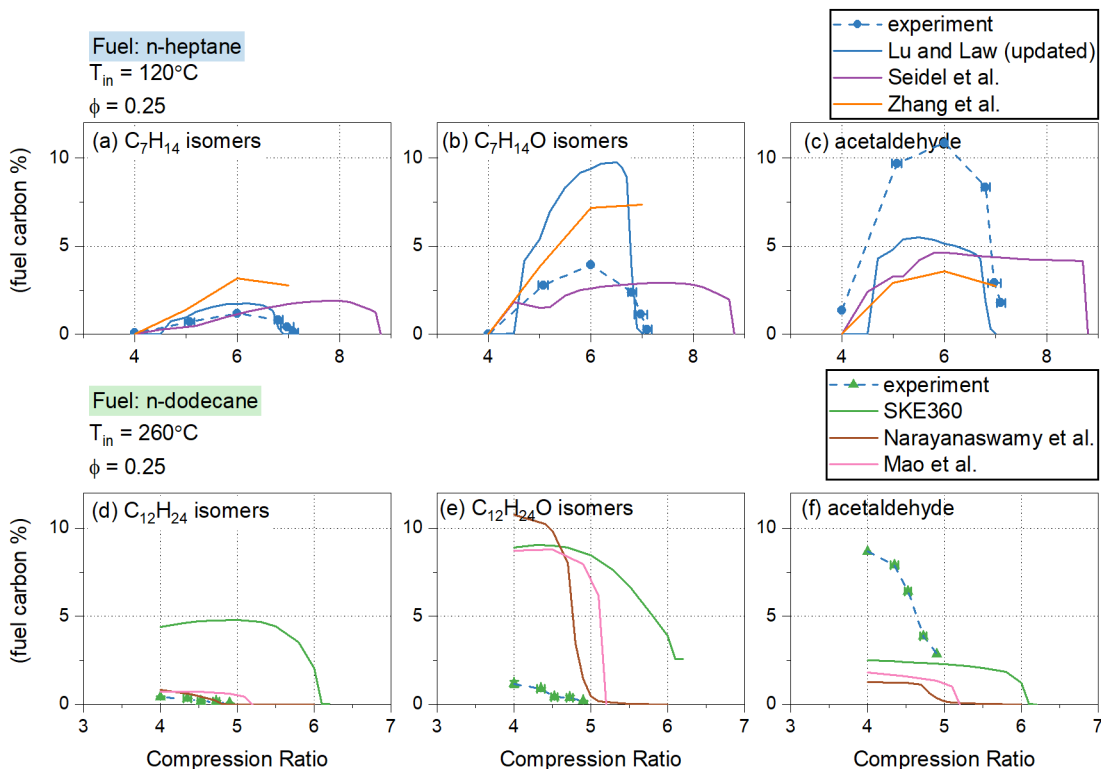
Figure 5.6: Conjugate olefins, cyclic ethers and acetaldehyde concentrations during n-heptane and n-dodecane oxidation.

Figure 5.7 shows the GC-FID signals at the retention time (RT) of 2-10 min from n-heptane and n-dodecane autoignition experiments. Usually, the peak for the fuel molecule is the strongest, and small peaks closest to the fuel molecule are conjugate olefins. For n-heptane, there are three n-heptene isomers.

1-Heptene's retention time overlaps with n-heptane's. Hence, 1-heptene was not able to be separated. Two major peaks were observed near the n-heptane peak. Mass spectrometry showed that both peaks were heptene isomers, but it was difficult to tell which was 2-heptene and 3-heptene, as their mass spectra were very similar. Herbinet
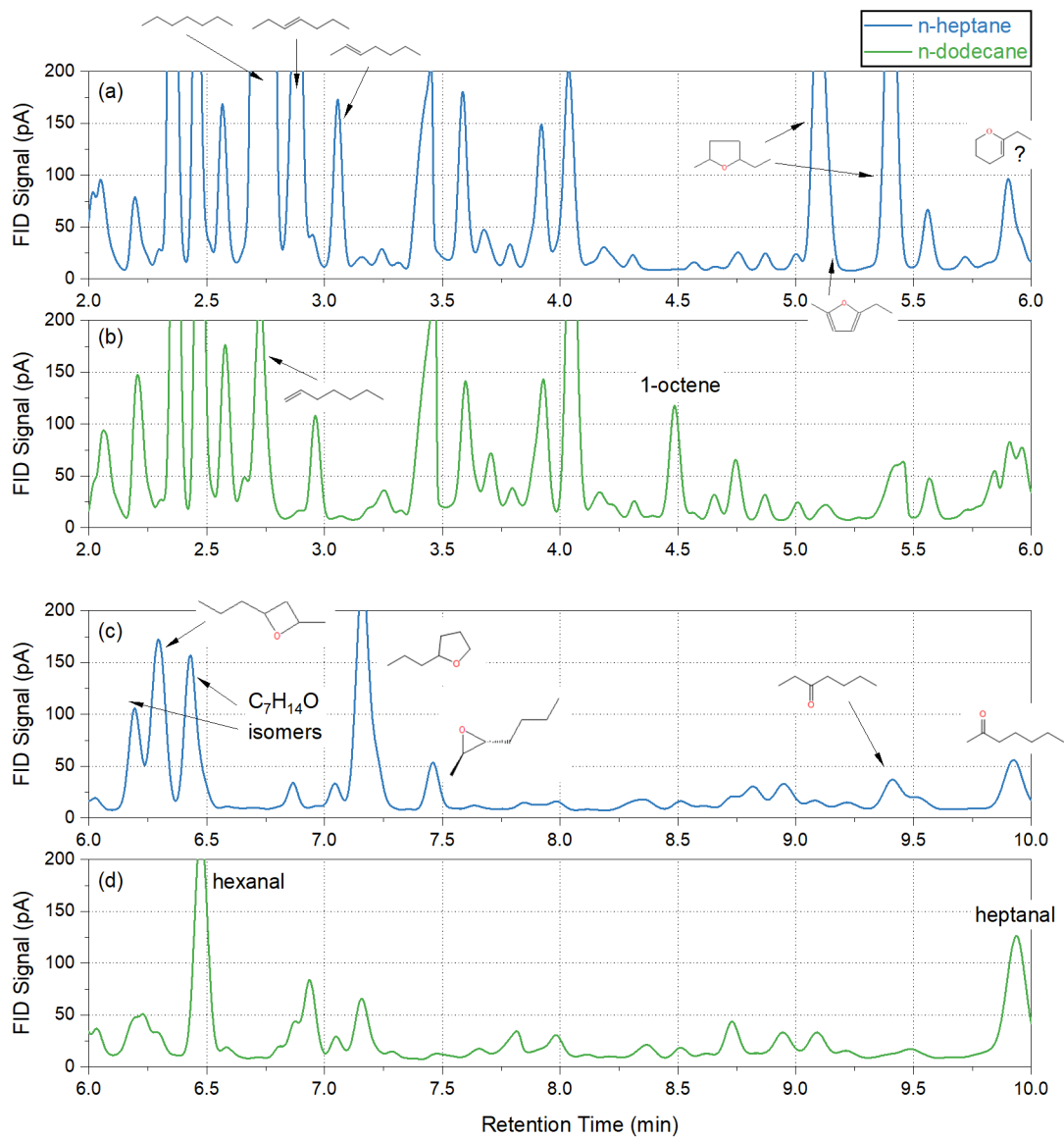
Figure 5.7: GC-FID signal from an n-heptane autoignition experiment at CR=6.0 and an n-dodecane autoignition experiment at $CR = 4.0$.

et al. [97] measured n-heptane oxidation intermediates at 10 bar and stoichiometric conditions in a JSR. They found that the three heptene isomers had similar concentrations at $600 - 900K$, with slightly more 3-heptene than 2-heptene and 1-heptene. Hence it's likely the higher peak in this study was 3-heptene, and the lower peak was 2-heptene.

Two major peaks at $RT = 5 - 5.5$ min had similar mass spectrums, and both were 2-ethyl-5-methyl-tetrahydrofuran. Herbinet et al. [97] obtained a similar chromatography using an HP-5 capillary column and marked those two peaks as cis- and trans- 2-ethyl-5-methyl tetrahydrofurans.

A third major peak at $RT = 5.92$ min was an unknown species with a molecular weight of 112, so it's likely a $C_7H_{14}O$ isomer. Figure 5.8 shows the mass spectrum of this species, which might be 2-ethyl-3,4-dihydropyran but needs confirmation.
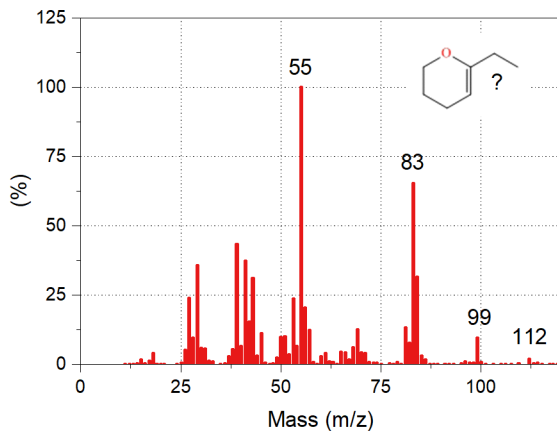
Figure 5.8: Mass spectrum of the species at the retention time of 5.92 min from an n-heptane autoignition experiment at $CR = 6.0$.

The retention time and concentrations of 2-propyl-tetrahydro-furan and 2- and 3-heptone were consistent with the chromatograms in Herbinet et al. Other major peaks at $RT = 5.75 - 6.75$ min were identified as $C_7H_{14}O$ isomers from their molecular ion peaks and retention time.

Figure 5.9 shows the GC-FID signal at $RT = 14 - 22$ min from an n-dodecane
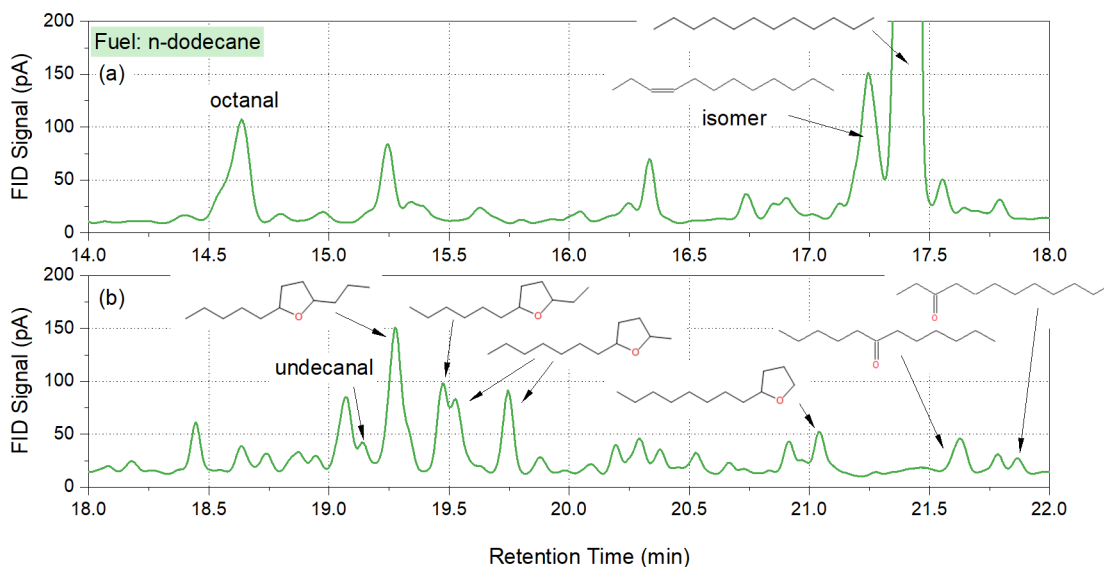
Figure 5.9: GC-FID signal from an n-dodecane autoignition experiment at $CR = 4.0$.
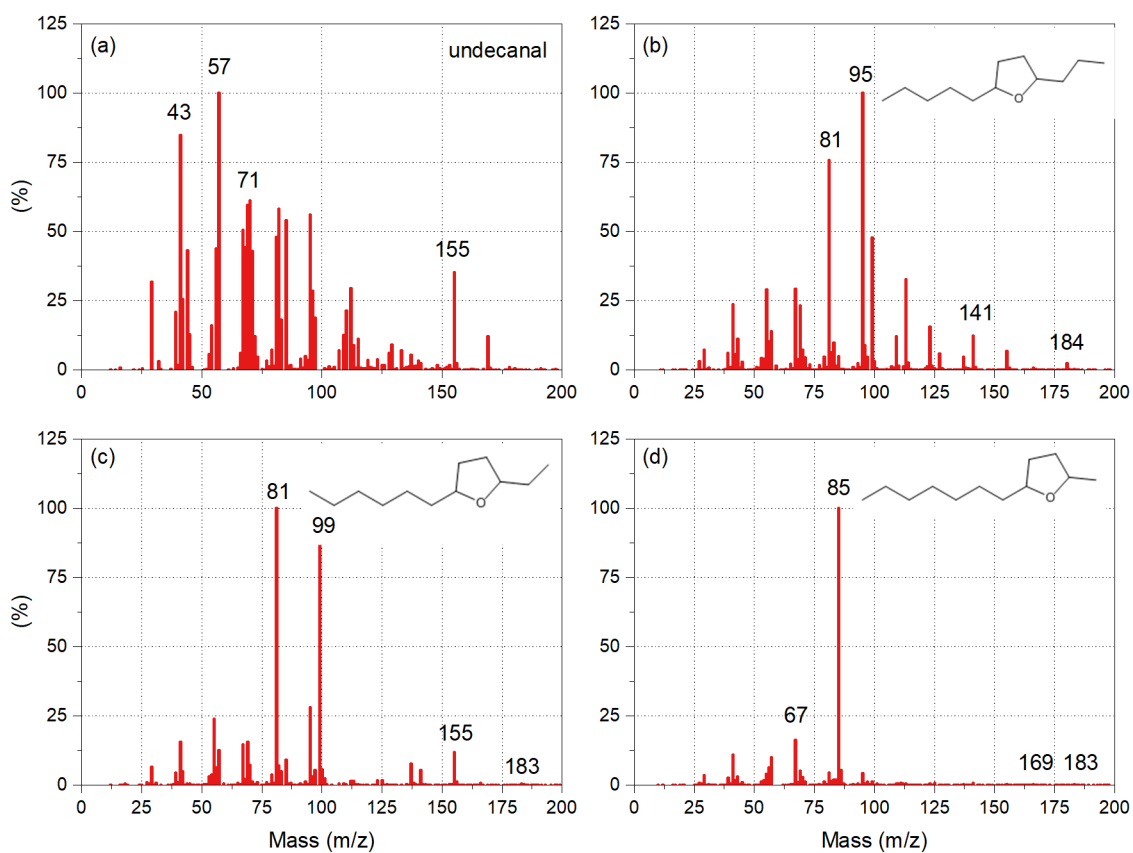
Figure 5.10: Mass spectrum of intermediate species during n-dodecane oxidation.
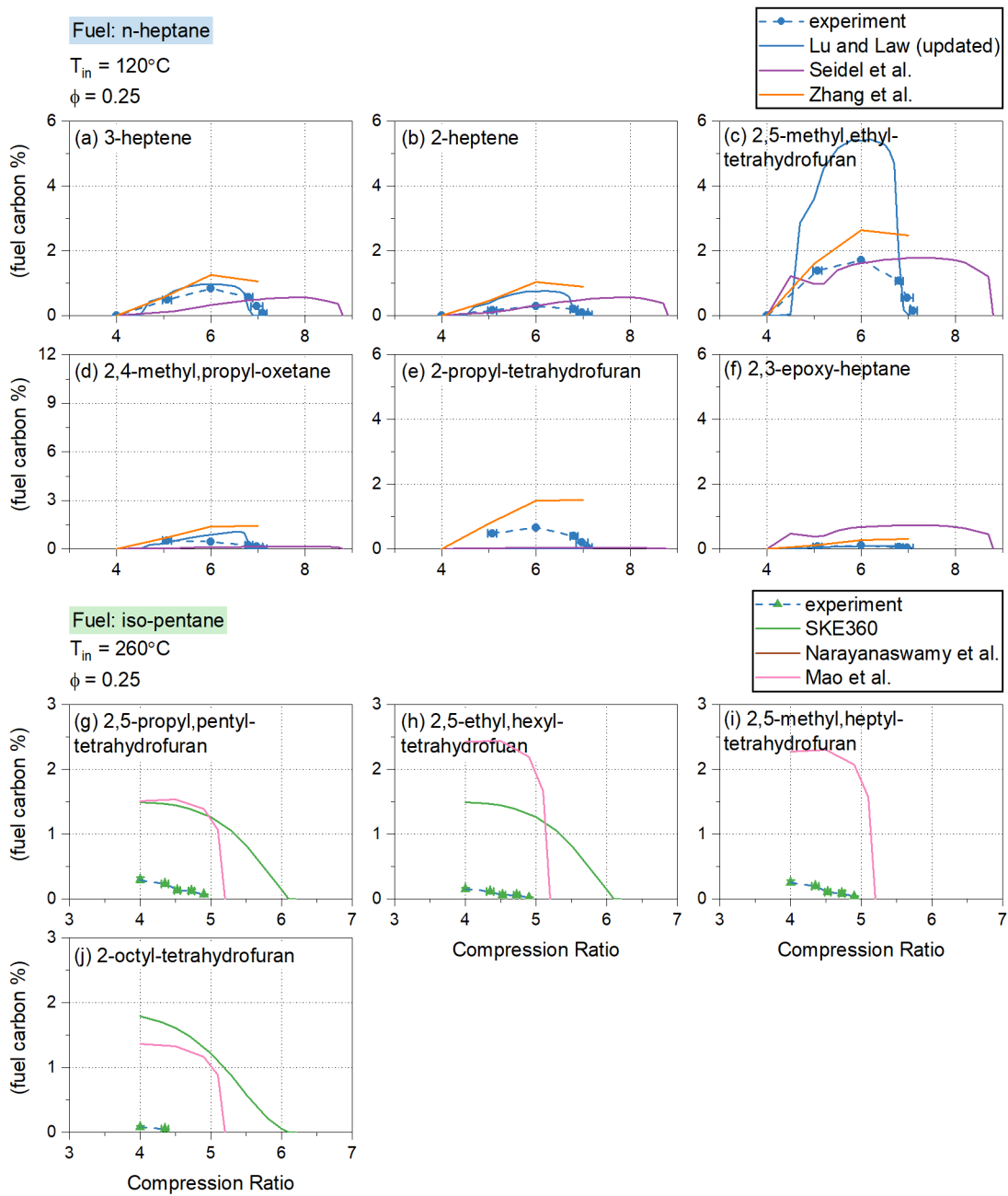
Figure 5.11: Concentrations of conjugate olefin and cyclic ether isomers during n-heptane and n-dodecane oxidation.

autoignition experiment. The dodecene peak was the one just before the n-dodecane peak. Because of strong coelution, dodecane isomers could not be separated from each other. Figure 5.10 shows the mass spectrums of $C_{12}H_{24}O$ isomers, identified using reference spectrums of tetrahydrofurans in Herbinet et al. [100]. Similar to $C_7H_{14}O$, major $C_{12}H_{24}O$ isomers are tetrahydrofurans.

Figure 5.11 shows the concentrations of each conjugate olefin and cyclic ether isomer. For both n-heptane and n-dodecane, the vast majority of cyclic ether intermediates are tetrahydrofurans, consistent with the observation of n-pentane oxidation in Chapter 4.

5.5.2 Other intermediate species

Acetaldehyde concentrations were shown in Figure 5.6. For all mechanisms evaluated, acetaldehyde production was significantly underestimated during n-heptane and n-dodecane oxidation. Zhang et al. [92] also observed significant underprediction for acetaldehyde during n-heptane oxidation in a JSR at $\phi = 0.25$.

Figure 5.12, 5.13 and 5.14 show other major intermediate species in n-heptane and n-dodecane oxidation. For both n-heptane and n-dodecane oxidation, the major intermediate species (other than conjugate olefins and cyclic ethers) were aldehydes and 1-alkenes. Among the aldehydes and alkenes, C_1 and C_2 species (formaldehyde, acetaldehyde and ethylene) were produced more than C_3 species (propanal, propenal, and propene). C_3 species were also produced more than C_4 species (butanal and butene), both being more than larger species $>C_4$. However, this trend was not always followed by the mechanisms. The trend for 1-alkenes of different carbon numbers was consistent with experiments of n-heptane oxidation in a JSR [19, 97], n-decane oxidation in a JSR [19], and n-dodecane oxidation in a shock tube [29, 101]. A zero-dimensional homogenous reactor simulation also showed that their mechanism didn't always follow this trend for 1-alkenes. Data on the formation of large aldehydes
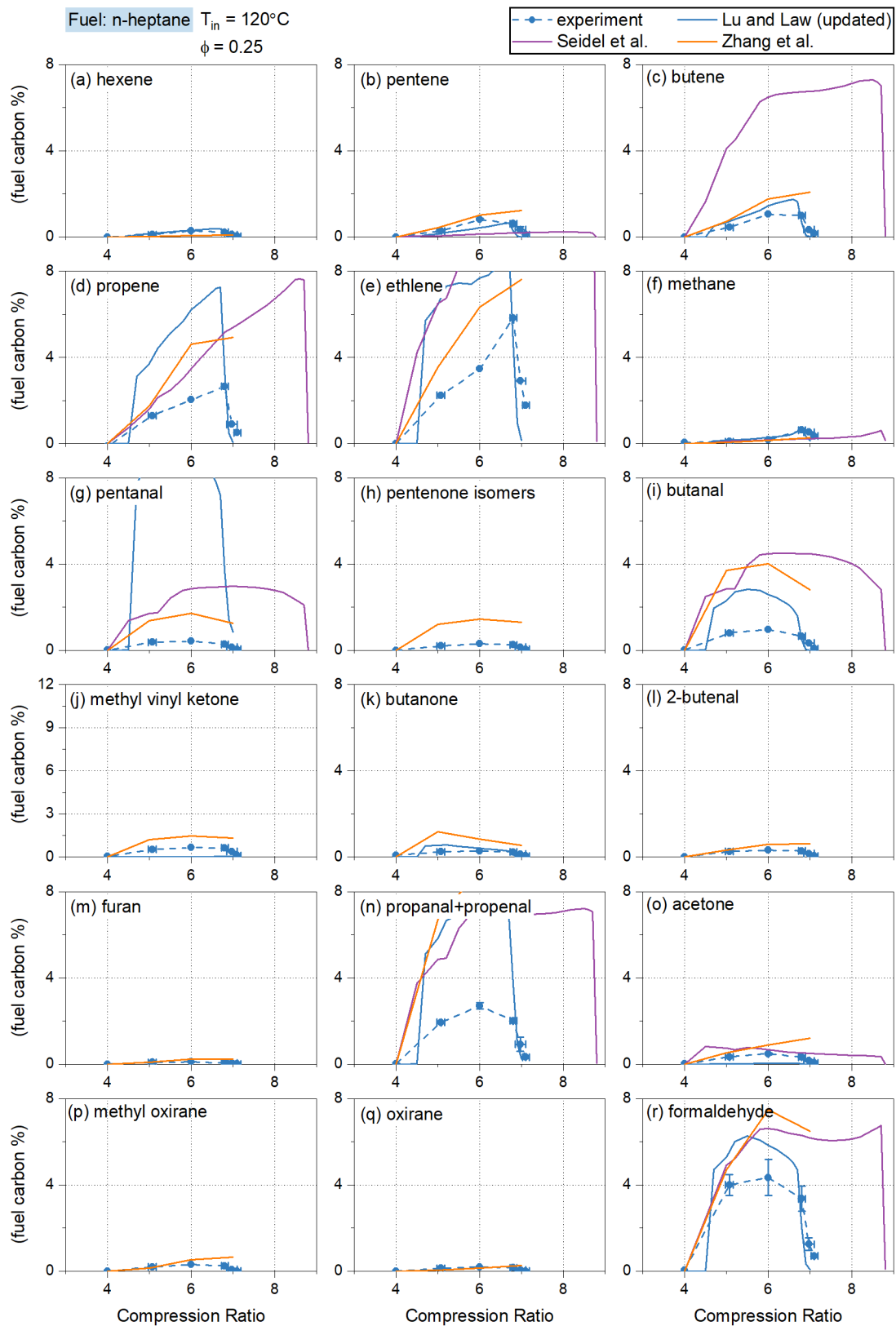
Figure 5.12: Alkenes and oxygenates during n-heptane oxidation.
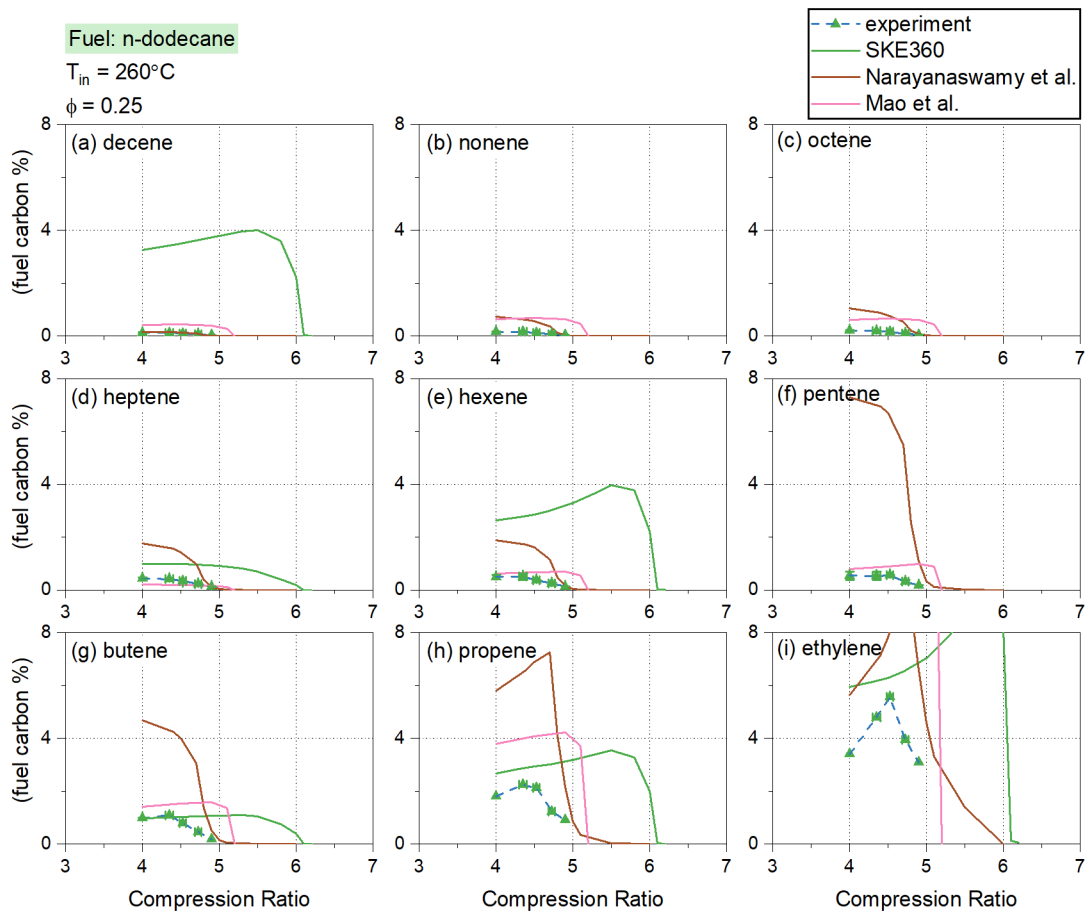
Figure 5.13: Alkenes during n-dodecane oxidation.
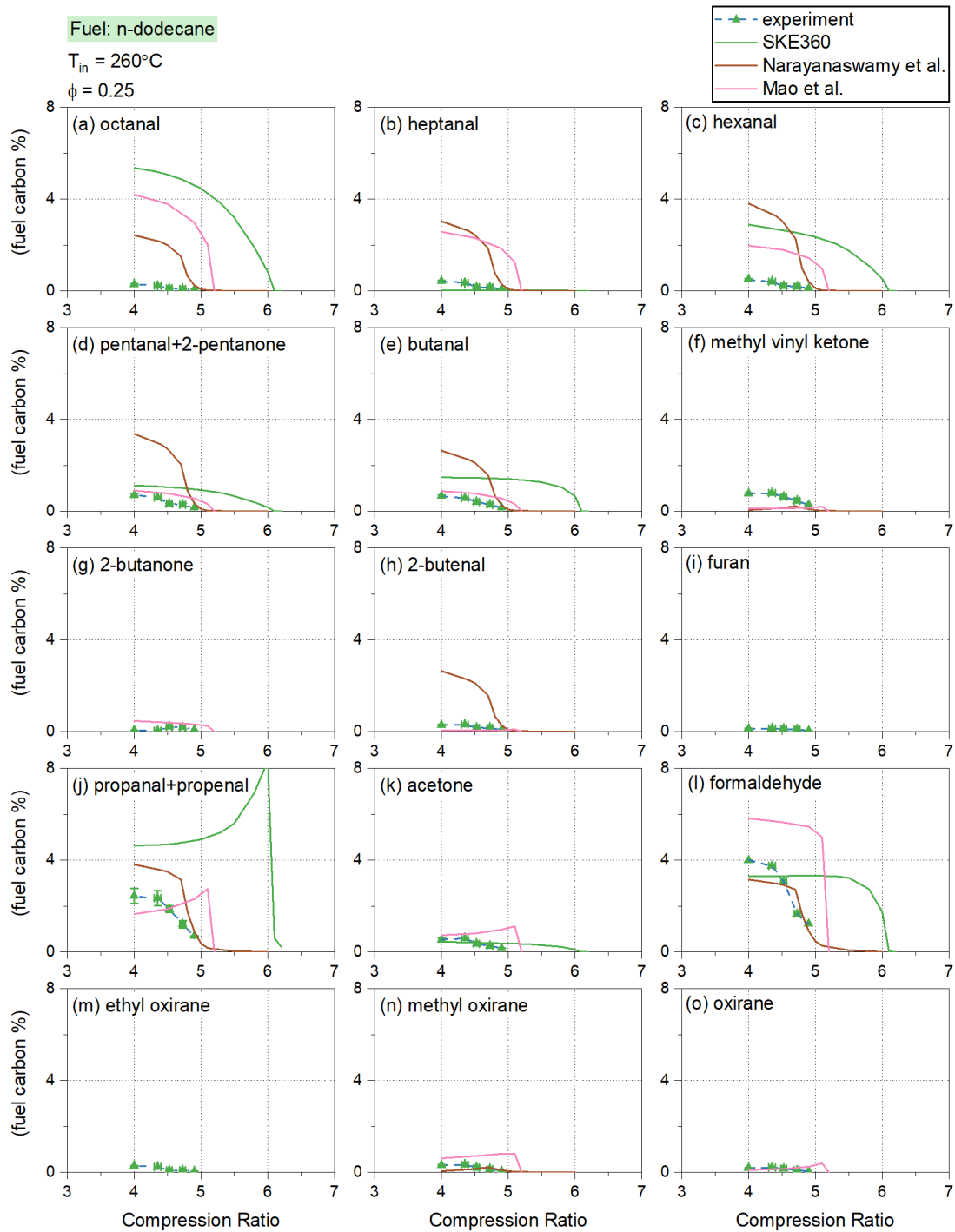
Figure 5.14: Oxygenates during n-dodecane oxidation.

were limited in the literature. During n-heptane oxidation in a JSR at stoichiometric conditions [19], acetaldehyde concentration was higher than propanal, which was higher than butanal.

5.5.3 General trends for intermediate species during normal alkane oxidation

Due to the similarity of species types and concentrations, we plotted concentrations of intermediates during oxidation of n-pentane, n-heptane, and n-dodecane in Figure 5.15.

In this comparison, concentrations of conjugate olefins and cyclic ethers decreased with increasing carbon number. Concentrations of other intermediate species were similar for the three n-alkanes. During NTC, aldehyde concentrations leveled out and slightly dropped at the end of NTC. Alkenes kept accumulating till the end of NTC.

For all three n-alkanes, CO peaked at around 50% of fuel carbon. Formaldehyde peaked at about 4% of fuel carbon. Acetaldehyde was around 9% of fuel carbon at the end of NTC. Propanal + propenal peaked at around 3% of fuel carbon during n-heptane and n-dodecane oxidation. Butanal + methyl vinyl ketone peaked at around 2% of fuel carbon for the three n-alkanes.

Ethylene peaked at around 6% of fuel carbon during n-heptane and n-dodecane oxidation. Propene peaked at about 3% and butene at around 1.5% of fuel carbon for the three n-alkanes. In a JSR measurement of oxidation intermediates at stoichiometric conditions, propene and butene concentrations were also very close during n-heptane and n-decane oxidation. This similarity was missed in their simulation [19].

This comparison shows that for n-alkanes of different sizes, at similar stages of oxidation, the formation of conjugate olefins and cyclic ethers was sensitive to the carbon chain length. In contrast, the formation of CO, aldehydes, and other alkenes were not sensitive to the carbon chain length. This trend was not always followed in
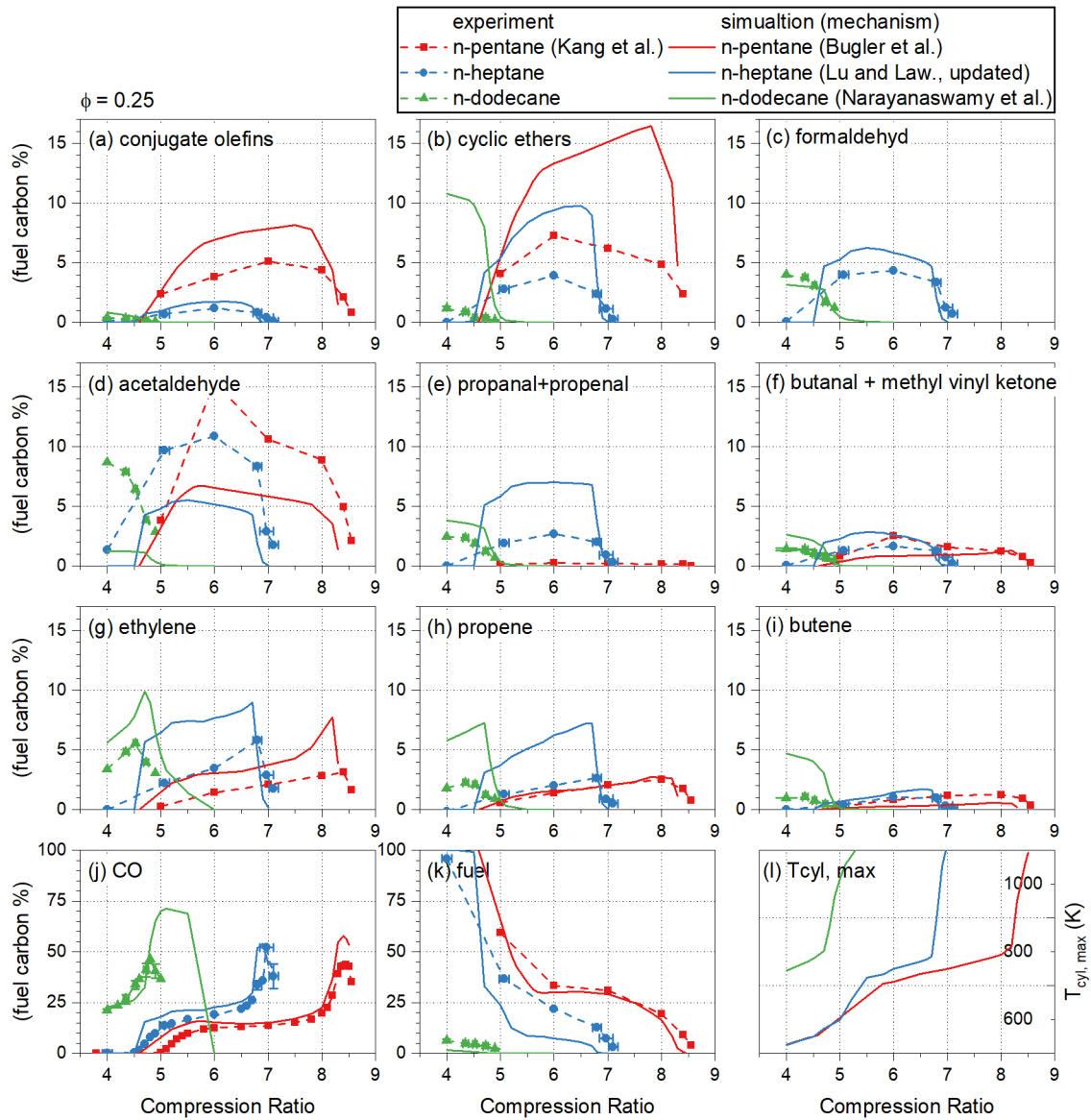
Figure 5.15: Intermediate species during n-pentane, n-heptane, and n-dodecane oxidation in the motored engine.

the mechanisms.

5.6   Conclusions

In this study, n-heptane and n-dodecane autoignition was investigated via coupled motored engine experiments and simulations.

In all evaluated mechanisms for n-heptane and n-dodecane, fuel reactivities were underestimated. It was demonstrated in two examples that the CO concentration from the motored engine experiment could be used as an evaluator of mechanism performance, could provide insight into the chemical model, and could be used as a prediction target for mechanism development and validation.

Intermediate species concentrations were measured during n-heptane and n-dodecane oxidation in the motored engine at lean conditions. Acetaldehyde production was underpredicted by all mechanisms evaluated.

In a comparison of n-pentane, n-heptane, and n-dodecane oxidation, the following trends for intermediate species were observed:

1. The concentrations of conjugate olefins and cyclic ethers were sensitive to the chain length of the normal alkane. The larger the normal alkane was, the fewer conjugation olefins and cyclic ethers were produced during oxidation.

2. Other intermediate species were less sensitive to the chain length of the normal alkane. For the three normal alkanes, major intermediate species were aldehydes and 1-alkenes. Aldehyde concentrations leveled out during NTC and dropped at the end of NTC. 1-Alkenes accumulated during NTC and peaked at the end of NTC. Concentrations for those species were also similar for the three normal alkanes.

These trends were not always followed calculations using the selected mechanisms

and these observations may be helpful for future mechanism development and validation.

Chapter 6

Autoignition of a Jet Fuel Surrogate and Pure Components in a Motored Engine: Experiment and Simulation

6.1 Experiment and simulation setup

The autoignition behavior of a jet fuel surrogate and its pure components were investigated in the motored engine experiment and simulation. The jet fuel surrogates were developed to emulate the physical and chemical properties of real jet fuels that are composed of hundreds of hydrocarbons [9]. Component fractions of the jet fuel surrogate are listed in Table 6.1.

Component	Volume Fraction (%)
n-Dodecane	47.84
iso-Cetane	11.29
Decalin	28.21
Toluene	12.66

Table 6.1: UM3 Jet-A surrogate components [9].

Engine experiments were performed at an engine speed of 600 RPM, an intake pressure of 1 bar, and an intake temperature of $260°C$ to fully vaporize all fuel com-

ponents. The equivalence ratio was kept at 0.25. The critical compression ratios (CCRs) of pure components and the surrogate were measured by gradually increasing the engine compression ratio until an intensive heat release event was observed. The exhaust gas was sampled to determine the species and concentrations during oxidation. An existing skeletal kinetic mechanism consisting of 360 species and 1851 reactions (refered to as SKE360 [9]) was evaluated by comparing the predicted species concentrations and heat release with measurements. The global reactivity, heat release profiles, and oxidation intermediates of test fuels are discussed in this chapter.

6.2 Global reactivity

Figure 6.1 shows the CO concentration, unreacted fuel concentration, and peak in-cylinder temperature in the surrogate and component autoignition experiments and simulation.

Two fuel components, n-dodecane, and decalin, exhibited strong low-temperature oxidation (LTO) behavior in the experiment, with significant CO production at lower compression ratios when the fuels were partially oxidized. CO accumulated during the transition from negative temperature coefficient (NTC) regime to high-temperature oxidation (HTO) and was converted to CO_2 quickly during HTO. The critical compression ratio prediction was significantly late for these two-stage fuels, and the peak [CO] prediction was slightly too low. Yu et al. [57] observed that an existing decalin mechanism slightly overpredicted the ignition delay time at low temperatures. This mechanism inaccuracy turned to be significant in the motored engine.

The other two fuel components, iso-cetane, and toluene exhibited negligible LTO behavior. The mechanism was effective for this feature of toluene. Although predicted CCR was too late for toluene, [CO] prediction was accurate at the beginning of HTO, showing that the toluene oxidation chemistry is accurate for the onset of ignition. Only minor modifications are needed. SKE360 predicted too strong LTO for iso-
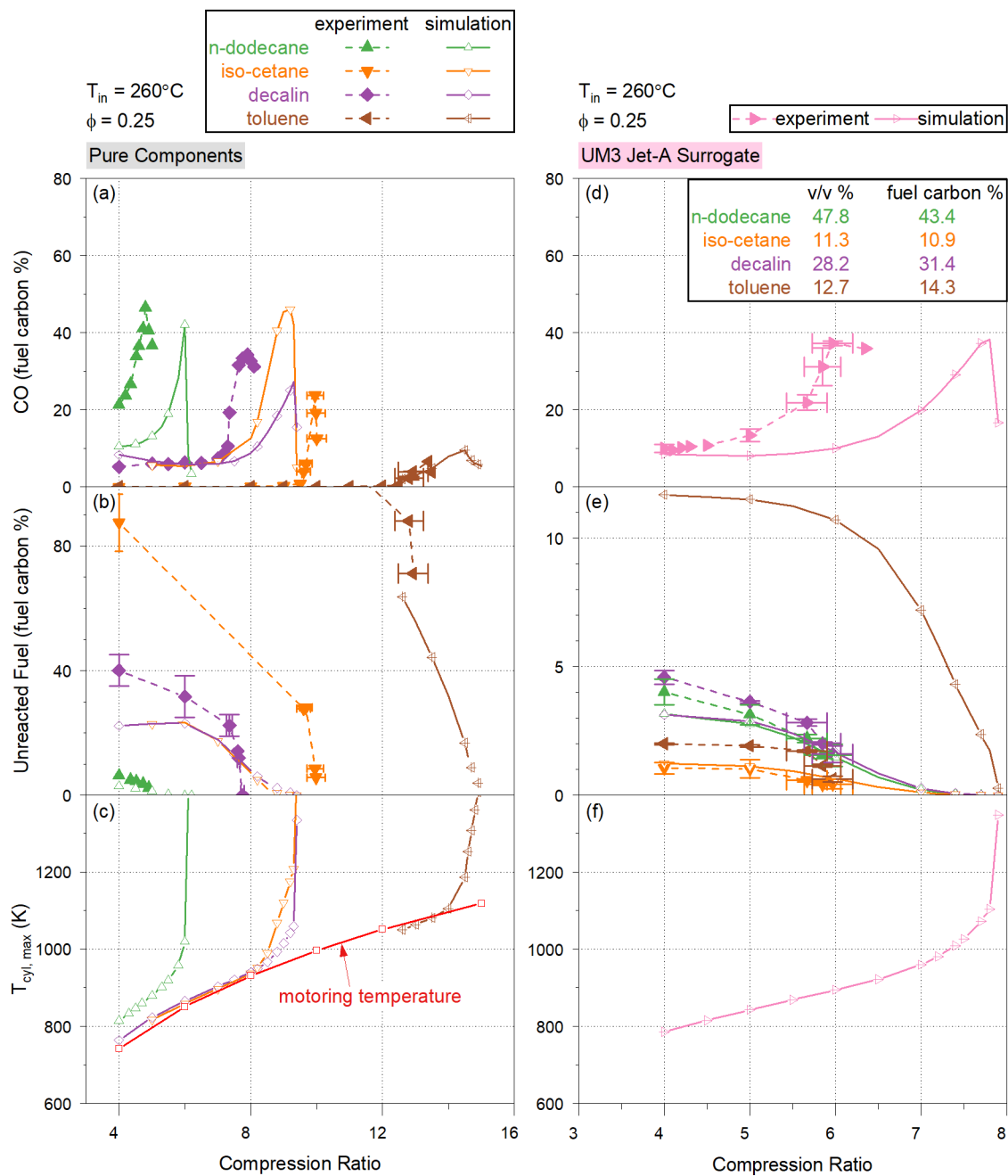
Figure 6.1: Autoignition of the pure components and the jet fuel surrogate in the motored engine.

cetane, consistent with the deficiency of an existing iso-cetane mechanism observed in an RCM. Kukkadapu and Sung [47] also found falsely predicted NTC in their ignition delay simulation, which was not detected in their RCM experiments.

Comparing the measured CO concentration during decalin and iso-cetane oxidation, decalin was significantly more reactive than iso-cetane and exhibited much stronger LTO. However, in the simulation, those two fuels had very similar LTO behavior, too similar [CO] curve, and too close CCRs. The bicyclic alkane decalin and the highly branched alkane iso-cetane are both less reactive than normal alkanes due to the branched structures, but the mechanism needs to be more effective for their difference.

The surrogate showed strong NTC behavior during oxidation, which comes from n-dodecane and decalin in the mixture. Instead of the reactive component being oxidized first and the unreactive component remaining as fuel molecule species, the low measured concentrations of unreacted fuel components at $CR = 4.0$ shows that all four components were significantly consumed at a similar level. Around 90% of all four components were consumed. Because iso-cetane, decalin, and toluene consumption were all enhanced considerably, the low remaining fuel concentrations were less likely due to mistakes during fuel blending. Additionally, carbon balance (THC+CO+CO$_2$ concentrations) was >95% near CCR, so the amount of fuel injected was correct, too, and sample loss was eliminated. A significant amount of small intermediate species were formed in the surrogate oxidation, as discussed in Section 6.4.4, which is consistent with the observation in fuel consumption. Hence, the observed oxidation enhancement for the other three components by n-dodecane was trustable. The causes of the oxidation enhancement will be discussed in 6.4.4.

Although all components were consumed at a fast rate, slight differences occurred for different components. Table 6.2 shows the component fractions in the surrogate formula and in remaining unreacted fuels at $CR = 4.0$. For the two alkanes

(n-dodecane and iso-cetane), fractions in unreacted fuel were lower than in the surrogate formula. For the bicyclic alkane decalin and the aromatic compound toluene, fractions in unreacted fuel were higher than in the surrogate formula. This comparison shows that n-dodecane and iso-cetane oxidized faster than decalin and toluene in the surrogate mixture. n-Dodecane is the most reactive among the four components, so it's reasonable for n-dodecane to oxidize at the highest rate. However, iso-cetane is less reactive than decalin, but the oxidation enhancement by the radical pool and heat from n-dodecane LTO made iso-cetane oxidize faster than decalin, showing that oxidation enhancement is not determined by the stand-alone reactivity of the enhanced component.

Component	UM3 Jet-A Surrogate	Unreacted Fuel, Experiment	Unreacted Fuel, Simulation
	(%)	(%)	(%)
n-Dodecane	43.4%	35.3%	16.5%
iso-Cetane	10.9%	9.29%	6.44%
Decalin	31.4%	37.8%	16.2%
Toluene	14.3%	17.6%	60.8%

Table 6.2: Component factions in UM3 Jet-A surrogate formula and in remaining unreacted fuel at $CR = 4.0$, as percentages of the total carbon.

In the simulation, although [CO] at $CR = 4.0$ and peak [CO] near CCR was accurately predicted for the surrogate mixture, the predicted transition from NTC to HTO was too late. It's likely that the overestimation of iso-cetane LTO compensated for the underestimation of n-dodecane LTO, so the predicted [CO] concentration at $CR = 4.0$ was better than for pure components.

The mechanism captured the enhanced consumption of decalin and iso-cetane but significantly underestimated the consumption of toluene in the mixture. Because both decalin and iso-cetane were predicted to have strong two-stage oxidation behaviors,

missing toluene consumption in the mixture indicates deficiencies in the single-stage fuel oxidation mechanism.

To better understand how the ignition process in the motored engine is related to the ignition delay timing measured in fundamental combustion facilities, the temperature-pressure trajectories in the compression stroke of a firing and a motoring cycle were plotted in Figure, on the 3D surface of the ignition delay timing in a homogeneous reactor (τ). It can be seen that at both firing at motoring conditions, the engine temperature and pressure increased from around 500K and 1 bar near IVC and went across a wide range. The temperature and pressure at the end of compression depended on the engine operating condition and the fuel property. In this motored engine, low-temperature (<750K) ignition delay timing is only important from 1 bar to 5 bar. Above 5 bar, only intermediate- to high-temperature ignition delay timing matters to the fuel autoignition. The integral of the reciprocal of tau could be used to estimate the ignition delay timing τ_{id} in changing conditions [66]:

$$\int_{t_{si}}^{t_{si}+\tau_{id}} \frac{1}{\tau}dt = 1 \tag{6.1}$$

where t_{si} is the start of injection, and could be considered as IVC in HCCI cycles. τ_{id} is the ignition delay timing in the HCCI cycle and is reached when this integral reaches 1. 6.2 shows the value of this integral, in-cylinder OH mass fraction, and in-cylinder temperature. The integral increased from zero near the first spike of OH, which was an indicator of the first-stage ignition at around 750K. When the integral reached 1, the timing was close to the second OH peak, which was an indicator of the second-stage ignition. τ_{id} did not agree perfectly with the second OH peak, because both the OH mass fraction and the in-cylinder temperature used to calculate the ignition delay timing were an average across the cylinder to simplify the calculation.
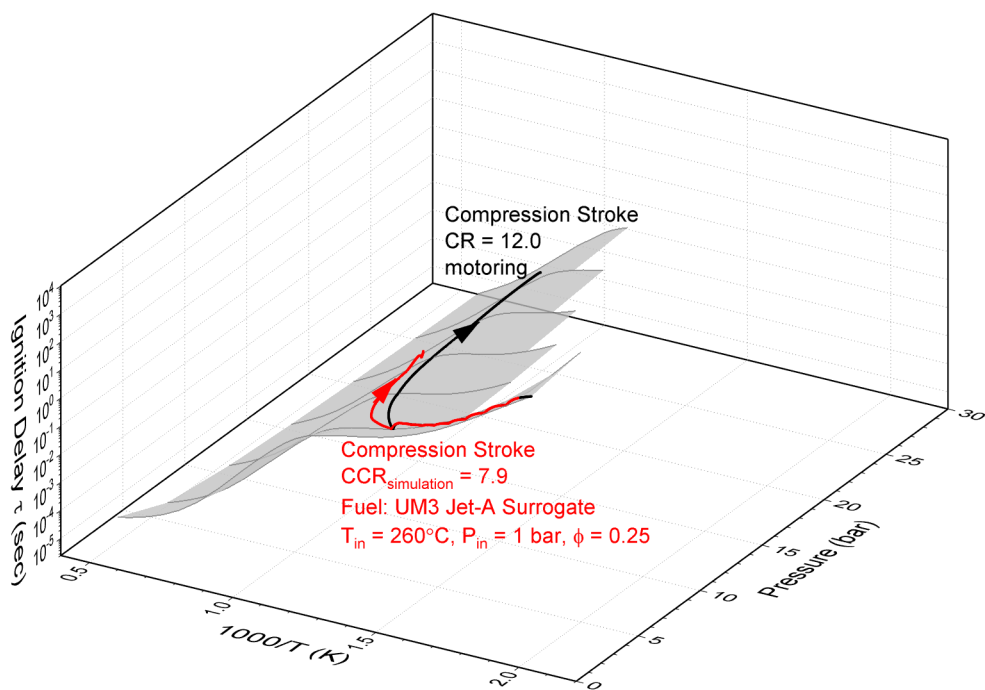
Figure 6.2: Simulated temperature-pressure trajectories of the engine cycles on the 3D surface plot of the ignition delay timing. The in-cylinder temperature and pressure was from the multizone simulation of the motored engine. The ignition delay timing of the UM3 Jet-A surrogate was from the homogeneous reactor simulation using Cantera and the kinetic mechanism SKE360, at $\phi = 0.25$.
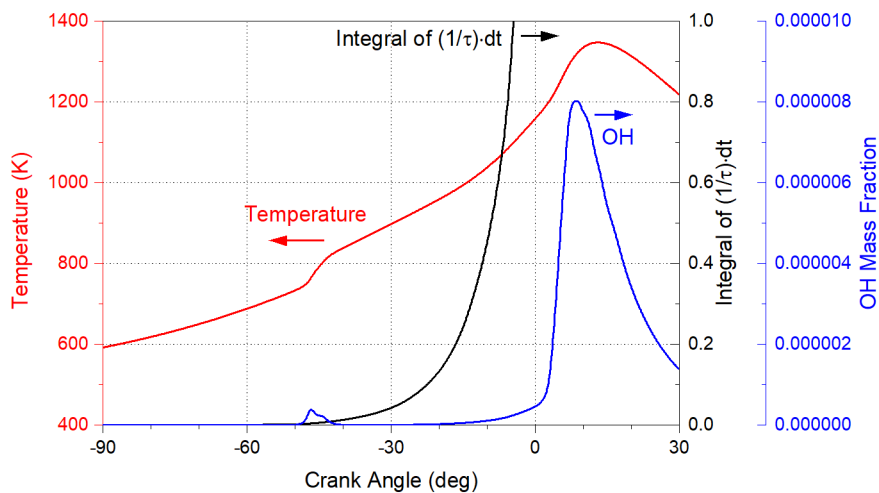
Figure 6.3: Simulated in-cylinder temperature, OH mass fraction and the calculation of the ignition delay timing at $\mathrm{CCR}_{simulation} = 7.9$ for the UM3 Jet-A surrogate.

6.3 Heat release analysis
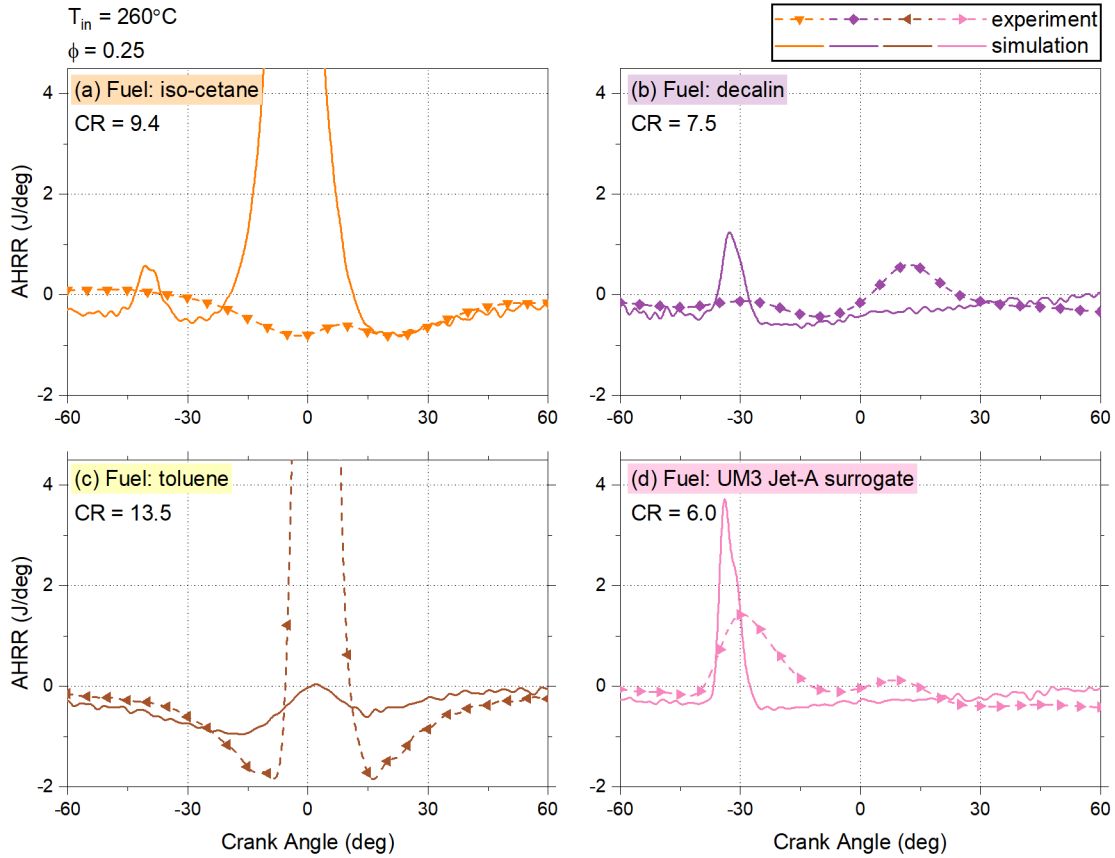
Figure 6.4: Apparent heat release rate of the pure components and jet fuel surrogate autoignition in the motored engine.

Figure 6.4 shows the apparent heat release rate (AHRR) for the pure components and surrogate mixture. A low-temperature heat release (LTHR) was falsely predicted for iso-cetane, and high-temperature heat release (HTHR) prediction was too intense. For decalin, LTHR was correctly predicted, but HTHR was under predicted. For toluene, the single-stage ignition behavior was captured in the simulation. The ignition timing prediction was fairly accurate, though the predicted amount of heat release was too small. For the surrogate mixture, LTHR was correctly predicted, and the timing prediction was pretty accurate, but the onset of HTO at this condition was missed in the simulation.

6.4 Intermediate species

6.4.1 Intermediate species during iso-cetane oxidation

Figure 6.5 and 6.6 shows oxygenate and hydrocarbon species concentrations during iso-cetane oxidation. Compared to normal alkanes, there was a significant amount of acetone production during iso-cetane oxidation, similar to the observation during neo-pentane oxidation. However, as a major low-temperature oxidation product, predicted acetone formation was too early in the oxidation process. Three oxygenate species (4,4,-dimethyl-2-pentanone, 2,2,4,4-tetramethyl-tetrahydrofuran, and 2-methyl-propanal) and six hydrocarbon species were not included in SKE360. Except for acetaldehyde and ethylene, all other species considered in the mechanism were significantly overpredicted.

Yu et al. [57] found that the iso-cetane NTC regime was at lower temperatures than mechanism prediction. In an RCM experiment at 20 bar and $\phi = 0.5$, isocetane oxidation entered the NTC regime at around $625K$ and HTO regime at around $740K$. Based on Yu et al. [57]'s observation, iso-cetane oxidation in the motored engine already entered the NTC and HTO regimes at $CR = 4.0$, where the peak cylinder temperature was $742K$ (from motoring simulation). Within one engine cycle, because the temperature window for LTO was narrow for iso-cetane, LTO behavior and species production were not significant. Yang and Boehman [58] used the concept of ceiling temperature to explain a similar observation in motored engine experiments. The ceiling temperature is the temperature at which the concentrations of $\dot{R}$ and RO_2 are equal ([102, 102]), meaning that O_2 addition to the fuel radical becomes less likely than β-scission of the fuel radical. Hence, oxidation enters the high-temperature regime. Yang and Boehman [58] mentioned that the ceiling temperature is high for reactive fuels, like n-heptane, and low for non-reactive fuels. [49] found that as the size of the branched alkane molecule increased, NTC moved towards low temper-
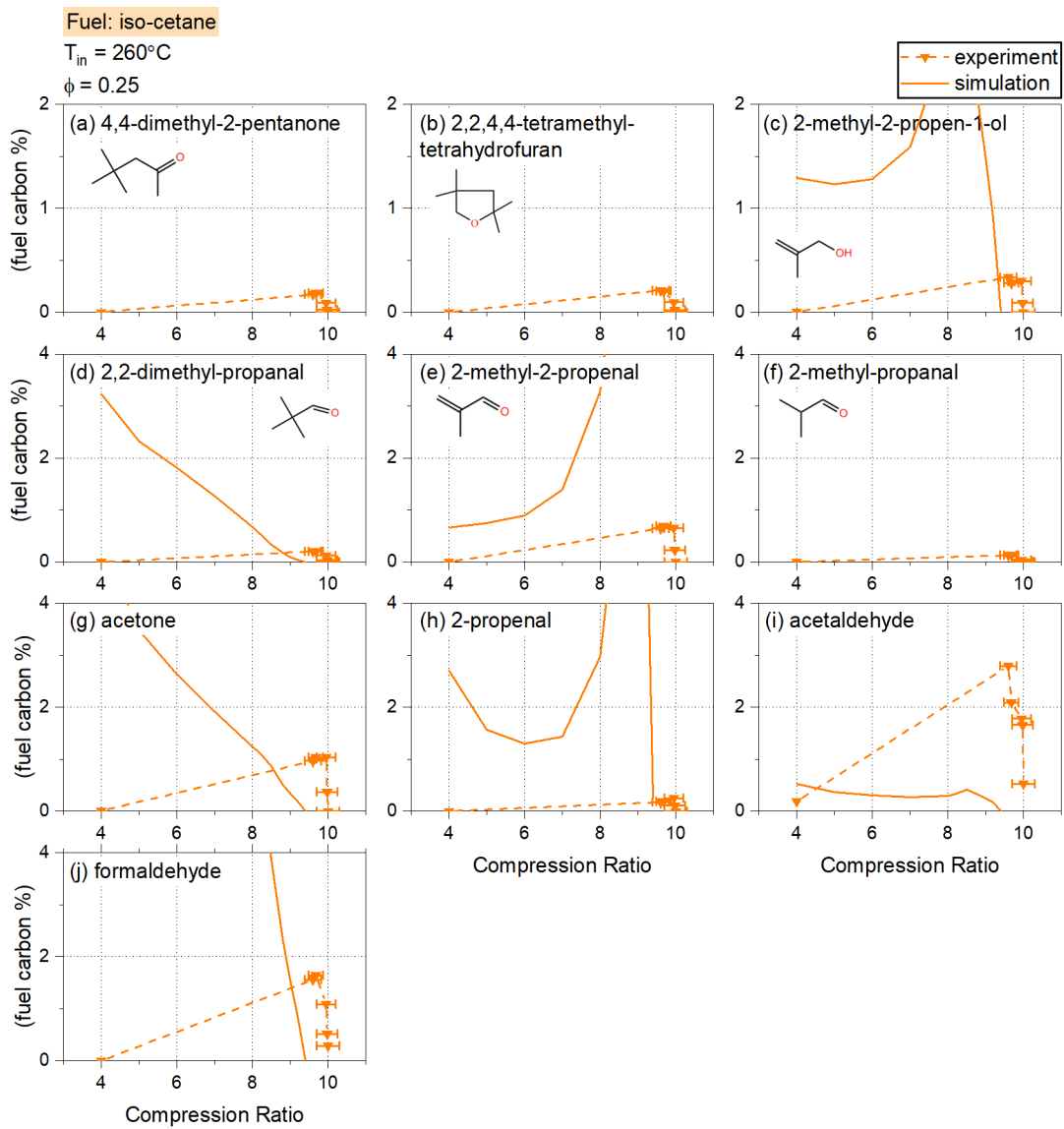
Figure 6.5: Oxygenate intermediates during iso-cetane oxidation.
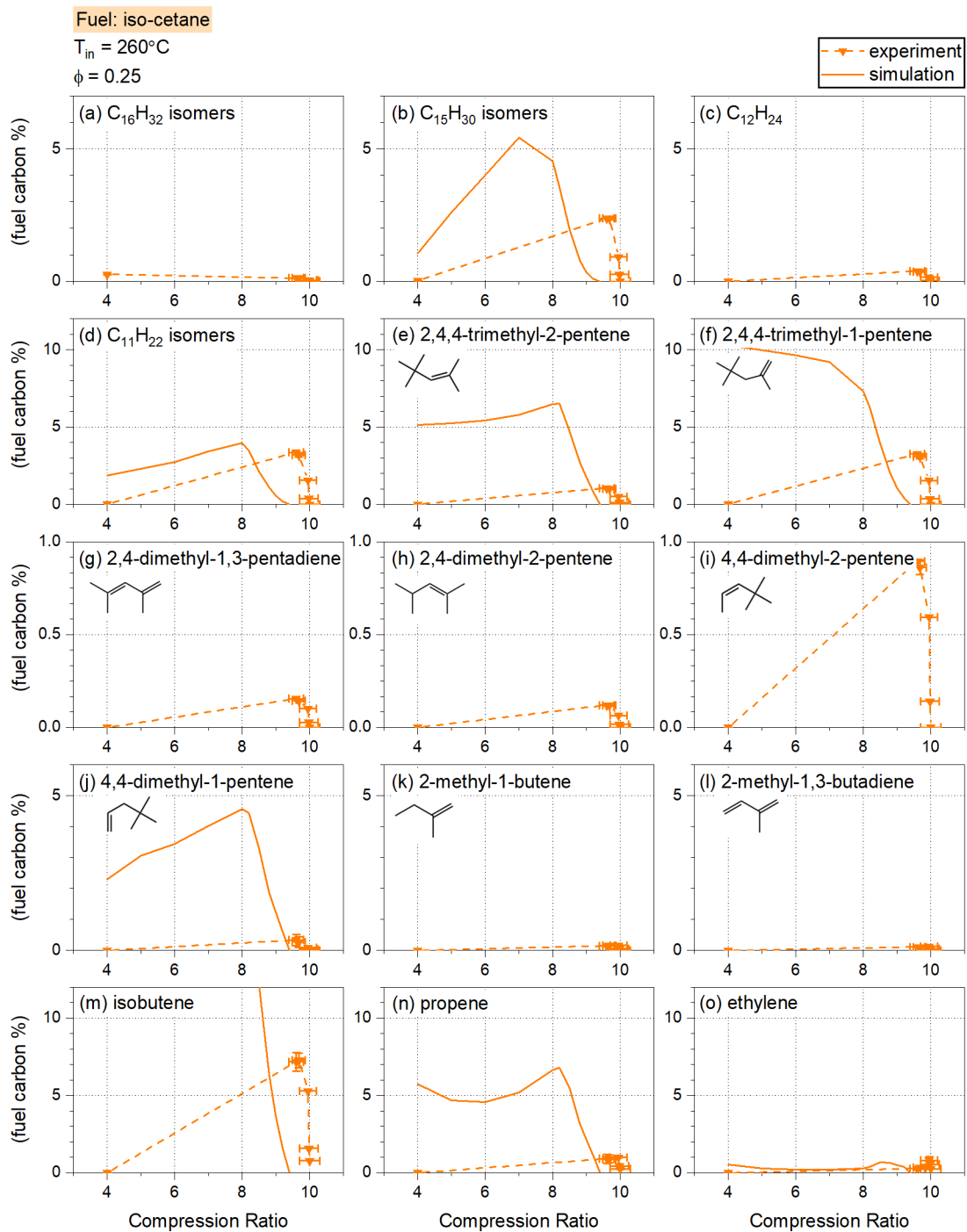
Figure 6.6: Hydrocarbon intermediates during iso-cetane oxidation.

atures. Compared to iso-octane, iso-cetane started to show NTC behavior at lower temperatures, meaning that the ceiling temperature of iso-cetane is significantly lower than iso-octane. Existing iso-cetane mechanisms were developed based on analogy to iso-octane oxidation, and this difference in ceiling temperature was not properly addressed.

This ceiling temperature concept explains the gap between experiment and simulation of iso-cetane oxidation in the motored engine. For example, in one engine cycle at $CR = 4.0$, as the mixture temperature increased from $T_{in} = 260°C$, the mixture at first entered the LTO regime and O_2 addition to fuel radicals was favored. However, the ceiling temperature was low, so after a very short period, O_2 addition stopped, and oxidation entered NTC and HTO regime. Because the window for LTO was narrow, O_2 addition and low-temperature chemistry were observed to be insignificant at the test condition. In contrast, in the simulation, O_2 addition continued because the ceiling temperature was set too high. Hence, in the mechanism, improvements are needed to lower the ceiling temperature and weaken O_2 addition to the fuel radical. Figure 6.7 shows significantly different reaction rates of $\dot{R} + O_2 \Leftrightarrow RO_2$ reactions in multiple iso-cetane mechanisms. Among the four mechanisms, the Wang et al. [50] mechanism showed a reasonable ceiling temperature estimation. Assuming an oxygen concentration of 0.044 $kmol/m^3$ at 15 bar, ceiling temperature is reached when the equilibrium constant

$$K = \frac{k_f}{k_r} = \frac{1}{[O_2]} \tag{6.2}$$

In the Wang et al. [50] mechanism, k_f is around $10^{10}/(kmol \cdot m^3 \cdot s)$ at all temperatures, so ceiling temperature is reached when the reverse rate constant

$$k_r = k_f[O_2] = 4.4 \times 10^8/s \tag{6.3}$$
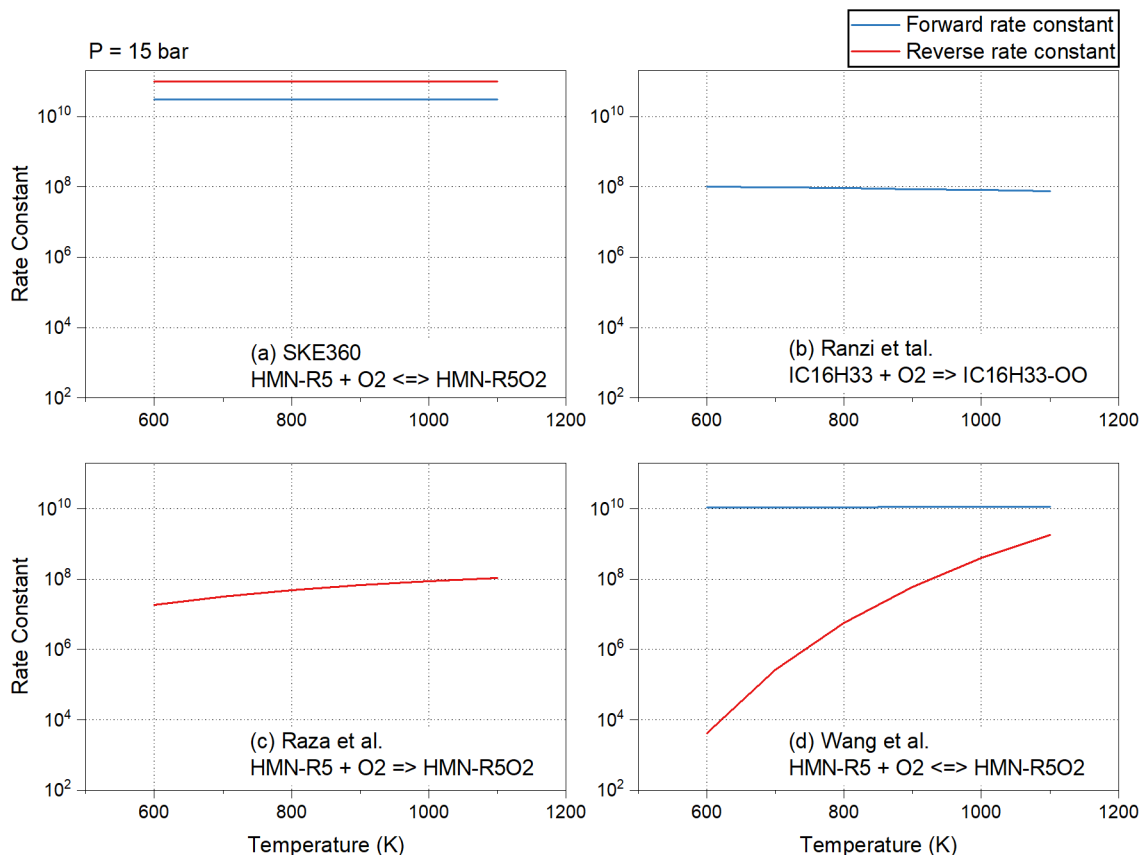
Figure 6.7: $R + O_2 \Leftrightarrow RO_2$ forward and reverse reaction rates in SKE360, the Ranzi et al. [30] mechanism, the Raza et al. [49] mechanism, and the Wang et al. [50] mechanism. The unit for concentration is $kmol/m^3$.

In Figure 6.7 (d), $k_r = 4.4 \times 10^8/s$ is correspondent to a temperature of 1000 to 1100K, which is a fairly good estimation for ceiling temperature, especially compared to other mechanisms. However, this ceiling temperature might still be too high for iso-cetane. n-Heptane and n-dodecane high-temperature oxidation started at around 950K in motored engine experiments and simulation. iso-Cetane, as a less reactive fuel, very likely has a lower ceiling temperature than 950K. This slight overestimation of ceiling temperature is consistent with the observation in Wang et al. [50] that the mechanism prediction missed the transition from NTC to HTO regime, as shown in Figure 6.8.

Intermediated species measurements also support the hypothesis that iso-cetane
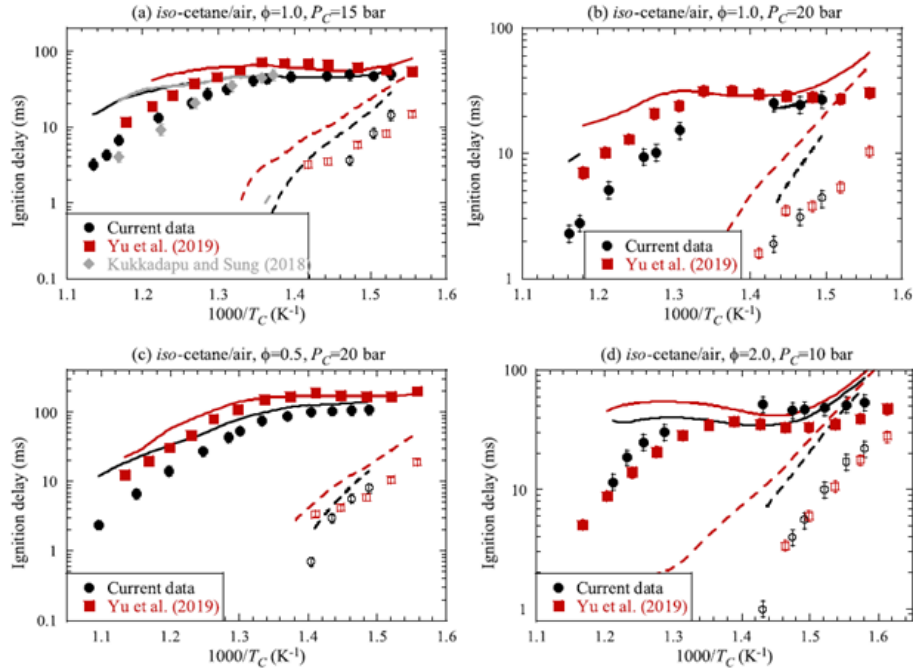
Figure 6.8: The Wang et al. [50] mechanism missed the transition from NTC to HTO. The figure is from [50].

oxidation already entered NTC and HTO regimes at $CR = 4.0$. A very small amount of $C_{16}H_{32}$ was detected at $CR = 4.0$, indicating a small amount of LTO was present. With an increased compression ratio, [$C_{16}H_{32}$] did not increase, which was different from all other species, showing that LTO had already ended. No significant $C_{16}H_{32}O$ was observed, also indicating that O_2 addition was not important at the test condition.

All major species $>C_8$ were alkenes. As shown in Figures 6.9 and 6.10, three major groups of peaks were observed in the GC-FID signal: $C_{16}H_{32}$ isomers, $C_{15}H_{30}$ isomers $C_{11}H_{22}$ isomers. Due to the lack of library and literature data reference, and the nature of highly-branched hydrocarbon molecules, it's difficult to reconstruct the molecule structure merely from MS.

There are eight carbon atoms in an iso-cetane molecular that have at least one hydrogen atom to lose, as shown in Figure 6.14, hence eight different fuel radicals. Three $C_{16}H_{32}$ isomers could be produced following an H-atom abstraction from the carbon atoms 4, 5, 6, or 7 and an O_2 addition to the carbon, with a double bond
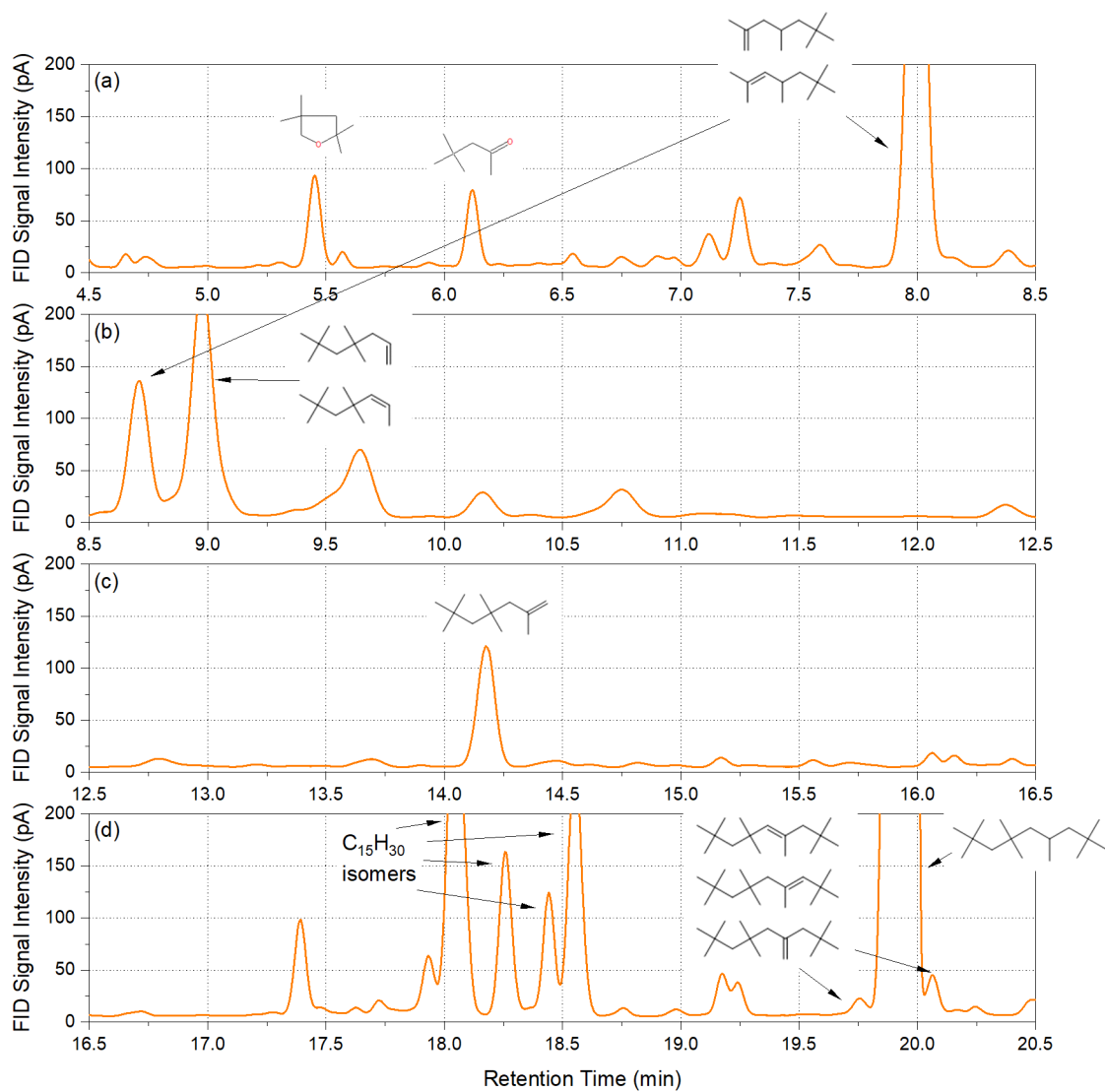
Figure 6.9: GC-FID signal from iso-cetane autoigntion experiment at $CR = 9.4$.
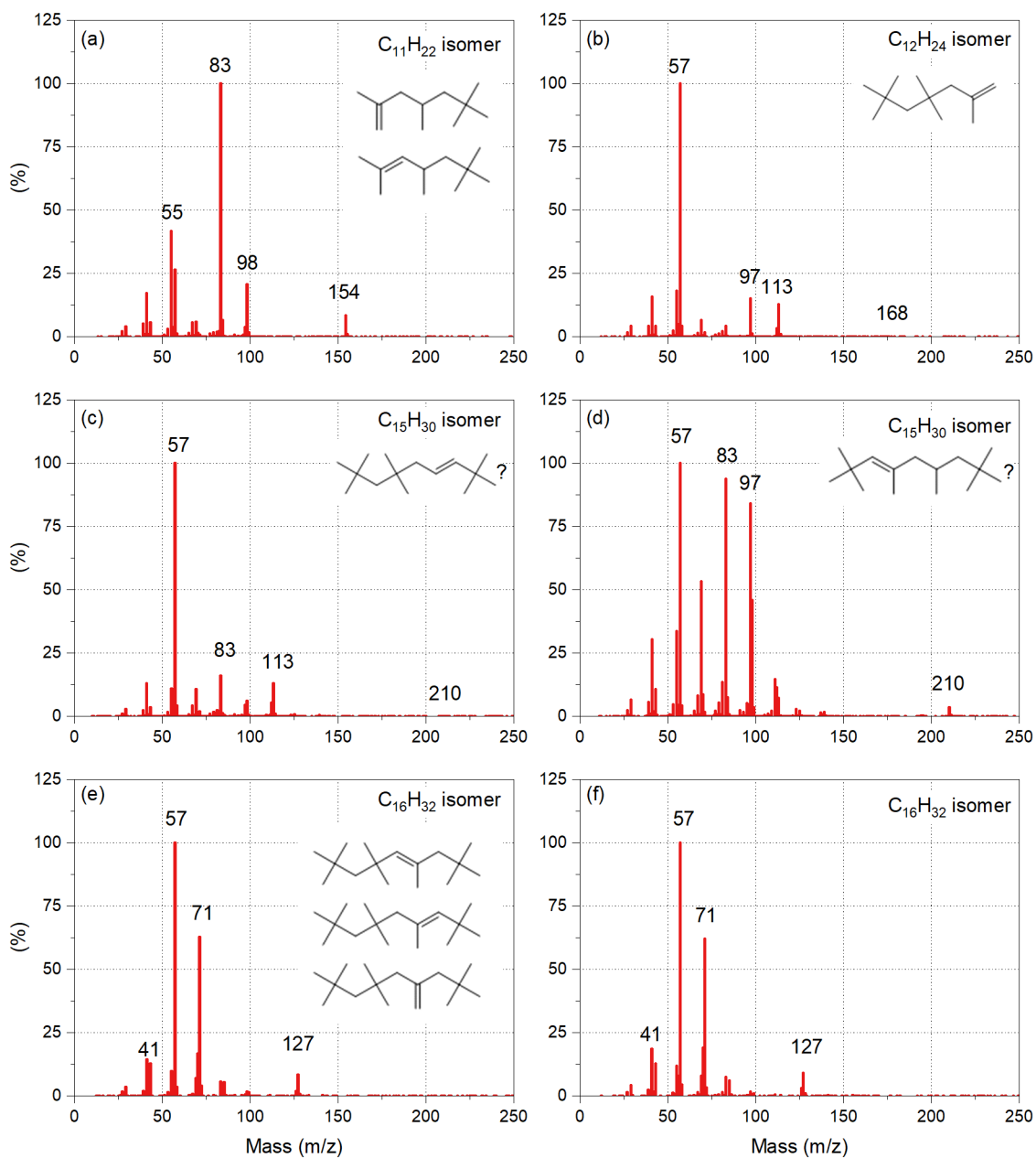
Figure 6.10: Mass spectrum of the species detected in iso-cetane oxidation experiment.

96
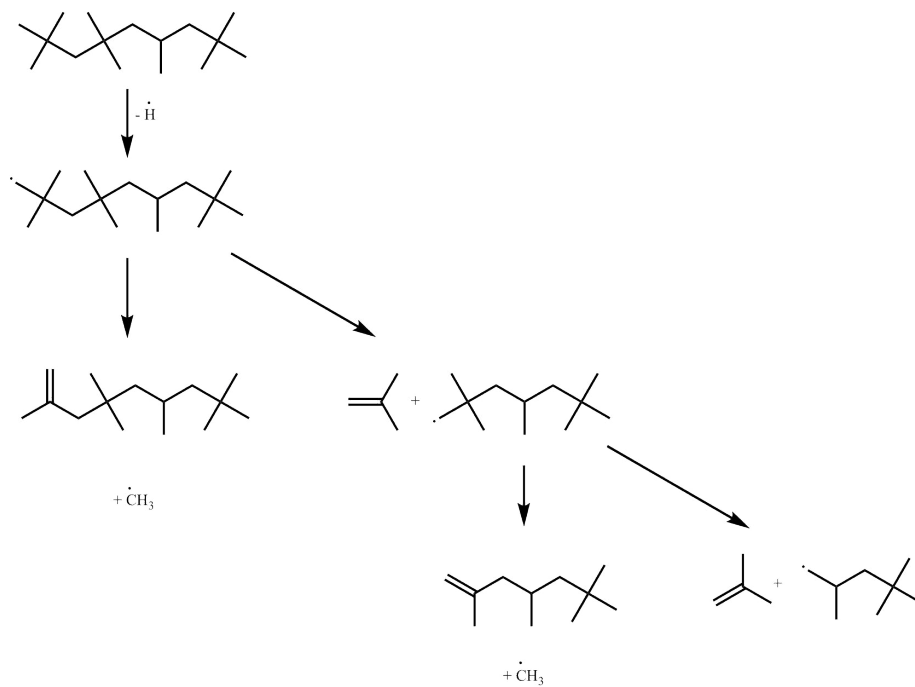
Figure 6.11: Alkene formation through β-scission pathways.
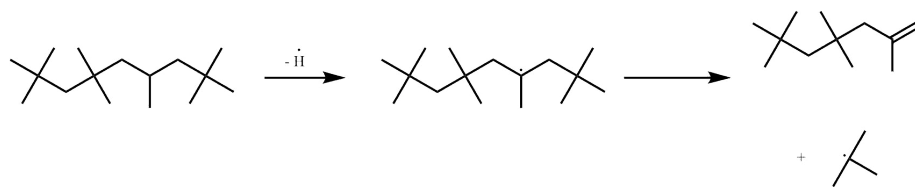
Figure 6.12: 2,4,4,6,6-Pentylmethyl-heptene production pathway.

C$_{16}$H$_{32}$ isomers

C$_{15}$H$_{30}$ isomers

C$_{11}$H$_{22}$ isomers

C$_8$H$_{16}$ isomers

C$_7$H$_{14}$ isomers
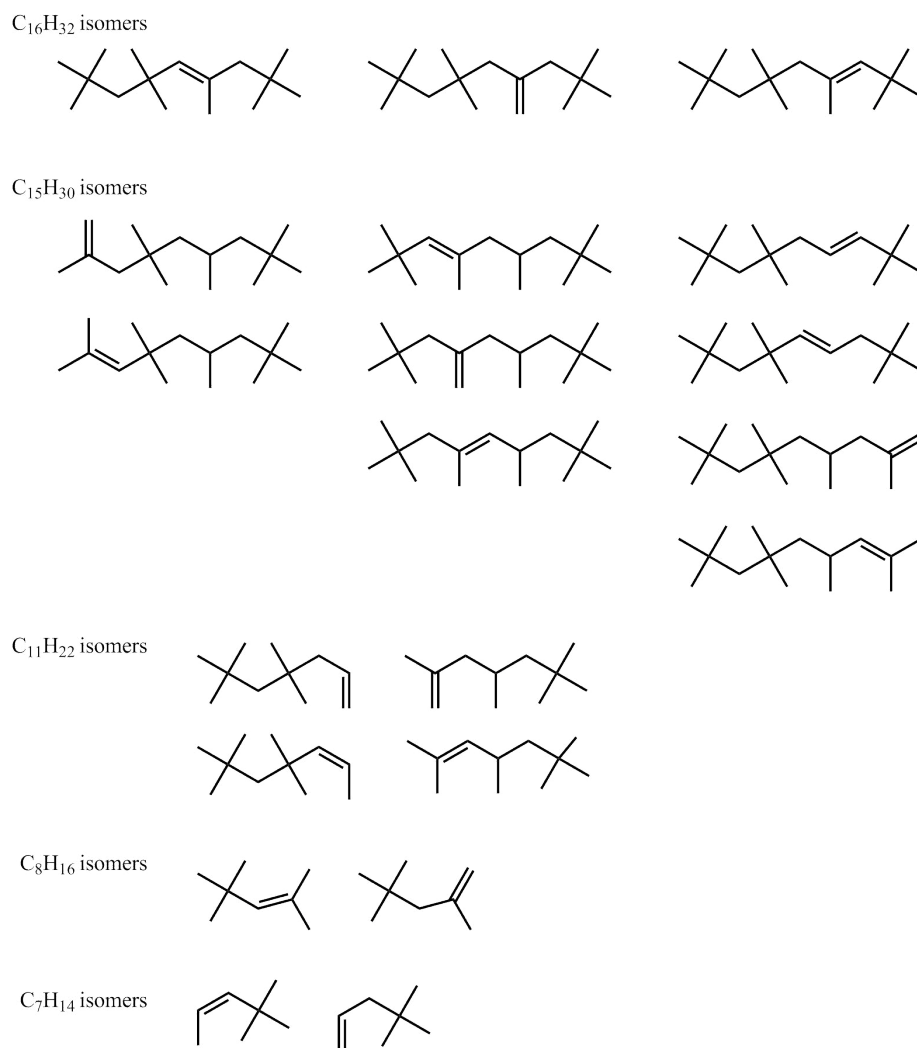
Figure 6.13: Alkene isomers that could possibly form in iso-cetane oxidation.

formed between site 5 and sites 4, 6, or 7. From the ceiling temperature discussion above, the formation of other alkenes was less likely via O_2 addition to fuel radicals. Instead, production was more likely through beta-scission of the fuel radicals. There could possibly be nine $C_{15}H_{30}$ isomers, four $C_{11}H_{22}$ isomers, two C_8H_{16} isomers, and two C_7H_{14} isomers, through pathways similar to those in Figure 6.11. Molecular structures of the isomers are shown in Figure 6.13.
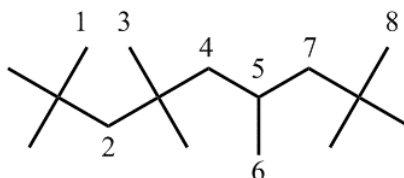
Figure 6.14: An iso-cetane molecule.

In addition to $C_{11}H_{22}$, $C_{15}H_{30}$ and $C_{16}H_{32}$ isomers, there was one single peak at $RT = 14.20$ min with a molecular weight of 168, being very likely $C_{12}H_{24}$. Formation of a $C_{12}H_{24}$ molecule involves losing a tert butyl group. It is unlikely to lose the tert butyl group connecting to carbon atom 2 in this process. The other carbon connecting to 2 is also a quaternary carbon, so 2 cannot form a double bond after losing the tert butyl group. Hence, the only possible structure of $C_{12}H_{24}$ is 2,4,4,6,6-pentylmethyl-heptene, with carbon 7 losing the tert butyl group and forming a double bond with 5. Figure 6.12 shows the pathway of 2,4,4,6,6-pentylmethyl-heptene formation.

6.4.2 Intermediate species during decalin oxidation

Major C_{10} species during decalin oxidation, as shown in Figure 6.15 were $C_{10}H_{16}O$ isomers, octahydronaphthalenes, hexahydronaphtalenes, tetralin, dialin and naphthalene, consistent with the results in Yang and Boehman [58]. C_8H_{12} and styrene, C_7H_{10} and toluene, cyclohexene, cyclohexadiene, and benzene were also detected but at lower concentrations compared to C_{10} species, showing that ring-opening of one ring first was less likely. The mechanism significantly overpredicted concentrations
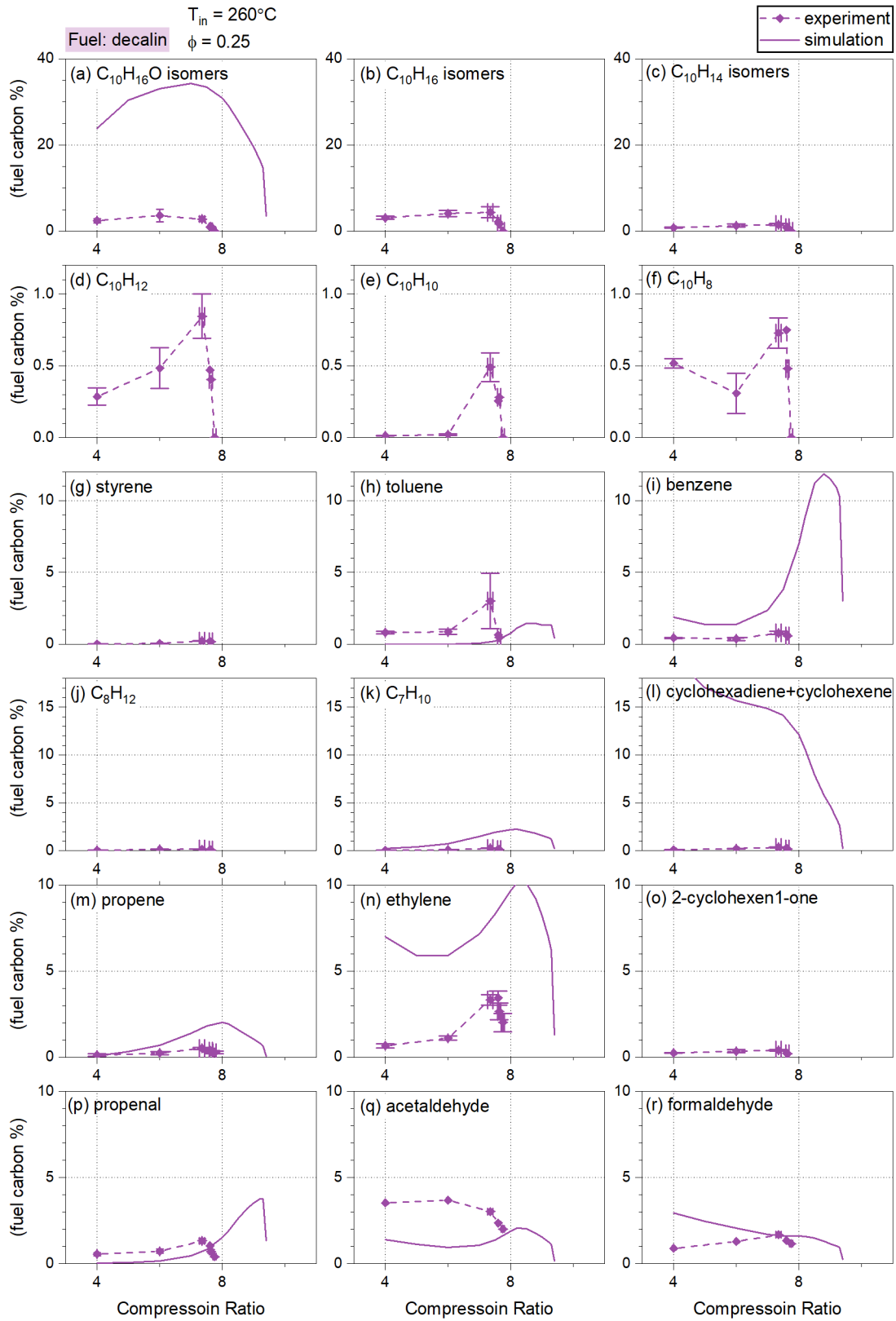
Figure 6.15: Species during decalin oxidation.

of benzene, cyclohexadiene, and cyclohexene. A flux analysis showed that the major fuel consumption pathways in the mechanism were ring-opening of one ring first, which Yang and Boehman [58] found was less favored due to higher activation energy and a stronger bond. Wang et al. [52] developed a mechanism based on analogy to MCH oxidation. Flux analysis of the Wang et al. [52] mechanism showed that the major fuel consumption pathways were via the formation of 1-decal radical or 2-decal radical, consistent with the reaction pathways proposed in Yang and Boehman [58]. Adding those two pathways is necessary in future development of the kinetics mechanism for the jet fuel surrogate.

6.4.3 Intermediate species during toluene oxidation

Low-temperature oxidation was found to be insignificant for toluene autoignition at the test conditions. Very simple intermediates were observed, primarily benzene and benzaldehyde.
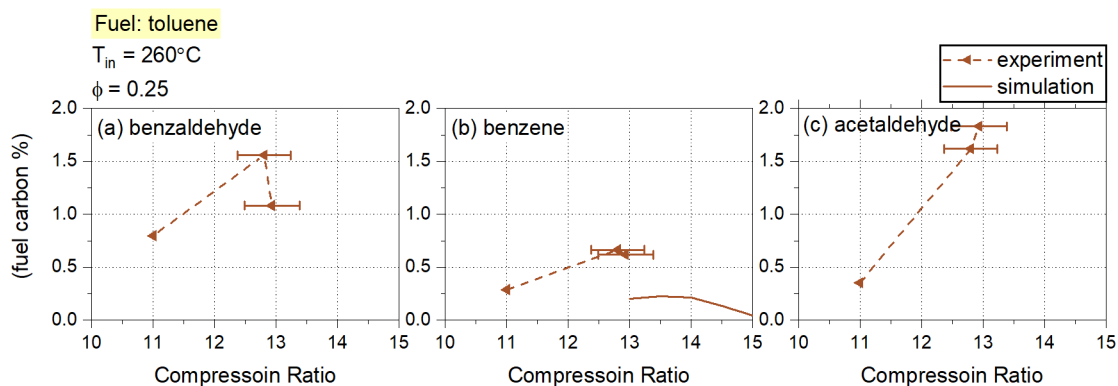
Figure 6.16: Species during toluene oxidation.

6.4.4 Intermediate species during jet fuel surrogate oxidation

The surrogate intermediate species was a mixture of the four component fuels' intermediate species, except for one new species: 2,2,4-trimethyl-pentane. 2,2,4-Trimethyl-pentane might be produced via β-scission of the fuel radical, at the same

101
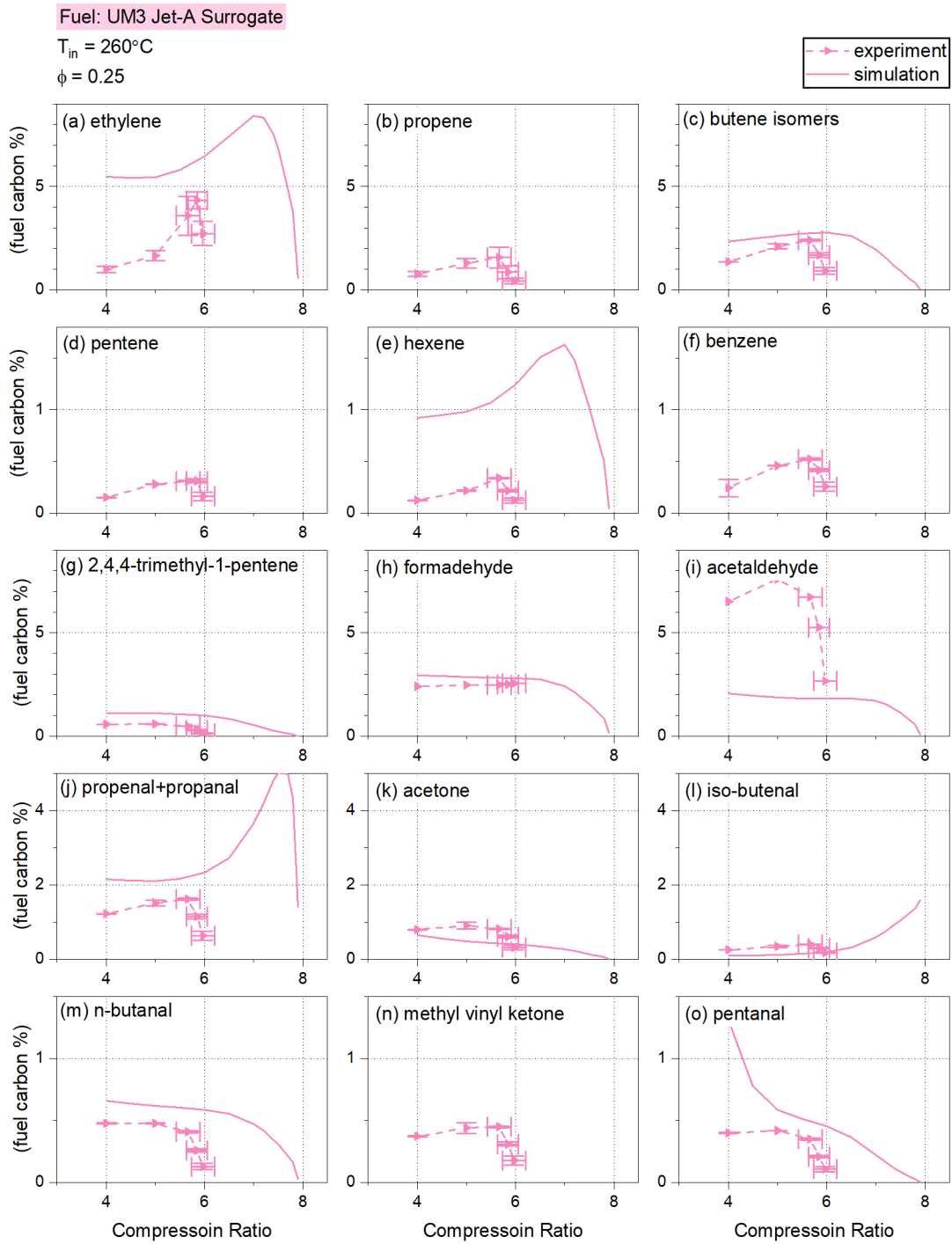
Figure 6.17: Species during the jet fuel surrogate oxidation.

time of 2,4,4-trimethyl-1-pentene formation. 2,4,4-Trimethyl-1-pentene was a major species in both the surrogate and iso-cetane oxidation. iso-Butanal production was also significant, which was another major species during iso-cetane oxidation.

Detection of those species indicates enhanced H-atom abstraction by radicals generated in other components' oxidation processes and consequently more fuel radicals. Those small species were produced from fuel radicals via β-scission reactions. At the same time, production of conjugate olefins and cyclic ethers was insignificant for iso-cetane, decalin and benzene in the mixture, meaning that the oxidation enhancement was not via correspondent chain-propagation pathways. O_2 addition might not be important for iso-cetane, decalin and toluene during oxidation of the surrogate mixture, while LTO of n-dodecane is still important. Improved quantification of oxygenated species, better separation of conjugate olefins and cyclic ethers, and an optimized mechanism would be helpful to further investigate the cross-reactions among pure components.

6.5   Conclusions

In this study, autoignition properties of a jet fuel surrogate and components were investigated in motored engine experiment and simulation. Reactivity, heat release, and oxidation intermediates were measured for pure components and the surrogate fuel. Performance of an existing jet fuel surrogate mechanism, SKE360, was evaluated.

The jet fuel surrogate mechanism underpredicted the surrogate reactivity, due to underestimated n-dodecane and decalin reactivity. The overestimated iso-cetane reactivity compensated for this deviation slightly and made [CO] prediction during LTO fairly accurate. Oxidation enhancement was predicted for iso-cetane and decalin, but toluene oxidation was significantly underpredicted in the mixture. The oxidation enhancement was due to increased H-atom abstraction by radicals generated in n-dodecane low-temperature oxidation. More fuel radicals were produced, and via β-

103

scission reactions more small intermediate species were produced. This enhancement was not determined by the stand-alone fuel reactivity and was more significant for iso-cetane than for decalin.

During iso-cetane autoignition, low-temperature chemistry was insignificant at the testing conditions, but its importance was overestimated in the mechanism. The $R +$ O_2 reaction rates need to be updated in SKE360 and in other mechanisms in the literature to eliminate O_2 addition to the fuel radicals.

Decalin exhibited strong NTC behavior, which was captured in the prediction, but the global reactivity was underestimated. The ring-opening pathways need major modification in the mechanism. The production of benzene, cyclohexadiene, and cyclohexene was overpredicted by more than 10 times during decalin oxidation, showing the opening of one ring in this bicyclic alkane molecule was overestimated. The two pathways breaking the C-C bond between the two tertiary carbons were the major low-temperature chain-branching pathways and need to be added.

Low-temperature oxidation was also found to be insignificant in toluene oxidation at the test conditions. This feature was successfully predicted. Although CCR prediction was slightly late, the onset of HTO was accurately predicted.

Chapter 7

Conclusions and Recommendations
for Future Work

7.1 Conclusions

Autoignition properties of a jet fuel surrogate and its pure components were investigated in coupled engine experiments and simulation. The cylinder pressure trace and oxidation intermediate species were measured to provide information for mechanism development and validation.

7.1.1 Multizone model reliability

For the purpose of mechanism evaluation, a multizone model was developed to simulate the homogeneous charge compression ignition (HCCI) process in a motored engine. In a simulation study for three pentane isomers, the model was found to be accurate for engine simulation and effective for mechanism validation.

7.1.2 Pentane isomers autoignition

In the simulation study for pentane isomers autoignition, an existing pentane isomers mechanism was found to be accurate for the prediction of reactivity, fuel consumption, and heat release for all three pentane isomers. At the same time, slight

105

improvements could be made in the mechanism, as low-temperature oxidation (LTO) was slightly overestimated for n- and neo-pentane and slightly underestimated for iso-pentane. The first-stage fuel consumption was overpredicted by 3.8% and 5.2% for n- and neo-pentane, and was underpredicted by 32.2% for iso-pentane.

For all pentane isomers considered, C_5 cyclic ethers were overpredicted by 148% and 58.9% for n- and neo-pentane, and by more than 20 times for iso-pentane. 2-Pentene and 2-methyl-2-butene production was overpredicted by 104% and 126%. Low-temperature chain-branching products acetaldehyde or acetone were underpredicted by 57.5% for n-pentane, 72.2% for iso-pentane and 58.6% for neo-pentane. Hence, specific 7- and 5-membered transition state (TS) ring pathways could be weakened, and 6-membered TS ring pathways could be enhanced. 4- and 8-Membered TS ring pathways also need to be added to include missing species. H-atom availability might be the dominant factor in conjugate elimination reactions, and its importance was underestimated. Specifically for iso-pentane, chain-branching pathways following first and second O_2 addition to the tertiary carbon were found to be unlikely.

In comparing the three pentane isomers, conjugate olefin production was found to be insensitive to the fuel structure. $C_5H_{10}O$ and acetaldehyde/acetone formation is sensitive to the fuel structure, with the least reactive pentane isomer, iso-pentane producing the least $C_5H_{10}O$ and acetaldehyde. The mechanism successfully predicted the trend for conjugate olefins and $C_5H_{10}O$ isomers. However, it was ineffective in predicting the difference in acetaldehyde/acetone production. The mechanism was accurate for fuel reactivity, indicating that reactivity prediction might be sensitive to chain-propagating reactions producing conjugate olefins and cyclic ethers, but not sensitive to the chain-branching reactions producing acetaldehyde/acetone.

7.1.3 n-Heptane and n-dodecane autoignition

In motored engine experiment and simulation, existing mechanisms for n-heptane and n-dodecane oxidation were evaluated, and all mechanisms underestimated fuel reactivities and acetaldehyde production. Although reaction pathways were similar, mechanisms showed disagreeing predictions for fuel reactivity, showing the importance of mechanism selection. An n-heptane mechanism was improved by updating the $H_2/O_2/CO$ submechanism, with the predicted critical compression ratio improved from 0.9 compression ratio higher to within 0.1 deviation from the measurements. CO concentration from the motored engine experiment could be used as an evaluator of mechanism performance, providing insight into the chemical model and direction for mechanism development.

In a comparison of n-pentane, n-heptane, and n-dodecane oxidation, the following trends for intermediate species were observed:

1. The concentrations of conjugate olefins and cyclic ethers were sensitive to the chain length of the normal alkane. The larger the normal alkane was, the fewer conjugation olefins and cyclic ethers were produced during oxidation.

2. Other intermediate species were less sensitive to the chain length of the normal alkane. For the three normal alkanes, major intermediate species were aldehydes and 1-alkenes. Aldehyde concentrations leveled out during negative temperature coefficient (NTC) and dropped at the end of NTC. 1-Alkenes accumulated during NTC and peaked at the end of NTC. Concentrations for those species were also similar for the three normal alkanes.

These trends were consistent with observations in the shock tube, the jet-stirred reactor, and in other motored engine studies. Still, they were not always followed in mechanisms and should be considered in future mechanism development.

7.1.4   Jet fuel surrogate and components autoignition

The jet fuel surrogate mechanism, SKE360, successfully predicted the low-temperature reactivity of the surrogate. However, the global reactivity was underpredicted due to underestimated n-dodecane and decalin reactivity.

In the jet fuel surrogate, oxidation of iso-cetane, decalin, and toluene was significantly enhanced, due to increased H-atom abstraction by radicals generated in n-dodecane LTO. More fuel radicals were produced, and via beta-scission reactions more small intermediate species were produced. This enhancement was not directly related to the stand-alone fuel reactivity and was more significant for iso-cetane than for decalin. Oxidation enhancement was predicted for iso-cetane and decalin with 1.87% and 5.45% deviation in fuel consumption from measurements, but toluene oxidation in the mixture was underpredicted by 79.1%.

During iso-cetane autoignition, low-temperature chemistry was insignificant at the testing conditions, but its importance was overestimated in the mechanism. The $\dot{R} + O_2$ reaction rates need to be improved to eliminate O_2 addition to the fuel radicals.

Decalin exhibited strong NTC behavior, which was captured in the prediction, but the global reactivity was underestimated. The production of benzene, cyclohexadiene, and cyclohexene was overpredicted by more than 10 times during decalin oxidation, showing the opening of one ring in this bicyclic alkane molecule was overestimated. The two pathways breaking the C-C bond between the two tertiary carbons were the major low-temperature chain-branching pathways but were missed in the mechanism.

7.2 Recommendations for future work

7.2.1 Kinetic mechanism development based on combustion intermediate species measurement and reaction pathways analysis

As discussed in Chapter 2, current chemical kinetic mechanisms still need to be improved to accurately predict observations and measurements in fundamental combustion facilities, while a lack of ignition data, especially at low temperatures and for intermediate combustion species, makes further mechanism development difficult. Previously, the ignition delay data at low temperatures were mainly measured in the rapid compression machine and, more recently, in the flow reactor. Combustion intermediate species were mainly measured in the flow and jet reactors. As a closer mimic and a simplification of real engines, the motored engine provides a realistic and practical way for generating ignition data at conditions that are related to and important in mechanism development and engine design.

This study demonstrated that the fuel reactivity and combustion intermediate species measured in a motored engine provided important information on fuel oxidation pathways. The coupled engine experiment and simulation showed that significant discrepancies exist and current reaction pathways and reaction rates need improvements. Methods and directions for improvements were proposed, but mechanism development is beyond the scope of this study. It is promising that the accuracy of existing mechanisms could be greatly improved by including new reaction pathways for missing intermediate species, re-evaluating the relative importance of competing pathways, and eliminating the uncertainties of important reactions. We are closer to having the kinetic mechanism that we will be confident to use in engine simulation and design.

7.2.2 Kinetic mechanism optimization with motored engine measurements as complementing constraints

A chemical kinetic mechanism for fuel oxidation may consist of thousands of reactions, while few of the reaction rates were directly measured. Most reaction rates were developed based on analogy to similar reactions and need to be optimized using indirect experimental measurements as prediction targets. The ignition delay timing measured in the shock tube and the rapid compression machine was usually used as these prediction targets. Important species time histories from flow and jet reactor experiments were also common prediction targets. While the question remains whether a high level of accuracy is necessary, studies found that mere fundamental combustion facility measurements may not be enough to develop a mechanism that could be used for reliable engine simulation. Motored engine measurements may need to be included as complementations to eliminate prediction uncertainties [22].

Methods developed in this study provides a potential to use motored engine data in large-scale mechanism optimization, while challenges remain before significant progress could be made. A problem with the current simulation model was parallelization. Even though the model currently runs with a single core, the computational cost is low, and the model has a strong capability to utilize very large detailed kinetic mechanisms. However, significantly higher computation speed must be achieved at a comparable level to the homogeneous reactor simulation that is currently used for mechanism optimization. The widely used optimization method involves sensitivity analysis to select important reactions and uncertainty minimization, both inducing high computational costs. New optimization methods, for example, the Evolutionary Algorithm [103], and fully connected neural networks, have been successful for optimization problems and are worth utilizing in kinetic mechanisms optimization.

BIBLIOGRAPHY

[1] A McIlroy, G McRae, V Sick, DL Siebers, CK Westbrook, PJ Smith, C Taatjes, A Trouve, AF Wagner, E Rohlfing, et al. Basic research needs for clean and efficient combustion of 21st century transportation fuels. Technical report, DOESC (USDOE Office of Science (SC)), 2006.

[2] Yu Zhang and André L Boehman. Experimental study of the autoignition of $C_8H_{16}O_2$ ethyl and methyl esters in a motored engine. *Combustion and flame*, 157(3):546–555, 2010.

[3] Dongil Kang, Doohyun Kim, Vickey Kalaskar, Angela Violi, and André L Boehman. Experimental characterization of jet fuels under engine relevant conditions–part 1: Effect of chemical composition on autoignition of conventional and alternative jet fuels. *Fuel*, 239:1388–1404, 2019.

[4] William J Pitz and Charles J Mueller. Recent progress in the development of diesel surrogate fuels. *Progress in Energy and Combustion Science*, 37(3): 330–350, 2011.

[5] Stephen Dooley, Sang Hee Won, Joshua Heyne, Tanvir I Farouk, Yiguang Ju, Frederick L Dryer, Kamal Kumar, Xin Hui, Chih-Jen Sung, Haowei Wang, et al. The experimental evaluation of a methodology for surrogate fuel formulation to emulate gas phase combustion kinetic phenomena. *Combustion and Flame*, 159(4):1444–1466, 2012.

[6] Charles K Westbrook, Marco Mehl, William J Pitz, Goutham Kukkadapu, Scott Wagnon, and Kuiwen Zhang. Multi-fuel surrogate chemical kinetic mechanisms for real world applications. *Physical Chemistry Chemical Physics*, 20(16):10588–10606, 2018.

[7] Doohyun Kim. *Conventional and Alternative Jet Fuels for Diesel Combustion: Surrogate Development and Insights into the Effect of Fuel Properties on Ignition.* PhD thesis, Department of Mechanical Engineering, The University of Michigan, 2016.

[8] Taewon Kim, Xi Luo, Mustafa Al-Sadoon, Ming-Chia Lai, Marcis Jansons, Doohyun Kim, Jason Martz, Angela Violi, and Eric Gingrich. Experimental validation of jet fuel surrogates in an optical engine. Technical report, SAE Technical Paper, 2017.

[9] Doohyun Kim, Jason Martz, and Angela Violi. The relative importance of fuel oxidation chemistry and physical properties to spray ignition. *SAE International Journal of Fuels and Lubricants*, 10(1):10–21, 2017.

[10] Henry J Curran. Developing detailed chemical kinetic mechanisms for fuel combustion. *Proceedings of the Combustion Institute*, 37(1):57–81, 2019.

[11] John Bugler, Kieran P Somers, Emma J Silke, and Henry J Curran. Revisiting the kinetics and thermodynamics of the low-temperature oxidation pathways of alkanes: a case study of the three pentane isomers. *The Journal of Physical Chemistry A*, 119(28):7510–7527, 2015.

[12] GA Pang, DF Davidson, and RK Hanson. Experimental study and modeling of shock tube ignition delay times for hydrogen–oxygen–argon mixtures at low temperatures. *Proceedings of the combustion institute*, 32(1):181–188, 2009.

[13] KA Heufer and HJSW Olivier. Determination of ignition delay times of different hydrocarbons in a new high pressure shock tube. *Shock Waves*, 20(4):307–316, 2010.

[14] Jiankun Shao, Rishav Choudhary, Yuzhe Peng, David F Davidson, and Ronald K Hanson. A shock tube study of n-heptane, iso-octane, n-dodecane and iso-octane/n-dodecane blends oxidation at elevated pressures and intermediate temperatures. *Fuel*, 243:541–553, 2019.

[15] H Li, ZC Owens, DF Davidson, and RK Hanson. A simple reactive gasdynamic model for the computation of gas temperature and species concentrations behind reflected shock waves. *International Journal of Chemical Kinetics*, 40(4): 189–198, 2008.

[16] S Scott Goldsborough, Simone Hochgreb, Guillaume Vanhove, Margaret S Wooldridge, Henry J Curran, and Chih-Jen Sung. Advances in rapid compression machine studies of low-and intermediate-temperature autoignition phenomena. *Progress in Energy and Combustion Science*, 63:1–78, 2017.

[17] Liang Yu, Yue Qiu, Yebing Mao, Sixu Wang, Can Ruan, Wencao Tao, Yong Qian, and Xingcai Lu. A study on the low-to-intermediate temperature ignition delays of long chain branched paraffin: Iso-cetane. *Proceedings of the Combustion Institute*, 37(1):631–638, 2019.

[18] Frederick L Dryer, Francis M Haas, Jeffrey Santner, Tanvir I Farouk, and Marcos Chaos. Interpreting chemical kinetics from complex reaction–advection–diffusion systems: Modeling of flow reactors and related experiments. *Progress in energy and combustion science*, 44:19–39, 2014.

[19] Anne Rodriguez, Olivier Herbinet, Xiangzan Meng, Christa Fittschen, Zhandong Wang, Lili Xing, Lidong Zhang, and Frédérique Battin-Leclerc. Hydroperoxide measurements during low-temperature gas-phase oxidation of n-heptane and n-decane. *The Journal of Physical Chemistry A*, 121(9):1861–1876, 2017.

[20] Frédérique Battin-Leclerc, Jérémy Bourgalais, Zied Gouid, Olivier Herbinet, Gustavo Garcia, Philippe Arnoux, Zhandong Wang, Luc-Sy Tran, Guillaume Vanhove, Laurent Nahon, et al. Chemistry deriving from ooqooh radicals in alkane low-temperature oxidation: A first combined theoretical and electron-ion coincidence mass spectrometry study. *Proceedings of the Combustion Institute*, 38(1):309–319, 2021.

[21] Zhandong Wang, Bingjie Chen, Kai Moshammer, Denisia M Popolan-Vaida, Salim Sioud, Vijai Shankar Bhavani Shankar, David Vuilleumier, Tao Tao, Lena Ruwe, Eike Bräuer, et al. n-heptane cool flame chemistry: Unraveling intermediate species measured in a stirred reactor and motored engine. *Combustion and Flame*, 187:199–216, 2018.

[22] Song Cheng. *Autoignition of pentane isomers in a spark-ignition engine: experiment & modeling uncertainty quantification*. PhD thesis, Department of Mechanical Engineering, The University of Melbourne, 2019.

[23] Charles K Westbrook, William J Pitz, Olivier Herbinet, Henry J Curran, and Emma J Silke. A comprehensive detailed chemical kinetic reaction mechanism for combustion of n-alkane hydrocarbons from n-octane to n-hexadecane. *Combustion and flame*, 156(1):181–199, 2009.

[24] Matthew A Oehlschlaeger, Justin Steinberg, Charles K Westbrook, and William J Pitz. The autoignition of iso-cetane at high to moderate temperatures and elevated pressures: Shock tube experiments and kinetic modeling. *Combustion and flame*, 156(11):2165–2172, 2009.

[25] Chitralkumar V Naik. Detailed chemical kinetic modeling of decalin combustion. In *7th US National Technical Meeting of the Combustion Institute*, 2011.

[26] Chitralkumar V Naik, William J Pitz, Charles K Westbrook, Magnus Sjöberg, John E Dec, John Orme, Henry J Curran, and John M Simmie. Detailed chemical kinetic modeling of surrogate fuels for gasoline and application to an HCCI engine. *SAE transactions*, pages 1381–1387, 2005.

[27] Yue-Xi Liu, Sandra Richter, Clemens Naumann, Marina Braun-Unkhoff, and Zhen-Yu Tian. Combustion study of a surrogate jet fuel. *Combustion and Flame*, 202:252–261, 2019.

[28] Sayak Banerjee, Rei Tangko, David A Sheen, Hai Wang, and C Tom Bowman. An experimental and kinetic modeling study of n-dodecane pyrolysis and oxidation. *Combustion and Flame*, 163:12–30, 2016.

[29] Yebing Mao, Mohsin Raza, Zhiyong Wu, Jizhen Zhu, Liang Yu, Sixu Wang, Lei Zhu, and Xingcai Lu. An experimental study of n-dodecane and the development of an improved kinetic model. *Combustion and Flame*, 212:388–402, 2020.

[30] Eliseo Ranzi, Alessio Frassoldati, Alessandro Stagni, Matteo Pelucchi, Alberto Cuoci, and Tiziano Faravelli. Reduced kinetic schemes of complex reaction systems: fossil and biomass-derived transportation fuels. *International Journal of Chemical Kinetics*, 46(9):512–542, 2014.

[31] Yachao Chang, Ming Jia, Yaodong Liu, Yaopeng Li, Maozhao Xie, and Hongchao Yin. Application of a decoupling methodology for development of skeletal oxidation mechanisms for heavy n-alkanes from n-octane to n-hexadecane. *Energy & Fuels*, 27(6):3467–3479, 2013.

[32] S Mani Sarathy, Charles K Westbrook, Marco Mehl, William J Pitz, Casimir Togbe, Philippe Dagaut, Hai Wang, Matthew A Oehlschlaeger, Ulrich Niemann, Kalyanasundaram Seshadri, et al. Comprehensive chemical kinetic modeling of the oxidation of 2-methylalkanes from c7 to c20. *Combustion and flame*, 158 (12):2338–2357, 2011.

[33] Krithika Narayanaswamy, Perrine Pepiot, and Heinz Pitsch. A chemical mechanism for low to high temperature oxidation of n-dodecane as a component of transportation fuel surrogates. *Combustion and Flame*, 161(4):866–884, 2014.

[34] Liming Cai, Heinz Pitsch, Samah Y Mohamed, Venkat Raman, John Bugler, Henry Curran, and S Mani Sarathy. Optimized reaction mechanism rate rules for ignition of normal alkanes. *Combustion and Flame*, 173:468–482, 2016.

[35] Meirong Zeng, Wenhao Yuan, Wei Li, Yan Zhang, and Yizun Wang. Investigation of n-dodecane pyrolysis at various pressures and the development of a comprehensive combustion model. *Energy*, 155:152–161, 2018.

[36] Yang Li, Chong-Wen Zhou, Kieran P Somers, Kuiwen Zhang, and Henry J Curran. The oxidation of 2-butene: A high pressure ignition delay, kinetic modeling study and reactivity comparison with isobutene and 1-butene. *Proceedings of the Combustion Institute*, 36(1):403–411, 2017.

[37] Debolina Dasgupta, Wenting Sun, Marc Day, and Tim Lieuwen. Sensitivity of chemical pathways to reaction mechanisms for n-dodecane. In *10th US National Combustion Meeting, College Park, Maryland*, 2017.

[38] Xiaoqing You, Fokion N Egolfopoulos, and Hai Wang. Detailed and simplified kinetic models of n-dodecane oxidation: The role of fuel cracking in aliphatic hydrocarbon combustion. *Proceedings of the Combustion Institute*, 32(1):403–410, 2009.

[39] Zhaoyu Luo, Sibendu Som, S Mani Sarathy, Max Plomer, William J Pitz, Douglas E Longman, and Tianfeng Lu. Development and validation of an n-dodecane skeletal mechanism for spray combustion applications. *Combustion theory and modelling*, 18(2):187–203, 2014.

[40] José M Desantes, J Javier López, José M García-Oliver, and Darío López-Pintor. Experimental validation and analysis of seven different chemical kinetic mechanisms for n-dodecane using a rapid compression-expansion machine. *Combustion and Flame*, 182:76–89, 2017.

[41] Tianfeng Lu, Max Plomer, Zhaoyu Luo, SM Sarathy, WJ Pitz, S Som, and DE Longman. Directed relation graph with expert knowledge for skeletal mechanism reduction. Technical report, Lawrence Livermore National Lab.(LLNL), Livermore, CA (United States), 2011.

[42] Hu Wang, Rolf Deneys Reitz, Mingfa Yao, Binbin Yang, Qi Jiao, and Lu Qiu. Development of an n-heptane-n-butanol-pah mechanism and its application for combustion and soot prediction. *Combustion and Flame*, 160(3):504–519, 2013.

[43] Tong Yao, Yuanjiang Pei, Bei-Jing Zhong, Sibendu Som, and Tianfeng Lu. A hybrid mechanism for n-dodecane combustion with optimized low-temperature chemistry. In *9th US national combustion meeting*, volume 5, 2015.

[44] Francisco Payri, Jose M García-Oliver, Ricardo Novella, and Eduardo J Pérez-Sánchez. Influence of the n-dodecane chemical mechanism on the cfd modelling of the diesel-like ecn spray a flame structure at different ambient conditions. *Combustion and Flame*, 208:198–218, 2019.

[45] Xiaohang Fang, Riyaz Ismail, and Martin Davy. A study on kinetic mechanisms of diesel fuel surrogate n-dodecane for the simulation of combustion recession. Technical report, SAE Technical Paper, 2019.

[46] Henry J Curran, Paolo Gaffuri, William J Pitz, and Charles K Westbrook. A comprehensive modeling study of iso-octane oxidation. *Combustion and flame*, 129(3):253–280, 2002.

[47] Goutham Kukkadapu and Chih-Jen Sung. Autoignition study of binary blends of n-dodecane/1-methylnaphthalene and iso-cetane/1-methylnaphthalene. *Combustion and Flame*, 189:367–377, 2018.

[48] Nour Atef, Goutham Kukkadapu, Samah Y Mohamed, Mariam Al Rashidi, Colin Banyon, Marco Mehl, Karl Alexander Heufer, Ehson F Nasir, Adamu Alfazazi, Apurba K Das, et al. A comprehensive iso-octane combustion model with improved thermochemistry and chemical kinetics. *Combustion and Flame*, 178:111–134, 2017.

[49] Mohsin Raza, Jizhen Zhu, Yebing Mao, Sixu Wang, and Xingcai Lu. The autoignition of heptamethylnonane at moderate-to-high temperatures and elevated pressures: Shock tube study and improved chemical kinetic model. *Fuel*, 281:118787, 2020.

[50] Mengyuan Wang, Goutham Kukkadapu, Ruozhou Fang, William J Pitz, and Chih-Jen Sung. Autoignition study of iso-cetane/tetralin blends at low temperature. *Combustion and Flame*, 228:415–429, 2021.

[51] P Dagaut, A Ristori, Alessio Frassoldati, Tiziano Faravelli, G Dayma, and E Ranzi. Experimental and semi-detailed kinetic modeling study of decalin oxidation and pyrolysis over a wide range of conditions. *Proceedings of the Combustion Institute*, 34(1):289–296, 2013.

[52] Mengyuan Wang, Kuiwen Zhang, Goutham Kukkadapu, Scott W Wagnon, Marco Mehl, William J Pitz, and Chih-Jen Sung. Autoignition of trans-decalin, a diesel surrogate compound: Rapid compression machine experiments and chemical kinetic modeling. *Combustion and Flame*, 194:152–163, 2018.

[53] ID Costa, JW Bozzelli, R Seiser, WJ Pitz, CK Westbrook, C Chen, R Fournet, K Seshadri, F Battin-Leclerc, and F Billaud. Chemical kinetic study of toluene oxidation under premixed and nonpremixed conditions. Technical report, Lawrence Livermore National Lab.(LLNL), Livermore, CA (United States), 2003.

[54] WK Metcalfe, S Dooley, and FL Dryer. Comprehensive detailed chemical kinetic modeling study of toluene oxidation. *Energy & Fuels*, 25(11):4915–4936, 2011.

[55] Wenhao Yuan, Yuyang Li, Philippe Dagaut, Jiuzhong Yang, and Fei Qi. Investigation on the pyrolysis and oxidation of toluene over a wide range conditions. ii. a comprehensive kinetic modeling study. *Combustion and Flame*, 162(1): 22–40, 2015.

[56] Goutham Kukkadapu, Dongil Kang, Scott W Wagnon, Kuiwen Zhang, Marco Mehl, Manuel Monge-Palacios, Heng Wang, S Scott Goldsborough, Charles K Westbrook, and William J Pitz. Kinetic modeling study of surrogate components for gasoline, jet and diesel fuels: C7-c11 methylated aromatics. *Proceedings of the Combustion Institute*, 37(1):521–529, 2019.

[57] Liang Yu, Zhiyong Wu, Yue Qiu, Yong Qian, Yebing Mao, and Xingcai Lu. Ignition delay times of decalin over low-to-intermediate temperature ranges: rapid compression machine measurement and modeling study. *Combustion and Flame*, 196:160–173, 2018.

[58] Yi Yang and André L Boehman. Oxidation chemistry of cyclic hydrocarbons in a motored engine: Methylcyclopentane, tetralin, and decalin. *Combustion and flame*, 157(3):495–505, 2010.

[59] Hsi-Ping S Shen, Jeremy Vanderover, and Matthew A Oehlschlaeger. A shock tube study of the auto-ignition of toluene/air mixtures at high pressures. *Proceedings of the Combustion Institute*, 32(1):165–172, 2009.

[60] Gaurav Mittal and Chih-Jen Sung. Autoignition of toluene and benzene at elevated pressures in a rapid compression machine. *Combustion and Flame*, 150(4):355–368, 2007.

[61] Roda Bounaceur, Isabelle Da Costa, René Fournet, Francis Billaud, and Frédérique Battin-Leclerc. Experimental and modeling study of the oxidation of toluene. *International journal of chemical kinetics*, 37(1):25–49, 2005.

[62] Wenhao Yuan, Yuyang Li, Philippe Dagaut, Jiuzhong Yang, and Fei Qi. Investigation on the pyrolysis and oxidation of toluene over a wide range conditions. i. flow reactor pyrolysis and jet stirred reactor oxidation. *Combustion and Flame*, 162(1):3–21, 2015.

[63] Shengkai Wang, David F Davidson, and Ronald K Hanson. Shock tube measurements of oh concentration time-histories in benzene, toluene, ethylbenzene and xylene oxidation. *Proceedings of the Combustion Institute*, 37(1):163–170, 2019.

[64] Marco Mehl, Olivier Herbinet, Patricia Dirrenberger, Roda Bounaceur, Pierre-Alexandre Glaude, Frédérique Battin-Leclerc, and William J Pitz. Experimental and modeling study of burning velocities for alkyl aromatic components relevant to diesel fuels. *Proceedings of the Combustion Institute*, 35(1):341–348, 2015.

[65] Yingjia Zhang, Kieran P Somers, Marco Mehl, William J Pitz, Roger F Cracknell, and Henry J Curran. Probing the antagonistic effect of toluene as a component in surrogate fuel models at low temperatures and high pressures. a case study of toluene/dimethyl ether mixtures. *Proceedings of the Combustion Institute*, 36(1):413–421, 2017.

[66] John B Heywood. *Internal combustion engine fundamentals*. McGraw-Hill Education, 2018.

[67] James P Szybist, André L Boehman, Daniel C Haworth, and Hibiki Koga. Premixed ignition behavior of alternative diesel fuel-relevant compounds in a motored engine experiment. *Combustion and Flame*, 149(1-2):112–128, 2007.

[68] Kwang Hee Yoo. *Effects of Gasoline Composition on Compression Ignition in a Motored Engine*. PhD thesis, Department of Mechanical Engineering, The University of Michigan, 2020.

[69] Yu Zhang, Yi Yang, and André L Boehman. Premixed ignition behavior of c9 fatty acid esters: A motored engine study. *Combustion and Flame*, 156(6): 1202–1213, 2009.

[70] RD Wilk, DN Koert, and NP Cernansky. Low-temperature carbon monoxide formation as a means of assessing the autoignition tendency of hydrocarbons and hydrocarbon blends. *Energy & fuels*, 3(3):292–298, 1989.

[71] A Agosta, NP Cernansky, DL Miller, Tiziano Faravelli, and Eet al Ranzi. Reference components of jet fuels: kinetic modeling and experimental results. *Experimental Thermal and Fluid Science*, 28(7):701–708, 2004.

[72] U.s. environmental protection agency. epact/v2/e-89: Assessing the effect of five gasoline properties on exhaust emissions from light-duty vehicles certified to tier 2 standards: Final report on program design and data collection. *Document number EPA-420-R-13-004.*

[73] Charlotte Sandstroem-Dahl, Lennart Erlandsson, Jan Gasste, and Magnus Lindgren. Measurement methodologies for hydrocarbons, ethanol and aldehyde emissions from ethanol fuelled vehicles. *SAE International Journal of Fuels and Lubricants*, 3(2):453–466, 2010.

[74] Ricardo Suarez-Bertoa, Michael Clairotte, Bertold Arlitt, Shigeru Nakatani, Leslie Hill, Klaus Winkler, Charlotte Kaarsberg, Thorsten Knauf, Rens Zijl-mans, Henry Boertien, et al. Intercomparison of ethanol, formaldehyde and acetaldehyde measurements from a flex-fuel vehicle exhaust during the wltc. *Fuel*, 203:330–340, 2017.

[75] Thomas Wallner. Correlation between speciated hydrocarbon emissions and flame ionization detector response for gasoline/alcohol blends. *Journal of Engineering for Gas Turbines and Power*, 133(8), 2011.

[76] WA Dietz. Response factors for gas chromatographic analyses. *Journal of Chromatographic Science*, 5(2):68–71, 1967.

[77] Janardhan Kodavasal, Matthew J McNenly, Aristotelis Babajimopoulos, Salvador M Aceves, Dennis N Assanis, Mark A Havstad, and Daniel L Flowers. An accelerated multi-zone model for engine cycle simulation of homogeneous charge compression ignition combustion. *International Journal of Engine Research*, 14 (5):416–433, 2013.

[78] Pinaki Pal, Christopher Kolodziej, Seungmok Choi, Sibendu Som, Alberto Broatch, Josep Gomez-Soriano, Yunchao Wu, Tianfeng Lu, and Yee Chee See. Development of a virtual cfr engine model for knocking combustion analysis. *SAE International Journal of Engines*, 11(6):1069–1082, 2018.

[79] Kai J Morganti. *A study of the knock limits of liquefied petroleum gas (LPG) in spark-ignition engines*. PhD thesis, Department of Mechanical Engineering, The University of Melbourne, 2013.

[80] Junseok Chang, Orgun Güralp, Zoran Filipi, Dennis Assanis, Tang-Wei Kuo, Paul Najt, and Rod Rask. New heat transfer correlation for an HCCI engine derived from measurements of instantaneous surface heat flux. *SAE transactions*, pages 1576–1593, 2004.

[81] Liming Cai and Heinz Pitsch. Mechanism optimization based on reaction rate rules. *Combustion and flame*, 161(2):405–415, 2014.

[82] Zhandong Wang and S Mani Sarathy. Third o2 addition reactions promote the low-temperature auto-ignition of n-alkanes. *Combustion and Flame*, 165: 364–372, 2016.

[83] N Hansen, G Kukkadapu, B Chen, S Dong, HJ Curran, CA Taatjes, AJ Eskola, DL Osborn, L Sheps, WJ Pitz, et al. The impact of the third o2 addition reaction network on ignition delay times of neo-pentane. *Proceedings of the Combustion Institute*, 38(1):299–307, 2021.

[84] Alena Sudholt, Liming Cai, and Heinz Pitsch. Laminar flow reactor experiments for ignition delay time and species measurements at low temperatures: Linear alkanes and dimethyl ether. *Combustion and Flame*, 202:347–361, 2019.

[85] Yu Cheng, Erjiang Hu, Xin Lu, Xiaotian Li, Jing Gong, Qianqian Li, and Zuohua Huang. Experimental and kinetic study of pentene isomers and n-pentane in laminar flames. *Proceedings of the Combustion Institute*, 36(1): 1279–1286, 2017.

[86] Anne Rodriguez, Olivier Herbinet, Zhandong Wang, Fei Qi, Christa Fittschen, Phillip R Westmoreland, and Frédérique Battin-Leclerc. Measuring hydroperoxide chain-branching agents during n-pentane low-temperature oxidation. *Proceedings of the Combustion Institute*, 36(1):333–342, 2017.

[87] John Bugler, Anne Rodriguez, Olivier Herbinet, Frédérique Battin-Leclerc, Casimir Togbé, Guillaume Dayma, Philippe Dagaut, and Henry J Curran. An experimental and modelling study of n-pentane oxidation in two jet-stirred reactors: The importance of pressure-dependent kinetics and new reaction pathways. *Proceedings of the Combustion Institute*, 36(1):441–448, 2017.

[88] Jérémy Bourgalais, Zied Gouid, Olivier Herbinet, Gustavo A Garcia, Philippe Arnoux, Zhandong Wang, Luc-Sy Tran, Guillaume Vanhove, Majdi Hochlaf, Laurent Nahon, et al. Isomer-sensitive characterization of low temperature oxidation reaction products by coupling a jet-stirred reactor to an electron/ion coincidence spectrometer: case of n-pentane. *Physical Chemistry Chemical Physics*, 22(3):1222–1241, 2020.

[89] Dongil Kang, Stanislav V Bohac, André L Boehman, Song Cheng, Yi Yang, and Michael J Brear. Autoignition studies of c5 isomers in a motored engine. *Proceedings of the Combustion Institute*, 36(3):3597–3604, 2017.

[90] Tianfeng Lu and Chung K Law. Linear time reduction of large kinetic mechanisms with directed relation graph: n-heptane and iso-octane. *Combustion and flame*, 144(1-2):24–36, 2006.

[91] Lars Seidel, Kai Moshammer, Xiaoxiao Wang, Thomas Zeuch, Katharina Kohse-Höinghaus, and Fabian Mauss. Comprehensive kinetic modeling and experimental study of a fuel-rich, premixed n-heptane flame. *Combustion and Flame*, 162(5):2045–2058, 2015.

[92] Kuiwen Zhang, Colin Banyon, John Bugler, Henry J Curran, Anne Rodriguez, Olivier Herbinet, Frédérique Battin-Leclerc, Christine B'Chir, and Karl Alexander Heufer. An updated experimental and kinetic modeling study of n-heptane oxidation. *Combustion and Flame*, 172:116–135, 2016.

[93] Alison M Ferris, Jesse W Streicher, Adam J Susa, David F Davidson, and Ronald K Hanson. A comparative laser absorption and gas chromatography study of low-temperature n-heptane oxidation intermediates. *Proceedings of the Combustion Institute*, 37(1):249–257, 2019.

[94] Marco Mehl, William J Pitz, Charles K Westbrook, and Henry J Curran. Kinetic modeling of gasoline surrogate components and mixtures under engine conditions. *Proceedings of the Combustion Institute*, 33(1):193–200, 2011.

[95] S Mani Sarathy, Efstathios-Al Tingas, Ehson F Nasir, Alberta Detogni, Zhandong Wang, Aamir Farooq, and Hong Im. Three-stage heat release in n-heptane auto-ignition. *Proceedings of the Combustion Institute*, 37(1):485–492, 2019.

[96] Dong He, Damien Nativel, Jürgen Herzler, Jay B Jeffries, Mustapha Fikri, and Christof Schulz. Laser-based co concentration and temperature measurements in high-pressure shock-tube studies of n-heptane partial oxidation. *Applied Physics B*, 126(8):1–11, 2020.

[97] Olivier Herbinet, Benoit Husson, Hervé Le Gall, and Frédérique Battin-Leclerc. An experimental and modeling study of the oxidation of n-heptane, ethylbenzene, and n-butylbenzene in a jet-stirred reactor at pressures up to 10 bar. *International Journal of Chemical Kinetics*, 52(12):1006–1021, 2020.

[98] Nesrine Belhadj, Roland Benoit, Philippe Dagaut, and Maxence Lailliau. Experimental characterization of n-heptane low-temperature oxidation products including keto-hydroperoxides and highly oxygenated organic molecules (homs). *Combustion and Flame*, 224:83–93, 2021.

[99] Hisashi Nakamura, Daniel Darcy, Marco Mehl, Colin J Tobin, Wayne K Metcalfe, William J Pitz, Charles K Westbrook, and Henry J Curran. An experimental and modeling study of shock tube and rapid compression machine ignition of n-butylbenzene/air mixtures. *Combustion and Flame*, 161(1):49–64, 2014.

[100] Olivier Herbinet, Sarah Bax, Pierre-Alexandre Glaude, Vincent Carré, and Frédérique Battin-Leclerc. Mass spectra of cyclic ethers formed in the low-temperature oxidation of a series of n-alkanes. *Fuel*, 90(2):528–535, 2011.

[101] Tomasz Malewicki and Kenneth Brezinsky. Experimental and modeling study on the pyrolysis and oxidation of n-decane and n-dodecane. *Proceedings of the combustion institute*, 34(1):361–368, 2013.

[102] A Roubaud, O Lemaire, R Minetti, and LR Sochet. High pressure auto-ignition and oxidation mechanisms of o-xylene, o-ethyltoluene, and n-butylbenzene between 600 and 900 k. *Combustion and flame*, 123(4):561–571, 2000.

[103] Andrea Bertolino, Magnus Fürst, Alessandro Stagni, Alessio Frassoldati, Matteo Pelucchi, C Cavallotti, T Faravelli, and Alessandro Parente. An evolutionary, data-driven approach for mechanism optimization: theory and application to ammonia combustion. *Combustion and Flame*, 229:111366, 2021.